Robust control of nonlinear systems from data

POLITECNICO DI TORINO

Ph.D. in Computer and Control Systems Engineering – XXIII cycle

Ph.D. Thesis

# Robust control from data for nonlinear dynamic systems


**Maria Carmela Signorile**

**Advisor**
Professor Massimo Canale

April 2012

# Contents

# Chapter 1

# Introduction

A general problem in the control field is to derive a model of the system to be controlled. The classical approach consists in building a mathematical model on the basis of the laws governing the system (e.g. mechanical, physical, economical) and then exploit it for designing a model-based control law that fulfills the desired specifications. However, such approach is not always possible for two main reasons: the uncomplete knowledge of the system laws and its nonlinearity which, respectively, do not enable to derive an accurate and tractable model. On the other hand, considering that the most of the existing systems are nonlinear, the model to be derived should be a trade-off between accuracy and tractability. Indeed, the accuracy of the model, employed to design the control system, plays a crucial role since the performance achievable by the controlled system strongly depends on the size of the modeling error. In the presence of a poor accurate model, not only a performance degradation may occurr, but the closed loop stability may also be missed.
The literature of nonlinear control usually assumes that the system to be controlled and its model are well known, altough this is not always true as pointed out above. In particular, the nonlinear models usually employed are neural networks or parametric models whose parameters are identified from input/output data of the process. Due to the nature of these models, does not exist a systematic procedure to obtain a suitable description of the uncertainty associated with them, which in turn hampers a systematic dealing of the robust stability.
Thus, in order to investigate the control of nonlinear and unknown systems, guaranteeing the stability of the closed loop system in the presence of model uncertainty, objective of this thesis is study the robust control of nonlinear dynamic systems from experimental data.
At this aim, a Nonlinear Set Membership (NSM) identification methodology is used to derive a data-based model. Such technique identifies a model from input/output data collected in previous experiments and provides a finite measure of the uncertainty associated to the model (see [1] for more details). The obtained model results to be accurate both in

linear and nonlinear conditions and its accuracy can be further improved using a greater quantity of data related to several experiments performed in different conditions for its identification. Moreover, when a NSM model is employed within a control scheme, the knowledge of its uncertainty bound is fundamental to study the robust stability of the closed loop control scheme.
Among the model-based control techniques, this thesis focuses on Nonlinear Internal Model Control (NIMC) and Nonlinear Model Predictive Control (NMPC), which both require a tractable as well as accurate model also in the presence of highly nonlinear dynamics and parameter uncertainties. For this purpose, two methodologies which employ a NSM model are proposed in this thesis: a Set Membership Internal Model Control (SIMC) and a Set Membership Model Predictive Control (SMPC) .
The novelty of SIMC consists in deriving the controller by cascading a filter describing the desired input/output system behavior and the inverse of the system model (see [2]). Such a novel procedure exploits the recent results on the right–inversion (see [3]) and does not require the knowledge and the invertibility of the system. This is a not negligible advantage because the inversion of nonlinear systems is not trivial and sometimes impossible. Moreover, a robust stability study shows that the obtained SIMC control structure is input/output stable with finite gain by imposing a small gain condition in the control design phase (see [4], [5]). This is the second main result proposed because usually, in literature, the stability of NIMC control loops is empirically verified a posteriori.
The SMPC methodology, instead, uses a NSM model to predict the system behavior and the its uncertainty bound to assess the robust stability of the proposed scheme (see [6]). In fact, at first, exploiting the uncertainty measure, it is shown that the SMPC control structure is robustly stable through an a posteriori stability analysis (see [7]). Then, a procedure to design a robust SMPC control law is proposed (see [8], [9]) and applied to control a nonlinear oscillator. In the case of SIMC and SMPC robust analysis, a vehicle yaw control system is designed to show the effectiveness of the proposed methodologies.
A minor research theme, dealt in this thesis, is the design of robust control law using the technology of Direct Virtual Sensors (DVSs). DVSs are software algorithms derived directly from input/output data by means the NSM identification technique. They are able to estimate a variable of interest of a system exploiting some measures already available [10]. It is shown that the direct identification from data implies a greater accuracy of the estimate w.r.t. the classical two steps approach (e.g. Kalman filter) [11]. Further, it is shown that using data collected in closed loop fashion allows to obtain a much accurate estimate than using open loop data [10, 11]. In this thesis, DVSs are used to develop a fault tolerant vehicle yaw control system: the DVS gets on duty and replaces the physical yaw rate sensor when a fault of the last one occurs. The DVS provides the estimate of the yaw rate which is the feedback variable guaranteeing the right working of the stability control system and hence the vehicle safety (see [12]). The novelty consists in the use of an estimated variable from experimental data for control purposes and, in particular, to replace the feedback variable. Moreover, the system in closed loop which employs the

DVS results to be robustly stable through an a posteriori analysis.
The thesis is organized as follows: Chapter 2 and 3 introduce, respectively, the proposed SIMC and SMPC methodologies and the results obtained in terms of performance and stability, while Chapter 4 introduces the technology of DVSs and its employment within the context of vehicle stability control systems. Finally, Appendix A introduces the NSM methodology used to derive the system model from data.

# Chapter 2

# Set Membership Internal Model Control

Internal Model Control (IMC) is a powerful technique which offers a practical and effective approach to the synthesis of control systems (for more details see e.g. [13]). Initially, the IMC scheme was introduced for linear systems, then it was extended to the case of nonlinear ones see e.g. [14]. The peculiar characteristic of IMC, see Figure 2.1, is that the control structure incorporates a model $\mathbf{f}_c$ of the system $\mathbf{f}_0$ to be controlled. In such a structure, a typical design approach consists in computing the controller $\mathbf{Q}$ by cascading the inverse of the system model with a suitably chosen filter which describes the desired input/output behavior and guarantees stability in the presence of plant model mismatch (see e.g. [13] and [14]).
Therefore, model inversion issues play a significant role in the design of IMC controllers.

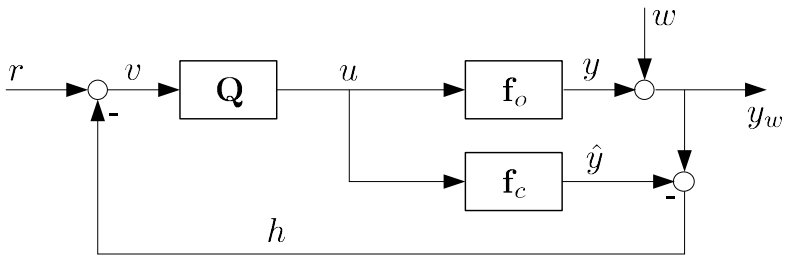


Figure 2.1. NIMC control system.

In the case of linear systems, these problems can be analyzed and, when possible, solved in a systematic way [15]. For nonlinear systems, instead, they are considerably more difficult because of the non invertibility of the system or the complex nonlinear dynamics which may characterize the system itself. In literature, the problem of inversion of nonlinear systems has been addressed both from theoretical, see e.g. [16], [17], [18], [19], [20]

and application point of view, see e.g. [21], [22], [23], [24]. In the context of Nonlinear Internal Model Control (NIMC), a possible solution is to identify the inverse model from data collected during suitable experiments on the system. Along this line of research, the contributions introduced in [19] and [25] solve the problem by means of neural networks. In this thesis, instead, the novel approach investigated consists in deriving the system model and its inverse directly from data [4]. In particular, the system model is obtained by means the NSM methodology as described in Appendix A, while, the inverse model is computed from the system model, previously identified, applying an inversion algorithm [26]. Therefore, the proposed methodology Set Membership Internal Model Control (SIMC), for nonlinear and unknown systems, consists in designing a NIMC structure including a NSM model and a controller obtained by cascading the inverse NSM model and a filter describing the desired input/output behavior. Moreover, a robust stability study shows that the derived SIMC control structure is input/output stable with finite gain by imposing a small gain condition in the control design phase (see [4], [5]). The effectiveness of the proposed approach is shown through a vehicle yaw control application [2].

## 2.1 Inversion of nonlinear systems

### 2.1.1 Problem formulation

Consider a nonlinear discrete-time dynamic system in regression form:

$$\begin{aligned} y^{t+1} &= f_o\left(\mathbf{y}^t, \mathbf{u}^t\right) \quad t \in \mathbb{Z} \\ \mathbf{y}^t &= [y^t; \ldots; y^{t-n_y}] \\ \mathbf{u}^t &= [u^t; \ldots; u^{t-n_u}] \end{aligned} \tag{2.1}$$

where $u^t \in U \subset \mathbb{R}$, $y^{t+1} \in Y \subset \mathbb{R}$, $f_o : \Phi \subset \mathbb{R}^n \to \mathbb{R}$, $n = n_y + n_u$. $U$, $Y$ and $\Phi$ are convex compact sets. The regression function $f_o$ is assumed differentiable. The notation $[\ldots;\ldots;\ldots]$ indicates vertical concatenation.
The regression system (2.1) is a nonlinear operator $\mathbf{f}_o$ mapping the initial condition $\mathbf{y}^0 \in Y^{n_y}$, and the input sequence $u = [u^1; u^2; \ldots] \in U^\infty \subset \mathbb{R}^\infty$ into an output sequence $y = [y^1; y^2; \ldots] \in Y^\infty \subset \mathbb{R}^\infty$. The operator $\mathbf{f}_o$ is defined as

$$y = \mathbf{f}_o\left(\mathbf{y}^0, u\right) = \left[\mathbf{f}_o^1\left(\mathbf{y}^0, u\right); \mathbf{f}_o^2\left(\mathbf{y}^0, u\right); \ldots\right] \tag{2.2}$$

where $\mathbf{f}_o : \mathbb{R}^\infty \to \mathbb{R}^\infty$, $\mathbf{f}_o^t : \mathbb{R}^{n_y+t} \to \mathbb{R}$. The notation $y = \mathbf{f}_o(u)$ will be used when it will be not needed to explicit the dependence on initial conditions.
The output of $\mathbf{f}_o$ at a time $\tau$ is given by

$$y^\tau = \mathbf{f}_o^\tau\left(\mathbf{y}^0, u\right) = \mathbf{f}_o^\tau\left(\mathbf{y}^0, [u^1; \ldots; u^\tau]\right) \tag{2.3}$$

where $\mathbf{f}_o^\tau(\mathbf{y}^0, u)$ is computed by iterating $\tau$ times the difference equation (2.1), starting from the initial condition $\mathbf{y}^0$. As indicated in (2.3), $\mathbf{f}_o^\tau(\mathbf{y}^0, u)$ depends only on the first $\tau$ samples of $u$. The notation $\mathbf{f}_o^\tau(\mathbf{y}^0, u)$ will be used if it will not needed to highlight this dependence, the notation $\mathbf{f}_o^\tau(\mathbf{y}^0, [u^1; \ldots; u^\tau])$ will be used otherwise.
The sequence $y$ is called *solution* of the system $\mathbf{f}_o$ corresponding to the initial condition $\mathbf{y}^0$ and to the input sequence $u$. A sequence $v$ is a solution of the system $\mathbf{f}_o$ if an initial condition $\mathbf{v}^0$ and an input sequence $u \in U$ exist such that $v = \mathbf{f}_o(\mathbf{v}^0, u)$.
Let us consider a system $\mathbf{f}^{-1}$ defined by

$$u = \mathbf{f}^{-1}\left(\mathbf{u}^0, v\right). \tag{2.4}$$

where $u = [u^1, u^2, \ldots]$, $u^t \in U$, $v = [v^1, v^2, \ldots]$, $v^t \in Y$, $\mathbf{u}^0 \in U^{n_u}$. Suppose that the output $u$ of $\mathbf{f}^{-1}$ is used as the input of $\mathbf{f}_o$:

$$y = \mathbf{f}_o\left(\mathbf{y}^0, u\right) = \mathbf{f}_o\left(\mathbf{y}^0, \mathbf{f}^{-1}\left(\mathbf{u}^0, v\right)\right) \tag{2.5}$$

where $y = [y^1, y^2, \ldots]$, $y^t \in Y$, $\mathbf{y}^0 \in Y^{n_y}$. Then, $\mathbf{f}^{-1}$ is called a *right-inverse* of $\mathbf{f}_o$ and $|v^t - y^t|$ is called *inversion error* of $\mathbf{f}^{-1}$. The notion of exact right-inverse is now introduced. Let $S_o$ be the set of all solutions of $\mathbf{f}_o$.

**Definition 1** *A system* $\mathbf{f}_{ex}^{-1}$ *is an* exact right-inverse *of* $\mathbf{f}_o$ *if*

$$e^\infty\left(\mathbf{f}_{ex}^{-1}, \mathbf{f}_o, S_o\right) \doteq \sup_{\substack{\mathbf{y}^0 \in Y^{n_y} \\ \mathbf{u}^0 \in U^{n_u} \\ v \in S_o}} \lim_{t\to\infty} \left|v^t - y^t\right| = 0. \qquad \blacksquare$$

According to this definition, a system is an exact right-inverse of $\mathbf{f}_o$ if its inversion error converges to zero for all initial conditions $\mathbf{y}^0 \in Y^{n_y}$ and $\mathbf{u}^0 \in U^{n_u}$, and for all solutions of $\mathbf{f}_o$. Note that the above definition requires the existence of $\lim_{t\to\infty} |v^t - y^t|$ for every $\mathbf{y}^0 \in Y^{n_y}$, $\mathbf{u}^0 \in U^{n_u}$, and $v \in S_o$.
In many cases, deriving an exact right-inverse of $\mathbf{f}_o$ may be difficult or even impossible, e.g. when $\mathbf{f}_o$ is characterized by unstable zero dynamics. In these cases, it is of interest to derive an approximate right-inverse with fading memory, since this property, as it will be shown later, ensures a bounded inversion error.

**Definition 2** *A system* $\mathbf{f}$ *has* fading memory *if, for any* $\alpha > 0$*, a* $N > 0$ *exists such that*

$$\left|\mathbf{f}^{k+\tau}\left(\mathbf{y}^0, [q; u]\right) - \mathbf{f}^{k+\tau}\left(\widehat{\mathbf{y}}^0, [\widehat{q}; u]\right)\right| < \alpha, \quad \tau \geq N$$

*for every* $k \geq 0$*, every initial conditions* $\mathbf{y}^0, \widehat{\mathbf{y}}^0$*, and every sequences* $q = [q^1; q^2; \ldots; q^k]$, $\widehat{q} = [\widehat{q}^1; \widehat{q}^2; \ldots; \widehat{q}^k]$, $u = [u^1; u^2; \ldots; u^\tau]$*, with* $q^t, \widehat{q}^t, u^t \in U$. $\blacksquare$

Thus, the output of a fading memory system essentially depends on the recent values of the input, while the influence of far past values of the input and of initial conditions is negligible. Note that the fading memory property is commonly used in nonlinear system identification, see e.g. [27], [28].
Let us now introduce the following right-inverse system:

$$\mathbf{f}_{fm}^{-1} \doteq \arg \min_{\mathbf{f}^{-1} \in \mathbf{FM}(\gamma_{inv})} e^{\infty}\left(\mathbf{f}^{-1}, \mathbf{f}_o, S_o\right) \tag{2.6}$$

where $\mathbf{FM}\left(\gamma_{inv}\right)$ is the set of all NFIR (Nonlinear Finite Impulse Response) systems of order $m_y$ with Lipschitz continuous regression function:

$$\mathbf{FM}\left(\gamma_{inv}\right) \doteq \left\{\mathbf{f} : u^t = f\left(y^{t+1}, \ldots, y^{t-m_y}\right), f \in \mathcal{F}\left(\gamma_{inv}\right)\right\} \tag{2.7}$$

$\mathcal{F}\left(\gamma\right)$ is the set of all functions with Lipschitz constant $\gamma$, see (7), and $\gamma_{inv} < \infty$ is the Lipschitz constant of the $\mathbf{f}_{fm}^{-1}$ regression function. Note that, the existence of an inverse $\mathbf{f}^{-1}$ having finite error $e^{\infty}$ is guaranteed by the facts that $Y$ is a compact set and that $\mathbf{f}^{-1} \in \mathbf{FM}\left(\gamma_{inv}\right)$.
According to (2.6), $\mathbf{f}_{fm}^{-1}$ is the best right-inverse of $\mathbf{f}_o$ within the set $\mathbf{FM}\left(\gamma_{inv}\right)$ and, due to its NFIR form, it is guaranteed to have fading memory. In general, $\mathbf{f}_{fm}^{-1}$ cannot be explicitly computed, since solving the optimization problem (2.6) is hard. However, an approximation $\widehat{\mathbf{f}}^{-1}$ of $\mathbf{f}_{fm}^{-1}$ can be identified from a set of data generated by the system (A.1). This approximation is described in regression form as

$$u^t = \widehat{f}^{-1}\left(\mathbf{y}^{t+1}\right) \tag{2.8}$$

$$\mathbf{y}^{t+1} = [y^{t+1}; \ldots; y^{t-m_y}] \tag{2.9}$$

where $\widehat{f}^{-1}$ is an approximation of the regression function $f_{fm}^{-1}$ defining $\mathbf{f}_{fm}^{-1}$. Note that the optimization problem (2.6) is fundamental, not for the explicit evaluation of $\mathbf{f}_{fm}^{-1}$ (which is hard), but for the proper definition of $\widehat{\mathbf{f}}^{-1}$.
In Subsection 2.1.2 optimal approximate right-inverses of the form (2.9) will be derived, i.e. right-inverses ensuring a tight bound on the inversion error $|v^t - y^t|$. In order to precisely define the notion of optimal right-inverse it is convenient to introduce the Feasible Inverse System Set:

*The **Feasible Inverse System Set**, denoted by $\mathbf{FSS}_{inv}$, is the smallest system set which, on the basis of the available information, is guaranteed to contain $\mathbf{f}_{fm}^{-1}$.*

The available information consists of all prior and experimental information that can be exploited in order to identify the unknown system $\mathbf{f}_{fm}^{-1}$. In Subsections 2.1.2 and 2.1.3, this information will be described in detail for the considered specific cases. The corresponding formal definitions of $\mathbf{FSS}_{inv}$ will be given as well. Let us also introduce the following bound on the inversion error:

$$e_{inv}\left(\widehat{\mathbf{f}}^{-1}, \mathbf{f}^{-1}, \mathbf{f}, S, m\right) \doteq \sup_{\substack{\mathbf{y}^0 \in Y^{n_y} \\ \mathbf{u}^0 \in U^{n_u}}} \sup_{\substack{t > m \\ v \in S}} \left|v^t - y^t\right|$$

where $y = \mathbf{f}\left(\mathbf{y}^0, \widehat{\mathbf{f}}^{-1}\left(\mathbf{u}^0, v\right)\right)$, and $v \in S \subseteq Y^\infty \subset \mathbb{R}^\infty$. The notion of optimal right inverse can now be given.

**Definition 3** *A system* $\mathbf{f}_{opt}^{-1}$ *is an* optimal right-inverse *of* $\mathbf{f}_o$ *if*

$$EO\left(\mathbf{f}_{opt}^{-1}, m\right) \doteq \sup_{\mathbf{f}^{-1} \in \mathbf{FSS}_{inv}} e_{inv}\left(\mathbf{f}_{opt}^{-1}, \mathbf{f}^{-1}, \mathbf{f}_o, S_o, m\right) = \inf_{\widehat{\mathbf{f}}^{-1}} \sup_{\mathbf{f}^{-1} \in \mathbf{FSS}_{inv}} e_{inv}\left(\widehat{\mathbf{f}}^{-1}, \mathbf{f}^{-1}, \mathbf{f}_o, S_o, m\right)$$

*for some* $m < \infty$. $EO$ *is called* worst-case inversion error. ■

Besides the cases where an exact right-inverse of the system $\mathbf{f}_o$ is difficult to derive, there are other situations, quite common in practical applications, where an exact right-inverse cannot be found since $\mathbf{f}_o$ is unknown and has to be identified from data. In these cases, it is useful to introduce the Feasible System Set:

*The* ***Feasible System Set****, denoted by* $\mathbf{FSS}$*, is the smallest system set which, on the basis of the available information, is guaranteed to contain* $\mathbf{f}_o$.

The available information consists of all prior and experimental information that can be exploited in order to identify the unknown system $\mathbf{f}_o$. In Subsections 2.1.2 and 2.1.3, this information will be described in detail for the considered specific cases. The corresponding formal definitions of $\mathbf{FSS}$ will also be given.

According to the above definition, $\mathbf{FSS}$ provides a description of the uncertainty associated with the identification process. Clearly, right-inverses ensuring a tight bound on the inversion error $|v^t - y^t|$ for all the systems in the uncertainty set $\mathbf{FSS}$ are of interest. Such right-inverses are called robustly optimal.

**Definition 4** *A system* $\mathbf{f}_{rob}^{-1}$ *is a* robustly optimal right-inverse *of* $\mathbf{f}_o$ *if*

$$ER\left(\mathbf{f}_{rob}^{-1}, m\right) \doteq \sup_{\substack{\mathbf{f} \in \mathbf{FSS} \\ \mathbf{f}^{-1} \in \mathbf{FSS}_{inv}}} e_{inv}\left(\mathbf{f}_{rob}^{-1}, \mathbf{f}^{-1}, \mathbf{f}, S, m\right) = \inf_{\widehat{\mathbf{f}}^{-1}} \sup_{\substack{\mathbf{f} \in \mathbf{FSS} \\ \mathbf{f}^{-1} \in \mathbf{FSS}_{inv}}} e_{inv}\left(\widehat{\mathbf{f}}^{-1}, \mathbf{f}^{-1}, \mathbf{f}, S, m\right)$$

*for some* $m < \infty$. $ER$ *is called* worst-case inversion error. ■

According to Definitions 3 and 4, optimal and robustly optimal right-inverses are systems for which finite bounds on the inversion error can be guaranteed, and these bounds are the tightest ones that can be achieved on the basis of the available information.

In the Subsections 2.1.2 and 2.1.3, the following problem will be considered: if $\mathbf{f}_o$ is known derive an exact right-inverse (when possible), or an optimal right-inverse. Otherwise, when $\mathbf{f}_o$ is unknown derive a robustly optimal right-inverse of $\mathbf{f}_o$.

**Note 1** *Altough this thesis focuses on unknown systems and thus models identified from data, the inversion of known systems is a prerequisite for introducing the inversion of data based models.*

### 2.1.2 Inversion of known system

Consider a generic nonlinear system $\mathbf{f}(\mathbf{y}^0, u)$ of the form (2.1) defined by a known regression function $f$. A right-inverse of $\mathbf{f}$ can be obtained using the following algorithm.

**Inversion Algorithm 1** *Compute the right-inverse* $\mathbf{f}^{-1}(\mathbf{u}^0, y)$ *of* $\mathbf{f}(\mathbf{y}^0, u)$ *through the following regression equation:*

$$\begin{array}{l} u^t = f^{-1}\left(\mathbf{u}^{t-1}, \mathbf{y}^{t+1}\right), \quad t > 0 \\ \mathbf{y}^{t+1} = [y^{t+1}; \ldots; y^{t-n_y}] \\ \mathbf{u}^{t-1} = [u^{t-1}; \ldots; u^{t-n_u}] \end{array} \tag{2.10}$$

*where* $\mathbf{u}^0 = [0; \ldots; 0]$ *and*

$$f^{-1}\left(\mathbf{u}^{t-1}, \mathbf{y}^{t+1}\right) \doteq \max\left(\mathcal{U}\right) \tag{2.11}$$

$$\mathcal{U} = \arg\min_{\mathfrak{u} \in U} \left| y^{t+1} - f\left(\mathbf{y}^t, [\mathfrak{u}; u^{t-1}; \ldots; u^{t-n_u}]\right)\right|. \tag{2.12}$$

■

The function $f^{-1}$ is computed by means of the scalar optimization problem (2.12), which can be easily solved using any one-dimensional optimization technique, see e.g. [29], [30], [31]. The set $\mathcal{U}$ of minimizers of $|y^{t+1} - f(\mathbf{y}^t, [\mathfrak{u}; u^{t-1}; \ldots; u^{t-n_u}])|$ may be composed of several elements. The $\max(\mathcal{U})$ is performed to select a unique value, so that the function $f^{-1}$ is properly defined.

**Remark 1** *Inversion Algorithm 1 does not require the invertibility of the function* $f$ *in order to compute* $f^{-1}$. ■

For fixed $\mathbf{y}^t$ and $[u^{t-1}; \ldots; u^{t-n_u}]$, $f(\mathbf{y}^t, [\mathfrak{u}; u^{t-1}; \ldots; u^{t-n_u}])$ is a function of $\mathfrak{u}$ only, i.e. $f(\mathbf{y}^t, [\mathfrak{u}; u^{t-1}; \ldots; u^{t-n_u}]) \equiv f(\mathfrak{u})$. For any $y^{t+1}$ in the codomain of $f(\mathfrak{u})$, we have $\min_{\mathfrak{u}} |y^{t+1} - f(\mathfrak{u})| = 0$, and then

$$y^{t+1} = f\left(\mathbf{y}^t, [f^{-1}\left(\mathbf{u}^{t-1}, \mathbf{y}^{t+1}\right); u^{t-1}; \ldots; u^{t-n_u}]\right). \tag{2.13}$$

The function $f^{-1}$ is thus an exact right-inverse of the function $f$ (with respect to $u^t$). Consider now the system $\mathbf{f}_o$ defined by the regression equation (2.1) and let

$$y = \mathbf{f}_o\left(\mathbf{y}^0, u\right), \quad u = \mathbf{f}_o^{-1}\left(\mathbf{u}^0, v\right) \tag{2.14}$$

where $\mathbf{f}_o^{-1}$ is the right-inverse of $\mathbf{f}_o$ computed by means of Inversion Algorithm 1. Note that even if the regression function $f_o^{-1}$ defining $\mathbf{f}_o^{-1}$ is an exact right-inverse of the function $f_o$ defining $\mathbf{f}_o$, this does not ensure that $\mathbf{f}_o^{-1}$ is a reliable right-inverse of $\mathbf{f}_o$. Indeed, $\mathbf{f}_o^{-1}$ is described by an autoregressive equation of the form (2.10), which in general may display unstable solutions and high sensitivity to initial conditions, and this may lead to large or even unbounded inversion errors. The following result shows that this does not happen if both the system and the inverse have fading memory.

**Theorem 1** *Assume that* $\mathbf{f}_o$ *and* $\mathbf{f}_o^{-1}$ *have fading memory. Then,* $\mathbf{f}_o^{-1}$ *is an exact inverse of* $\mathbf{f}_o$.

**Proof.** This theorem is a direct consequence of the fact that $\mathbf{f}_o$ and $\mathbf{f}_o^{-1}$ have fading memory. ■

Theorem 1 assumes that the inverse $\mathbf{f}_o^{-1}$ computed by means of Inversion Algorithm 1 has fading memory. However, this assumption may not hold, e.g. in the case of unstable zero dynamics of $\mathbf{f}_o$. In order to overcome this problem, an approach based on the identification from data of the inverse $\mathbf{f}_{fm}^{-1}$ defined in (2.6) is now proposed.

The data set used for identification is the following:

$$\begin{aligned} D_{inv}^{sim} &\doteq \left\{ \left( \widetilde{\mathbf{y}}^t, \widetilde{u}_a^t \right), \quad t \in \mathcal{T} \right\} \\ \widetilde{\mathbf{y}}^t &= [y^t; \ldots; y^{t-m_y}] \\ \widetilde{u}_a^t &= f_o^{-1}(u^{t-1}, \ldots, u^{t-n_u}, y^t, \ldots, y^{t-n_y}) \end{aligned} \tag{2.15}$$

where $\mathcal{T} \doteq \{-T+1, -T+2, ...,0\}$, $(u^t, y^t)$ are obtained by simulation of the system (2.1), and $f_o^{-1}$ is computed from $f_o$ according to (2.11). Note that the direct identification of $f_o^{-1}$ from the data $(y^t, u^t)$, $t \in \mathcal{T}$, without using the values $\widetilde{u}_a^t$, may not be possible since in general the regression function $f_o$ is not invertible.
Let $y$ be the output of the system (2.1) corresponding to the input $u$ and to the initial condition $\mathbf{y}^0$. Then,

$$u = \mathbf{f}_{fm}^{-1}(y) + d_{nf} \tag{2.16}$$

where $\mathbf{f}_{fm}^{-1}(y)$ is defined in (2.6) and $d_{nf} \doteq u - \mathbf{f}_{fm}^{-1}(y)$. For large $m_y$ and $\gamma_{inv}$, $d_{nf}$ can be interpreted as the non fading memory part of $\mathbf{f}_o^{-1}$. Since $\mathbf{f}_{fm}^{-1} \in \mathbf{FM}(\gamma_{inv})$, $\gamma_{inv} < \infty$, and $Y$ and $U$ are compact sets, we have that $d_{nf}$ is tightly bounded as $\|d_{nf}\|_\infty \leq \eta$, for some $\eta < \infty$.
Consider now the system $\mathbf{f}_o$ defined by the regression equation (2.1) and let

$$y = \mathbf{f}_o\left(\mathbf{y}^0, u\right), \quad u = \mathbf{f}_a^{-1}(v)$$

where $\mathbf{f}_a^{-1}$ is a system of the form (2.9) with regression function $f_a^{-1}$. Let $f_a^{-1}$ be an approximation of $f_{fm}^{-1}$ (the regression function defining $\mathbf{f}_{fm}^{-1}$) identified from the data $D_{inv}^{sim}$ defined in (2.16) by means of the NSM method summarized in Chapter A. Let $r_I^{inv}$ be the corresponding radius of information in $l_\infty$ norm (see (9) for the definition of radius of information). Since $\mathbf{f}_o$ has fading memory, then it can be described as

$$y = \mathbf{f}_o\left(\mathbf{y}^0, u\right) = \widehat{\mathbf{f}}_o(u) + d_{trunc} \tag{2.17}$$

where $\widehat{\mathbf{f}}_o$ is an NFIR system defined by a regression equation $y^{t+1} = \widehat{f}_o(u^t, \ldots, u^{t-m_u})$, and $d_{trunc}$ is a "small" truncation error, tightly bounded as $\|d_{trunc}\|_\infty \leq \mu$, for some

$\mu < \infty$. The regression function $\widehat{f}_o$ is Lipschitz continuous, since it is obtained by a finite number of $f_o$ compositions, and $f_o$ is assumed Lipschitz continuous. Then, let $\Gamma < \infty$ be the $\ell_\infty$ Lipschitz constant of $\widehat{f}_o$, i.e. a constant such that $\left|\widehat{f}_o(\mathbf{u}) - \widehat{f}_o(\widehat{\mathbf{u}})\right| / \left\|\mathbf{u} - \widehat{\mathbf{u}}\right\|_\infty \leq \Gamma$, for any $\mathbf{u}, \widehat{\mathbf{u}} \in U^{m_u+1}$. Note that $\Gamma$ and $\mu$ can be estimated from a set of data generated by (2.1) by means of the validation analysis presented in [1].
The available information is the following:

- The system $\mathbf{f}_o$ is known and has fading memory.
- The inverse $\mathbf{f}_o^{-1}$ is known but has not fading memory. The inverse $\mathbf{f}_{fm}^{-1}$ defined in (2.6) is unknown, but it is known that $\mathbf{f}_{fm}^{-1} \in \mathbf{FM}\left(\gamma_{inv}\right)$ and $\left|\widetilde{u}_a^t - f_{fm}^{-1}\left(\widetilde{\mathbf{y}}^{t+1}\right)\right| \leq \eta$, $t \in \mathcal{T}$.

On the basis of this information, the Feasible Inverse System Set is defined as

$$\mathbf{FSS}_{inv} \doteq \left\{\mathbf{f} \in \mathbf{FM}\left(\gamma_{inv}\right) : \left|\widetilde{u}_a^t - f_{fm}^{-1}\left(\widetilde{\mathbf{y}}^{t+1}\right)\right| \leq \eta, t \in \mathcal{T}\right\}. \tag{2.18}$$

This definition allows us to present the following result.

**Theorem 2** *Assume that* $\mathbf{f}_o$ *has fading memory. Then, for any* $m_u < \infty$, $\mathbf{f}_a^{-1}$ *is an optimal right-inverse of* $\mathbf{f}_o$*, with worst-case inversion error given by*

$$EO\left(\mathbf{f}_a^{-1}, m_u\right) = \inf_{\widehat{\mathbf{f}}^{-1}} \sup_{\mathbf{f}^{-1} \in \mathbf{FSS}_{inv}} e_{inv}\left(\widehat{\mathbf{f}}^{-1}, \mathbf{f}^{-1}, \mathbf{f}_o, S_o, m_u\right) = 2\mu + \Gamma r_I^{inv} + \Gamma\eta \tag{2.19}$$

*where* $\mu, \Gamma, \eta, r_I^{inv} < \infty$*, and* $S_o$ *is the set of all solutions of* $\mathbf{f}_o$*.*

Theorem 2 can be interpreted as follows. The inversion error of the optimal right-inverse $\mathbf{f}_a^{-1}$ is tightly bounded by the sum of three terms: $2\mu$, $\Gamma r_I^{inv}$, and $\Gamma\eta$. The first one can be made arbitrarily small by choosing a sufficiently large $m_u$ in (2.17). The second one can be made arbitrarily small by improving the inverse approximation accuracy, measured by $r_I^{inv}$. This can be accomplished by using a sufficiently informative data set, i.e. a data set which gives a good exploration of the involved regressor domains (a method for assessing the degree of information of a given data set is presented in [32]). The third term accounts for the non fading memory part of $\mathbf{f}_o^{-1}$ and in general cannot be made as small as desired.

### 2.1.3 Inversion of data-based model

Assume that the system $\mathbf{f}_o$ defined by (2.1) is not known, but a set of noise-corrupted measurements $(\widetilde{\mathbf{y}}^t, \widetilde{\mathbf{u}}^t, \widetilde{y}^{t+1})$ of $(\mathbf{y}^t, \mathbf{u}^t, y^{t+1})$, is available:

$$D_{dir}^{meas} \doteq \left\{(\widetilde{\mathbf{y}}^t, \widetilde{\mathbf{u}}^t, \widetilde{y}^{t+1}), \quad t \in \mathcal{T}\right\}. \tag{2.20}$$

where $t \in \mathcal{T} \doteq \{-T+1, -T+2, \ldots, 0\}$. Assume that $\mathbf{f}_o$ has fading memory and that these measurements have been collected in an open-loop experiment.
Let $\mathbf{f}_c$ be a model of $\mathbf{f}_o$ identified from these data using the NSM method described in Appendix A, and let $r_I$ be the corresponding radius of information in $l_\infty$ norm. Let $\mathbf{f}_c^{-1}$ be the right-inverse of $\mathbf{f}_c$, computed by means of Inversion Algorithm 1. Let

$$y = \mathbf{f}_o\left(\mathbf{y}^0, u\right), \quad u = \mathbf{f}_c^{-1}\left(\mathbf{u}^0, v\right)$$

where $v \in S_c \subseteq Y^\infty \subset \mathbb{R}^\infty$, and $S_c$ is the set of all solutions of $\mathbf{f}_c$. Since $\mathbf{f}_o$ and $\mathbf{f}_c^{-1}$ have fading memory, it follows that $\mathbf{f}_o$ can be described as in (2.17), and $\mathbf{f}_c^{-1}$ can be described as

$$u = \mathbf{f}_c^{-1}\left(\mathbf{u}^0, v\right) = \widehat{\mathbf{f}}_c^{-1}(v) + \widehat{d}_{trunc} \tag{2.21}$$

where $\widehat{\mathbf{f}}_c^{-1}$ is an NFIR system defined by a regression equation $u^t = \widehat{f}_c^{-1}(v^t, \ldots, v^{t-m_y})$, and $\widehat{d}_{trunc}$ is a "small" truncation error, tightly bounded as $\left\|\widehat{d}_{trunc}\right\|_\infty \leq \mu^{inv}$, for some $\mu^{inv} < \infty$.
The available information is the following:

- The system $\mathbf{f}_o$ is unknown, but it is known that $\mathbf{f}_o \in \mathbf{FM}_o$, where $\mathbf{FM}_o$ is the set of all systems of the form (2.1) with fading memory, and that $f_o \in FFS$, where $FFS$ is the *Feasible Function Set* defined as

  $$FFS \doteq \{f \in \mathcal{F}(\gamma)\colon \left|\widetilde{y}^{t+1} - f\left(\widetilde{\mathbf{y}}^t, \widetilde{\mathbf{u}}^t\right)\right| \leq \varepsilon, t \in \mathcal{T}\}$$

  see also (A.4). Here, $\mathcal{F}(\gamma)$ is the set of all functions with Lipschitz constant $\gamma$and $\varepsilon$ is a tight bound on $|\widetilde{y}^{t+1} - f_o(\widetilde{\varphi}^t)|$, see (7).

- The inverse $\mathbf{f}_o^{-1}$ is unknown. The inverse $\mathbf{f}_c^{-1}$ is known and has fading memory.

On the basis of this information, the Feasible System Set is defined as

$$\mathbf{FSS} \doteq \left\{\mathbf{f} \in \mathbf{FM}_o : y^{t+1} = f\left(\mathbf{y}^t, \mathbf{u}^t\right), f \in FFS\right\}. \tag{2.22}$$

This definition allows us to present the following result.

**Theorem 3** *Assume that* $\mathbf{f}_o$ *and* $\mathbf{f}_c^{-1}$ *have fading memory. Then, for any* $\overline{m} \doteq \max(m_u, m_y) < \infty$, $\mathbf{f}_c^{-1}$ *is a robustly optimal right-inverse of* $\mathbf{f}_o$*, with worst-case inversion error given by*

$$ER\left(\mathbf{f}_c^{-1}, \overline{m}\right) = \inf_{\widehat{\mathbf{f}}^{-1}} \sup_{\mathbf{f} \in \mathbf{FSS}} e_{inv}\left(\widehat{\mathbf{f}}^{-1}, \mathbf{f}_c^{-1}, \mathbf{f}, S_c, \overline{m}\right) = 2\mu + 2\Gamma\mu^{inv} + \Lambda r_I \tag{2.23}$$

*where* $\mu, \mu^{inv}, \Lambda, \Gamma, r_I < \infty$*, and* $S_c$ *is the set of all solutions of* $\mathbf{f}_c$*.*

Theorem 3 can be interpreted as follows. The inversion error of the robustly optimal right-inverse $\mathbf{f}_c^{-1}$ is tightly bounded by the sum of three terms: $2\mu$, $2\Gamma\mu^{inv}$, and $\Lambda r_I$. The first two terms can be made arbitrarily small by choosing sufficiently large $m_u$ and $m_y$ in (2.17) and (2.21). The third one can be made arbitrarily small by improving the approximation accuracy, measured by $r_I$. This can be accomplished by using a sufficiently informative data set (see [32]).
Theorem 3 assumes that $\mathbf{f}_c^{-1}$ has fading memory, but this assumption may not always hold. In order to overcome this problem, an approach based on the identification from data of a robustly optimal inverse is now proposed.
The data set used for identification is the following:

$$\begin{array}{c} D_{inv}^{meas} \doteq \{(\widetilde{\mathbf{y}}^{t+1}, \widetilde{u}_a^t), \quad t \in \mathcal{T}\} \\ \widetilde{\mathbf{y}}^{t+1} = [\widetilde{y}^{t+1}; \ldots; \widetilde{y}^{t-m_y}] \\ \widetilde{u}_a^t = f_c^{-1}(\widetilde{u}^{t-1}, \ldots, \widetilde{u}^{t-n_u}, \widetilde{y}^{t+1}, \ldots, \widetilde{y}^{t-n_y}) \end{array} \tag{2.24}$$

where $\mathcal{T} \doteq \{-T+1, -T+2, ...,0\}$, $(\widetilde{u}^t, \widetilde{y}^t)$ are noise-corrupted measurements of $(u^t, y^t)$, $f_c^{-1}$ is computed from $f_c$ according to (2.11), and $f_c$ is the regression function of the model $\mathbf{f}_c$.
Consider now the system $\mathbf{f}_o$ defined by the regression equation (2.1) and let

$$y = \mathbf{f}_o\left(\mathbf{y}^0, u\right), \quad u = \mathbf{f}_a^{-1}\left(v\right)$$

where $\mathbf{f}_a^{-1}$ is a system of the form (2.9) with regression function $f_a^{-1}$. Let $f_a^{-1}$ be an inverse identified from the data $D_{inv}^{meas}$ defined in (2.24) by means of the NSM method summarized in Appendix A. $f_a^{-1}$ is an approximation of $f_{fm}^{-1}$, the regression function of $\mathbf{f}_{fm}^{-1}$, where $\mathbf{f}_{fm}^{-1}$ is defined in (2.6), with $\mathbf{f}_o \to \mathbf{f}_c$, $S_o \to S_c$. Let $r_I^{inv}$ be the radius of information in $L_\infty$ norm associated to $f_a^{-1}$ (see (9) for the definition of radius of information). Consider that $\mathbf{f}_o$ can be described as in (2.17).
The available information is the following:

- The system $\mathbf{f}_o$ is unknown, but it is known that $\mathbf{f}_o \in \mathbf{FM}_o$ with $f_o \in FFS$.
- The inverse $\mathbf{f}_o^{-1}$ is unknown. The inverse $\mathbf{f}_c^{-1}$ is known but has not fading memory. The inverse $\mathbf{f}_{fm}^{-1}$, defined in (2.6) with $\mathbf{f}_o \to \mathbf{f}_c$, $S_o \to S_c$, is unknown. It is known that $\mathbf{f}_{fm}^{-1} \in \mathbf{FM}\left(\gamma_{inv}\right)$ and $\left|\widetilde{u}_a^t - f_{fm}^{-1}\left(\widetilde{\mathbf{y}}^{t+1}\right)\right| \leq \eta$, $t \in \mathcal{T}$.

On the basis of this information, the Feasible System Set is given by (2.22), the Feasible Inverse System Set is given by (2.18).

**Theorem 4** *Assume that $\mathbf{f}_o$ has fading memory. Then, for any $\overline{m} \doteq \max\left(m_u, m_y\right) < \infty$, $\mathbf{f}_a^{-1}$ is a robustly optimal right-inverse of $\mathbf{f}_o$, with worst-case inversion error given by*

$$ER\left(\mathbf{f}_a^{-1}, \overline{m}\right) = \inf_{\widehat{\mathbf{f}}^{-1}} \sup_{\substack{\mathbf{f} \in \mathbf{FSS} \\ \mathbf{f}^{-1} \in \mathbf{FSS}_{inv}}} e_{inv}\left(\widehat{\mathbf{f}}^{-1}, \mathbf{f}^{-1}, \mathbf{f}, S_c, \overline{m}\right) = 2\mu + \Lambda r_I + \Gamma r_I^{inv} + \Gamma\eta \tag{2.25}$$

*where $\mu, \Lambda, \Gamma, \eta, r_I, r_I^{inv} < \infty$, and $S_c$ is the set of all solutions of $\mathbf{f}_c$.*

Theorem 4 can be interpreted as follows. The inversion error of the robustly optimal right-inverse $\mathbf{f}_a^{-1}$ is tightly bounded by the sum of four terms: $2\mu$, $\Lambda r_I$, $\Gamma r_I^{inv}$, and $\Gamma\eta$. The first one can be made arbitrarily small by choosing sufficiently large $m_u$ and $m_y$ in (2.17) and (2.9). The second and the third terms can be made arbitrarily small by improving the approximation accuracies, measured by $r_I$ and $r_I^{inv}$. This can be accomplished by using a sufficiently informative data set (see [32]). The fourth one accounts for the non fading memory part of $\mathbf{f}_o^{-1}$ and in general cannot be made as small as desired.

**Remark 2** *Consider a system with non-zero relative degree:*

$$y^t = f_o\left(\mathbf{y}^{t-1}, \mathbf{u}^{t-k}\right), \quad k > 0.$$

*The proposed inversion methods can be applied also in this case without significant modifications, using the input signal $q^t \doteq u^{t-k}$. This clearly leads to a delay in the inversion process, but this delay cannot be avoided using only the information considered here.* ■

**Remark 3** *The approximate inverse $\mathbf{f}_a^{-1}$ can be used instead of $\mathbf{f}_o^{-1}$ or $\mathbf{f}_c^{-1}$ also when these exact inverses have fading memory, in order to improve the computation efficiency in on-line applications.* ■

## 2.2 Set Membership Internal Model Control

In this Section, the inversion method from data introduced in Section 2.1.3 is used to design a robust Set Membership Internal Model Control (SIMC), see [33]).
Consider the control scheme in Figure 2.1, $\mathbf{f}_o$ is the unknown plant to be controlled, $\mathbf{f}_c$ is a model of $\mathbf{f}_o$ and $\mathbf{Q}$ is the controller. The feedback system $\mathbf{T}$ having input $(r, w)$ and output $y_w$ is defined by

$$y_w = \mathbf{T}(r, w).$$

From Figure 2.1, we have that

$$\begin{aligned} y_w = w + y = w + \mathbf{f}_o(u) = w + \mathbf{f}_o\mathbf{Q}(v) = \\ = w + \mathbf{f}_o(\mathbf{Q}(r - w - \zeta)) \end{aligned} \tag{2.26}$$

where $\zeta = y - \widehat{y} = \mathbf{f}_o(u) - \mathbf{f}_c(u)$. This relationship shows that, if $\mathbf{f}_c = \mathbf{f}_o$ and $\mathbf{Q} = \mathbf{f}_c^{-1}$, then the perfect control $y_w = r$ is achieved, i.e. exact tracking and total disturbance rejection.
Clearly, the perfect control cannot be obtained in practical applications, due to the facts that only approximate models can actually be identified from a finite set of data and that exact inversion may not be possible. However, a robust SIMC control can be designed, able to give stability and a tight bound on the *tracking error* $|r^t - y_w^t|$ for all the plants $\mathbf{f}_o \in \mathbf{FSS}$.
The following SIMC control scheme is proposed:

- The plant $\mathbf{f}_o$ is represented according to (2.17):

$$y^t = \widehat{f}_o\left(\mathbf{u}^t\right) + d^t_{trunc} \tag{2.27}$$

  where $\mathbf{u}^t = [u^t; \ldots; u^{t-m_u}]$ and $d_{trunc}$ is a "small" truncation error accounting for the initial condition $\mathbf{y}^0$ and for $u^k$, $k < t - m_u$. This truncation error is tightly bounded as $\|d_{trunc}\|_\infty \leq \mu$, for some $\mu < \infty$.

- The model $\mathbf{f}_c$ of $\mathbf{f}_o$ is identified from a set of data $(\widetilde{y}^t, \widetilde{u}^t)$, $t \in \mathcal{T}$, by means of the nonlinear SM method summarized in Appendix A. This model is given by

$$\widehat{y}^t = f_c\left(\mathbf{u}^t\right)$$

  where $f_c$ has Lipschitz constant $\Gamma$. Let us also define $\gamma_{res}$ as the Lipschitz constant of $\widehat{f}_o - f_c$. Note that $\gamma_{res}$ can be estimated by means of the validation procedure introduced in [1].

- The controller is $\mathbf{Q} = \mathbf{f}_a^{-1}$, where $\mathbf{f}_a^{-1}$ is an inverse of $\mathbf{f}_o$ identified from the data $D^{meas}_{inv}$ defined in (2.24), by means of the method of Subsection 2.1.3. $\mathbf{f}_a^{-1}$ is represented in NFIR form as

$$u^t = f_a^{-1}\left(\mathbf{v}^{t-1}\right)$$

  where $\mathbf{v}^{t-1} = [v^{t-1}; \ldots; v^{t-m_v}]$. Note that a delay between $v$ and $u$ has been inserted in this controller in order to avoid algebraic loops in the SIMC control structure. The Lipschitz constant $\gamma_{inv}$ of $f_a^{-1}$ is chosen such that

$$\gamma_{inv}\gamma_{res} < 1. \tag{2.28}$$

Let $\eta$ be the bound on the non fading memory part of $\mathbf{f}_c^{-1}$ (the exact inverse of $\mathbf{f}_c$). Let $r_I^{inv}$ be the radius of information associated to $f_a^{-1}$.
The case $\mathbf{Q} = \mathbf{f}_a^{-1}\mathbf{G}$, where $\mathbf{G}$ is a linear filter with unitary gain which can be inserted to improve the dynamic properties of the control system, can be treated as a trivial extension.
In order to evaluate the robustness of this control system, consider that the available information is the following:

- The system $\mathbf{f}_o$ is unknown, but it is known that $\mathbf{f}_o \in \mathbf{FM}_o$ with $f_o \in FFS$.
- The model $\mathbf{f}_c$ is known.
- The inverse $\mathbf{f}_o^{-1}$ is unknown. The inverse $\mathbf{f}_c^{-1}$ is known but, in general, it has not fading memory. The inverse $\mathbf{f}_{fm}^{-1}$, defined in (2.6) with $\mathbf{f}_o \to \mathbf{f}_c$, $S_o \to S_c$, is unknown. It is known that $\mathbf{f}_{fm}^{-1} \in \mathbf{FM}\left(\gamma_{inv}\right)$ and $\left|\widetilde{u}_a^t - f_{fm}^{-1}\left(\widetilde{\mathbf{y}}^{t+1}\right)\right| \leq \eta$, $t \in \mathcal{T}$.

On the basis of this information, the Feasible System Set is given by (2.22), the Feasible Inverse System Set is given by (2.18).

### 2.2.1 Robustness analysis

Let us now introduce the following stability notion (see e.g. [34]).

**Definition 5** *A nonlinear system* $\mathbf{f}$ *is finite-gain* $\ell_\infty$ *stable (with bias) if finite and non-negative* $\lambda$ *and* $\beta$ *exist such that*

$$\left\|\mathbf{f}\left(u\right)\right\|_\infty \leq \lambda \left\|u\right\|_\infty + \beta$$

*for every* $u = [u^1; u^2; \ldots] \in \ell_\infty$. ■

Let us define the following tight bound on the tracking error:

$$e_{nimc}\left(\widehat{\mathbf{Q}}, \widehat{\mathbf{f}}, \mathbf{f}^{-1}, \mathbf{f}, S, m\right) \doteq \sup_{\mathbf{y}^0 \in Y^{n_y}} \sup_{\substack{t>m \\ r\in S}} \left|r^t - y_w^t\right|$$

where $r \in S \subseteq Y^\infty \subset \mathbb{R}^\infty$ and $S$ is the set of all solutions of $\mathbf{f}_c$. A robust SIMC controller is defined as follows.

**Definition 6** *The SIMC control system is said* robust *if the feedback system* $y_w = \mathbf{T}(r, w)$ *is finite-gain* $\ell_\infty$ *stable for all* $\mathbf{f}_o \in \mathbf{FSS}$*, and*

$$EI\left(\mathbf{Q}, \mathbf{f}_c, m\right) \doteq \sup_{\substack{\mathbf{f}\in\mathbf{FSS} \\ \mathbf{f}^{-1}\in\mathbf{FSS}_{inv}}} e_{nimc}\left(\mathbf{Q}, \mathbf{f}_c, \mathbf{f}^{-1}, \mathbf{f}, S, m\right) = \inf_{\widehat{\mathbf{Q}},\widehat{\mathbf{f}}} \sup_{\substack{\mathbf{f}\in\mathbf{FSS} \\ \mathbf{f}^{-1}\in\mathbf{FSS}_{inv}}} e_{nimc}\left(\widehat{\mathbf{Q}}, \widehat{\mathbf{f}}, \mathbf{f}^{-1}, \mathbf{f}, S, m\right)$$

*for some* $m < \infty$. $EI\left(\mathbf{Q}, \mathbf{f}_c, m\right)$ *is called* worst-case tracking error. ■

**Theorem 5** *Consider the SIMC control system in Figure 2.1, where* $\mathbf{f}_c$ *and* $\mathbf{Q}$ *are the model and controller described above.*
*(i) The SIMC control system is robust.*
*(ii) For any* $\overline{m} \doteq \max\left(m_u, m_v\right) < \infty$*, the worst-case tracking error is given by*

$$EI\left(\mathbf{Q}, \mathbf{f}_c, \overline{m}\right) = \inf_{\widehat{\mathbf{Q}},\widehat{\mathbf{f}}} \sup_{\substack{\mathbf{f}\in\mathbf{FSS} \\ \mathbf{f}^{-1}\in\mathbf{FSS}_{inv}}} e_{nimc}\left(\widehat{\mathbf{Q}}, \widehat{\mathbf{f}}, \mathbf{f}^{-1}, \mathbf{f}, S, \overline{m}\right) = 2\mu + \Gamma r_I^{inv} + \Gamma\eta \quad (2.29)$$

*where* $\mu, \Gamma, \eta, r_I^{inv} < \infty$*, and* $S_c$ *is the set of all solutions of* $\mathbf{f}_c$.

**Proof.** Since $\gamma_{res}$ is the Lipschitz constant of $\Delta = \widehat{f_o} - f_c$, we have that

$$\left|\Delta\left(\mathbf{u}^t\right) - \Delta\left(\mathbf{0}\right)\right| \leq \gamma_{res}\left\|\mathbf{u}^t - \mathbf{0}\right\|_\infty, \quad \forall t$$

Then,

$$\left|\Delta\left(\mathbf{u}^t\right)\right| = \left|\widehat{f_o}\left(\mathbf{u}^t\right) - f_c\left(\mathbf{u}^t\right)\right| \leq \gamma_{res}\left\|\mathbf{u}^t\right\|_\infty + \left|\Delta\left(\mathbf{0}\right)\right|, \quad \forall t.$$

Since $\widehat{\mathbf{f}}_o$ and $\mathbf{f}_c$ are NFIR systems, this implies that

$$\left\|\mathbf{f}_o(u) - \mathbf{f}_c(u)\right\|_\infty \leq \left\|\widehat{\mathbf{f}}_o(u) - \mathbf{f}_c(u)\right\|_\infty + \mu \leq \gamma_{res}\left\|u\right\|_\infty + \left|\Delta(\mathbf{0})\right| + \mu. \tag{2.30}$$

Following similar argumentations, it can be shown that

$$\left\|\mathbf{f}_a^{-1}(v)\right\|_\infty \leq \gamma_{inv}\left\|v\right\|_\infty + \left|f_a(\mathbf{0})\right|, \tag{2.31}$$

$$\left\|\mathbf{f}_o(u)\right\|_\infty \leq \Gamma\left\|u\right\|_\infty + \left|\widehat{f}_o(\mathbf{0})\right| + 2\mu. \tag{2.32}$$

Consider now the feedback system in Figure 2.2, which is equivalent to the one in Figure 2.1. Inequalities (2.30), (2.31) and (2.28) imply that the stability condition $\gamma_{res}\gamma_{inv} < 1$ of the small gain theorem is satisfied, see e.g. [34]. Consequently, the feedback system $v = \widehat{\mathbf{T}}(r, w)$ is finite-gain $\ell_\infty$ stable.
From this result, and from inequalities (2.31) and (2.32), it follows that the feedback system $y_w = \mathbf{T}(r, w)$ is also finite-gain $\ell_\infty$ stable. This holds for all $\mathbf{f}_o \in \mathbf{FSS}$, thus proving claim (i).
Claim (ii) can be proven considering that, as it can be easily seen in Figure 2.1,

$$r - y_w = v - \widehat{y}. \tag{2.33}$$

Note that $\widehat{y} = \mathbf{f}_c(\mathbf{f}_a^{-1}(v))$, where $\mathbf{f}_a^{-1}$ is the approximated inverse of $\mathbf{f}_c$. Then, according to Theorem 2,

$$\left|v^t - y^t\right| \leq 2\mu + \Gamma r_I^{inv} + \Gamma\eta \tag{2.34}$$

for any $\overline{m} \doteq \max(m_u, m_v) < \infty$. As shown in the proof of Theorem 2 the bound (2.34) is tight. Claim (ii) follows from (2.33). ■

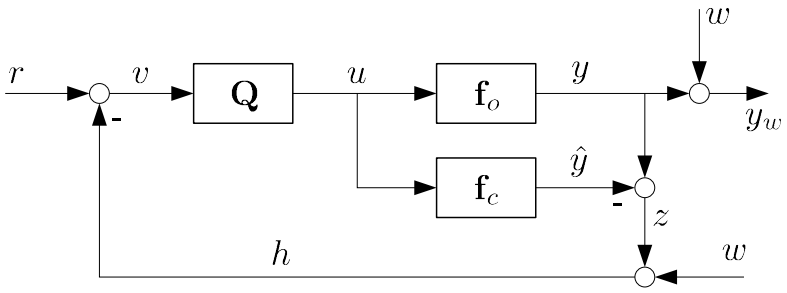


Figure 2.2. Feedback system.

Theorem 5 shows that the tracking error is bounded by the sum three terms: $2\mu$, $\Gamma r_I^{inv}$, and $\Gamma\eta$. The first one can be made arbitrarily small if sufficiently large $m_u$ and $m_y$ are chosen. The second one can be reduced by using a SM optimal model $\mathbf{f}_c$ of $\mathbf{f}_o$. In this way, an arbitrarily small value of $\gamma_{res}$ can be obtained (it can be proven that $\gamma_{res} \leq \Gamma$)

and thus a "large" value of $\gamma_{inv}$ can be used to design $\mathbf{f}_a^{-1}$, see (2.28). The larger is $\gamma_{inv}$, the larger is the set $\mathcal{F}(\gamma_{inv})$, the smaller is $\mathbf{f}_c^{-1}(\mathbf{u}^0, y) - \mathbf{f}_{fm}^{-1}(y)$, the smaller is $\eta$. Note that, in some cases, $\eta$ cannot be reduced to 0 even using a "large" $\gamma_{inv}$. In these cases, $\eta$ limits the accuracy performance that can be achieved by an SIMC approach. A similar situation happens in linear IMC, when the plant to control has some unstable zero and cannot be fully inverted, [35]. The third one can be made "small" deriving an accurate approximation $\mathbf{f}_a^{-1}$ of $\mathbf{f}_{fm}^{-1}$, so that $r_I^{inv}$ is "small". This requirement can be met by using a sufficiently informative data set, i.e. a data set which gives a good exploration of $f_c^{-1}$ domain (see [32]).

**Remark 4** *The present SIMC control scheme takes advantage of the output feedback and gives better tracking/inversion accuracy with respect to the inversion schemes presented in Section 2.1, where feedback is not used. Indeed, the SIMC tracking error bound (2.29), obtained not using the knowledge of the system* $\mathbf{f}_o$*, is the same as the one given in Theorem 2, where* $\mathbf{f}_o$ *is assumed to be known. The tracking error bound (2.29) is smaller than the one provided in Theorem 4, which has been derived on the basis of the same information used here. In any case the SIMC control scheme allows for noise attenuation (see the example in Subsection 2.3), a task that cannot be accomplished using only open loop inversion. On the other hand, it must be noted that output feedback is not always practicable.* ■

**Remark 5** *Since data are supposed to be collected in open loop experiments, the plant must be stable. In principle, the case of unstable plants can be treated by means of closed loop identification techniques. However, closed-loop identification of unstable nonlinear systems is an open research area which goes behind the scopes of this work.* ■

**Remark 6** *In most of the papers available in the literature, the SIMC control system is designed and its stability is empirically verified a posteriori. On the contrary, the SIMC technique proposed here allows us to impose closed loop stability in the design phase.* ■

## 2.3 Vehicle yaw control application

In this Section, the proposed SIMC design approach is employed to develop a vehicle yaw control.

Yaw stability control systems have been introduced in order to significantly enhance safety and handling properties of vehicles (see e.g. [36] and [37]) by modifying their passive dynamic behavior using suitable control structures and actuation devices. In particular, in this paper, a vehicle equipped with a front steer-by-wire actuator, based on a classical rack and pinion steering system (see e.g. [38]) is considered.

In the considered application, the objective is the control of the vehicle yaw rate $\dot{\psi}(t)$ in

order to improve its handling and understeer performance by suitably acting on the steering angle $\delta(t)$ by means of a front steer by wire actuation device. Referring to the SIMC structure of Figure 2.1, the variable to control $y$ is thus the yaw rate $\dot{\psi}$. The reference $r$ is the desired yaw rate sequence. The output $y_w$ is the measured yaw rate. The control input $u$ is the steering angle $\delta$.
In this example, it is assumed that a vehicle model is not available and the SIMC controller is designed directly from data. To this end, a set of about $7000$ values of $\dot{\psi}$ and $\delta$ have been generated simulating the nonlinear vehicle single track model described in [37], and imposing a suitably designed handwheel course composed of quick ramps and constant intervals plus a random signal with a sampling time of $0.05$ s. The values of $\dot{\psi}$ have been corrupted by a white noise having a noise-to-signal standard deviation ratio of $3\%$.
From this data set, a NFIR model $\mathbf{f}_c$ of the vehicle has been identified using the SM methodology described in Appendix A. The model is described in regression form by

$$\dot{\psi}^{t+1} = f_c(\delta^t, \ldots, \delta^{t-m_u}) \tag{2.35}$$

where a regressor length $m_u = 30$ has been considered.
The $\ell_\infty$ gain (see (2.30)) of the model error has been evaluated as

$$\gamma_{res} = 0.056.$$

Then, the inverse model $\mathbf{f}_c^{-1}$ computed according to Inversion Algorithm 1 has been implemented:

$$\delta^t = f_c^{-1}(\dot{\psi}^{t+1}, \delta^{t-1}, \ldots, \delta^{t-m_u}) \tag{2.36}$$

However, this inverse model displayed an unstable behavior in some maneuvers, indicating that the fading memory assumption required by Theorem 3 was not satisfied. Therefore, an approximation $\mathbf{f}_a^{-1}$ has been identified, described in regression form by

$$\delta^t = f_a^{-1}(\dot{\psi}^{t+1}, \ldots, \dot{\psi}^{t-m_u})$$

for which the fading memory property is guaranteed by definition. The approximation $f_a^{-1}$ has been obtained by means of the NSM method, using the following data set: $\widetilde{\varphi}^t = [\tilde{\dot{\psi}}^t, \tilde{\delta}^{t-1}, \ldots, \tilde{\delta}^{t-n_u}]$, $\tilde{y}^{t+1} = f_c^{-1}(\widetilde{\varphi}^t)$, $t \in \mathcal{T}$ where $\tilde{\dot{\psi}}^t$ and $\tilde{\delta}^t$ are the measured values of $\dot{\psi}^t$ and $\delta^t$.
The controller has been chosen as $\mathbf{Q} = \mathbf{f}_a^{-1}\mathbf{G}$, where the filter $\mathbf{G}$ is the linear second order filter $\mathbf{G}(s) = 1/(1 + s/2)^2$, inserted in order to improve the dynamic properties of the feedback system.
In order to evaluate the SIMC control structure performance, simulations have been performed using the nonlinear single track model considered in the identification to describe the vehicle dynamics. In Figure 2.3 the results for a 40° step steer maneuver performed at 100 km/h are shown. In particular, the course of the yaw rate $\dot{\psi}(t)$ for the controlled vehicle is reported (solid line) and compared with the desired behavior (dashed line) and

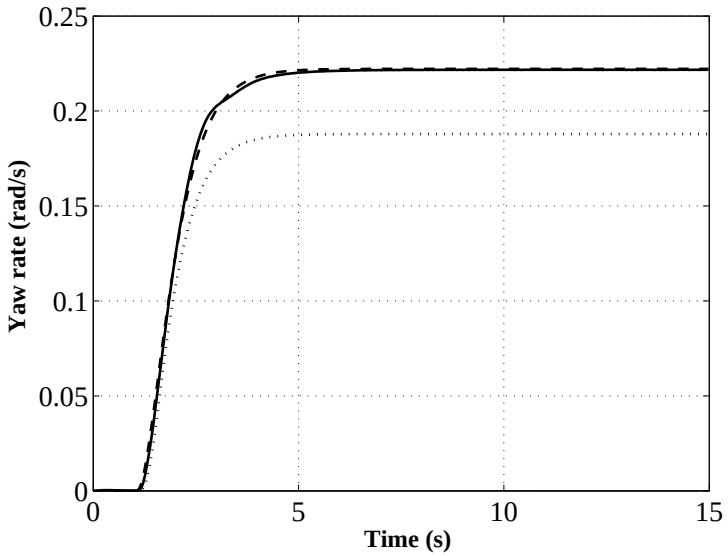


Figure 2.3. Step steer maneuver. Dashed line: reference. Solid line: controlled vehicle (SIMC). Dotted line: uncontrolled vehicle.

with the uncontrolled one (dotted line). From Figure 2.3, it can be seen that zero steady state error is achieved and good transient behavior performance is obtained in terms of readiness and damping.

The performance of the SIMC control has also been tested in the presence of a strong disturbance. A simulation has been performed, where the steering angle $\delta$ has been kept null, and a bump disturbance $w$ of amplitude $0.033$ rad/s lasting $3$ s has been introduced. This situation may happen for example when the vehicle is traveling on a motorway and a blast of wind comes, giving a yaw rate deviation of $0.033$ rad/s in the absence of a control action. The result of this simulation is shown in Figure 2.4. The solid and dotted line represent, respectively, the yaw rate of controlled and uncontrolled vehicle. It can be noted that a significant disturbance attenuation is achieved by the SIMC control. In particular, the yaw rate deviation is reduced by about $66\%$ with respect to the uncontrolled vehicle.

Finally, a comparison with the standard linear IMC design is presented. In order to make proper and significant such a comparison, a control design from data approach has been followed as done in the SIMC case. In particular, the same data set used to obtain the model (2.35) has been employed to identify an ARX model by suitably choosing its structure in order to minimize the $\ell_\infty$ norm of the model error. The application of this procedure gives rise to a fourth order minimum phase system described by the transfer function $M_{\dot{\psi},\delta}(z)$ between the steering angle $\delta$ and the yaw rate $\dot{\psi}$. The $\ell_\infty$ gain of the model error is given by

$$\gamma_{res,lin} = 0.11.$$

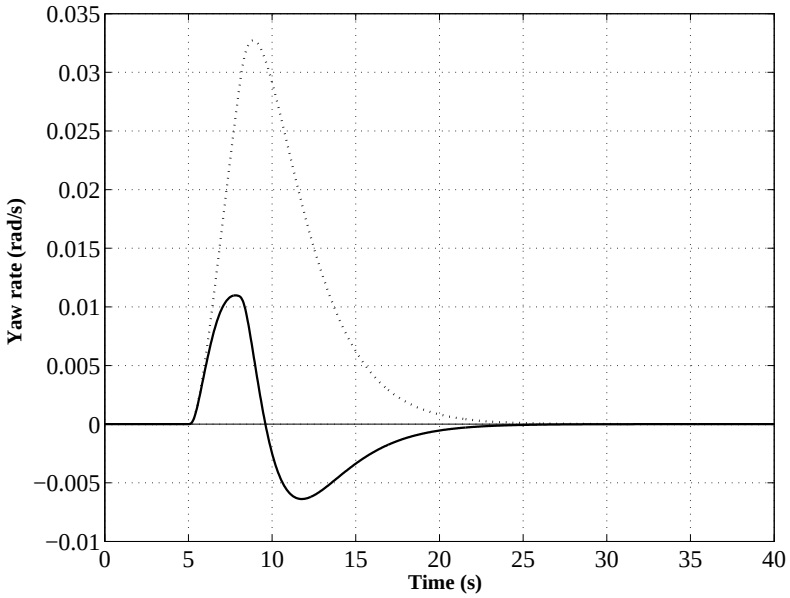


Figure 2.4. Bump disturbance. Thin line: reference yaw rate. Dotted line: yaw rate of the uncontrolled vehicle. Solid line: yaw rate of the controlled vehicle.

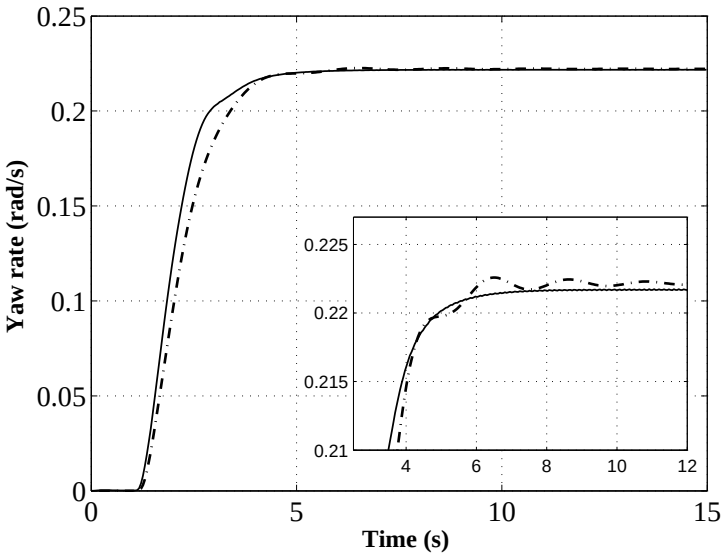


Figure 2.5. Step steer maneuver. Solid line: controlled vehicle (SIMC). Dash-dot line: controlled vehicle (linear IMC)

As expected, the linear model gives rise to a less accurate result in terms of modeling error. The linear IMC controller $Q(s)$ has been obtained through the standard procedure (see e.g. [39]) described by

$$Q(s) = G(s)M_{\dot{\psi},\delta}^{-1}(s)$$

where $M_{\dot{\psi},\delta}(s)$ is the continuous time counterpart of $M_{\dot{\psi},\delta}(z)$ and $G(s)$ is a strictly proper transfer function which describes the desired performance. In particular, in order to make a realistic comparison $G(s)$ has been chosen equal to the filter $G(s) = \mathbf{G}(s) = 1/(1 + s/2)^2$ employed in the SIMC design.

In Figure 2.5 the performance comparison between the SIMC and IMC designs is reported for the 40° step steer maneuver performed at 100 km/h previously considered. In particular, in Figure 2.5 the yaw rate behavior obtained by the nonlinear controller is reported (solid line) together with the one achieved by the linear controller (dash-dot line). It can be seen that the SIMC design shows better performance than IMC both in terms of response speed and damping properties and similar characteristics in terms of steady state accuracy.

# Chapter 3

# Set Membership Model Predictive Control

## 3.1 Nonlinear Model Predictive Control

Consider the following nonlinear discrete–time state space model:

$$x_{t+1} = g(x_t, u_t) \qquad t \in \mathbb{Z} \tag{3.1}$$

where $g : \mathbb{R}^{m+1} \to \mathbb{R}^m$ is a nonlinear function, $u_t \in \mathbb{R}$ and $x_t \in \mathbb{R}^m$ are the system input and state respectively.
Assume that the problem is to regulate the system state to the origin under some input and state constraints. By defining the prediction horizon $N_p$ and the control horizon $N_c \leq N_p$, it is possible to define a cost function $J_t(U, x_{t|t})$ of the form

$$J_t(U, x_{t|t}) = \sum_{j=0}^{N_p-1} L(x_{t+j|t}, u_{t+j|t}) + \Psi(x_{t+Np|t}) \tag{3.2}$$

The per-stage cost function $L(\cdot)$ and the terminal state cost $\Psi(\cdot)$ are suitably chosen and tuned according to the desired control performance. $L(\cdot)$ is typically continuous and convex in its arguments. The cost function $J_t(\cdot)$ is evaluated on the basis of the predicted state values $x_{t+j|t}$, $j \in [1, N_p]$ obtained using the model (3.1), the input sequence $U_t = [u_{t|t} \dots u_{t+N_c-1|t}]$ and the initial state $x_{t|t} = x_t$. The sequence $U_t$ is a decision variable in the problem, while the remaining input values $[u_{t+N_c|t}, ..., u_{t+N_p-1|t}]$ can be computed according to different strategies [40], [41].
The Nonlinear Model Predictive Control (NMPC) control is computed according to the Receding Horizon (RH) strategy:

1. At time instant $t$, get the state $x_{t|t} \doteq x_t$

2. Solve the optimization problem

$$\min_{U} \quad J_t(U, x_{t|t}) \tag{3.3a}$$

subject to

$$x_{t+j+1|t} = g(x_{t+j|t}, u_{t+j|t}),\ j \in [0, Np-1] \tag{3.3b}$$

$$x_{t+j|t} \in \mathbb{X}, j \in [1, N_p] \tag{3.3c}$$

$$u_{t+k|t} \in \mathbb{U}, k \in [0, N_p - 1] \tag{3.3d}$$

$$stabilizing\ constraints \tag{3.3e}$$

where the input and state constraints are represented by a set $\mathbb{X} \subseteq \mathbb{R}^m$ and a compact set $\mathbb{U} \subseteq \mathbb{R}$, both containing the origin in their interiors; denote with $U_t^* = [u_{t|t}^* \dots u_{t+N_c-1|t}^*]$ the minimizer of (3.3)

3. Apply the first element of $U_t^*$ as the actual control action $u_t = u_{t|t}^*$.

4. Repeat the whole procedure at the next sampling time $t+1$.

Possible additional *stabilizing constraints* (e.g. state contraction, terminal set) can be included in (3.3e) in order to ensure stability of the controlled system.
A model derived from physical laws is usually employed as model of the plant (3.1) to be controlled. In this work, instead, an approximated model derived from data by means a Nonlinear Set Membership (NSM) methodology is used.

## 3.2 Set Membership Model Predictive Control

Let consider the plant $f_o$ (2.1) and its NSM model $f_c$ (A.8) identified from data by means the NSM technique (see Appendix A). $f_o$ and $f_c$ can be re-written in state space form, by using $u_t$ as input value and $x_t$ as pseudo–state:

$$\begin{aligned} x_t &\doteq [y_t \cdots y_{t-n_y} u_{t-1} \cdots u_{t-n_u}] \\ &= [x_t^{(1)} \cdots x_t^{(n_y+1)} x_t^{(n_y+2)} \cdots x_t^{(n_y+n_u+1)}] \in \mathbb{R}^{n-1} \end{aligned} \tag{3.4}$$

The state space equation of the plant (2.1) results to be

$$x_{t+1} = f_o^{SS}(x_t, u_t) \tag{3.5}$$

where $f_o^{SS} : \mathbb{R}^n \to \mathbb{R}^{n-1}$ is defined as:

$$f_o^{SS}(x_t, u_t) \doteq \begin{bmatrix} f_o(x_t^{(1)}, \ldots, x_t^{(n_y+1)}, u_t, x_t^{(n_y+2)}, \ldots, x_t^{(n_y+n_u+1)}) \\ x_t^{(1)} \\ \vdots \\ x_t^{(n_y)} \\ u_t \\ \vdots \\ x_t^{(n_y+n_u)} \end{bmatrix} \tag{3.6}$$

Note that since $f_o(\cdot)$ is assumed to be Lipschitz continuous with constant $\gamma$, function $f_o^{SS}(\cdot)$ in (3.6) results to be Lipschitz continuous too, with constant $L_0 = \sqrt{1+\gamma^2}$:

$$\begin{aligned} & ||f_o^{SS}(x_1, u_1) - f_o^{SS}(x_2, u_2)||_2^2 = \\ = \; & ||f_o(\cdot) - f_o(\cdot)||_2^2 + ||x_1^{(1)} - x_2^{(1)}||_2^2 + \ldots + ||u_1 - u_2||_2^2 + \ldots + ||x_1^{(n_u+n_y)} - x_2^{(n_u+n_y)}||_2^2 = \\ \leq \; & (1+\gamma^2)\left(||x_1^{(1)} - x_2^{(1)}||_2^2 + \ldots + ||u_1 - u_2||_2^2 + \ldots + ||x_1^{(n_u+n_y)} - x_2^{(n_u+n_y)}||_2^2\right) = \\ = \; & (1+\gamma^2)\left(||x_1 - x_2||_2^2 + ||u_1 - u_2||_2^2\right) = L_0^2\left(||x_1 - x_2||_2^2 + ||u_1 - u_2||_2^2\right) \end{aligned} \tag{3.7}$$

Applying the same procedure to the model $f_c$ (A.8) leads to the state space description

$$x_{t+1} = f_c^{SS}(x_t, u_t) \tag{3.8}$$

where

$$f_c^{SS}(x_t, u_t) \doteq \begin{bmatrix} f_c(x_t^{(1)}, \ldots, x_t^{(n_y+1)}, u_t, x_t^{(n_y+2)}, \ldots, x_t^{(n_y+n_u+1)}) \\ x_t^{(1)} \\ \vdots \\ x_t^{(n_y)} \\ u_t \\ \vdots \\ x_t^{(n_y+n_u)} \end{bmatrix} \tag{3.9}$$

By construction, taking into account Theorem 8, function $f_c^{SS}(\cdot)$ in (3.9) is also Lipschitz continuous with constant $L_c = \sqrt{1+\gamma^2}$ (i.e. $L_c = L_0$).
Moreover, it can be shown that the estimation error is upper bounded by $\mathcal{R}_I$:

$$\|f_o^{SS} - f_c^{SS}\|_\infty \leq \mathcal{R}_I. \tag{3.10}$$

The SMPC law is derived according to the RH strategy described in Section 3.1, by using the model (A.8). The resulting controller is a static function of the pseudo–state $x_t$, i.e.

$u_t = \kappa(x_t)$, defined on a compact set $\mathcal{X}$ of values of $x$ where the optimization problem is feasible. Note that $\mathcal{X} \subseteq \mathbb{R}^{n-1}$ is a subset of $\Phi \subseteq \mathbb{R}^n$. Now, from (3.10) the following bound on the model uncertainty can be obtained:

$$\sup_{x \in \mathcal{X}} \|f_o^{SS} - f_c^{SS}\|_2 \leq \mathcal{R}_I \tag{3.11}$$

Note that the bound (3.11) can be derived because only the first components of the model equations (3.6) and (3.9) are different, so that the 2-norm of the difference $f_o^{SS}(x) - f_c^{SS}(x)$ is equivalent to the absolute value of the difference $f_o(\phi) - f_c(\phi)$.
When the predictive controller $u_t = \kappa(x_t)$ is applied to the systems (3.5) and (3.8), the following autonomous systems are obtained

$$x_{t+1} = f_o^{SS}(x_t, \kappa(x_t)) = F^o(x_t) \tag{3.12}$$
$$x_{t+1} = f_c^{SS}(x_t, \kappa(x_t)) = F^c(x_t) \tag{3.13}$$

Now, notations $\phi^o(t, x_0) = \underbrace{F^o(F^o(\dots F^o}_{t \text{ times}}(x_0)\dots))$ and
$\phi^c(t, x_0) = \underbrace{F^c(F^c(\dots F^c}_{t \text{ times}}(x_0)\dots))$ denote the state trajectories of systems (3.12) and (3.13), respectively.
Moreover, the following assumptions are made:

**Assumption 1** *The control law $u_t = \kappa(x_t)$ is a Lipschitz continuous function over $\mathcal{X}$, with constant $L_\kappa$.*

**Assumption 2** *The autonomous system (3.13) is uniformly asymptotically stable at the origin for any initial condition $x_0 \in \mathcal{X}$, i.e. it is stable and*

$$\forall \epsilon > 0, \forall \xi > 0 \quad \exists\, \tau \in \mathbb{N}\, s.t.\, ||\phi^c(t+\tau, x_0)||_2 < \epsilon, \quad \forall t \geq 0, \forall x_0 \in \mathcal{X} : ||x_0||_2 \leq \xi \tag{3.14}$$

Assumption 1 is related to the structure of the optimization problem (i.e. the regularity of model (3.10) and employed cost function and constraint sets, see e.g. [42, 43]), while Assumption 2 can be satisfied with a suitable choice of the cost function $J_t$ (3.2) and of the stabilizing constraints (3.3c) (see e.g. [40]- [41]).
Define the closed loop one step prediction error as

$$e(x_t) \doteq f_o^{SS}(x_t, \kappa(x_t)) - f_c^{SS}(x_t, \kappa(x_t)). \tag{3.15}$$

Due to (3.11), the prediction error (3.15) results to be bounded:

$$\|e(x_t)\|_2 \leq \mathcal{R}_I = \mu \tag{3.16}$$

Finally, according to Assumption 1, the function $f_c^{SS}(\cdot)$ in (3.13) results to be Lipschitz continuous over $\mathcal{X}$, with constant $L_{cl} = \sqrt{(1+L_\kappa^2)(1+L_c^2)}$:

$$\begin{aligned}
& ||f_c^{SS}(x_1,\kappa(x_1)) - f_c^{SS}(x_2,\kappa(x_2))||_2^2 = \\
= \;& ||f_c(\cdot) - f_c(\cdot)||_2^2 + ||x_1^{(1)} - x_2^{(1)}||_2^2 + \ldots + ||\kappa(x_1) - \kappa(x_2)||_2^2 + \ldots \\
+ \;& ||x_1^{(n_u+n_y)} - x_2^{(n_u+n_y)}||_2^2 = \\
\leq \;& L_c^2 \left( ||x_1^{(1)} - x_2^{(1)}||_2^2 + \ldots + ||\kappa(x_1) - \kappa(x_2)||_2^2 + \ldots + ||x_1^{(n_u+n_y)} - x_2^{(n_u+n_y)}||_2^2 \right) + \\
+ \;& ||x_1^{(1)} - x_2^{(1)}||_2^2 + \ldots + ||\kappa(x_1) - \kappa(x_2)||_2^2 + \ldots + ||x_1^{(n_u+n_y)} - x_2^{(n_u+n_y)}||_2^2 = \\
\leq \;& L_c^2||x_1 - x_2||_2^2 + L_c^2 L_\kappa^2||x_1 - x_2||_2^2 + ||x_1 - x_2||_2^2 + L_\kappa^2||x_1 - x_2||_2^2 = \\
= \;& (1+L_c^2)(1+L_\kappa^2)||x_1 - x_2||_2^2 = L_{cl}^2||x_1 - x_2||_2^2
\end{aligned} \tag{3.17}$$

## 3.3 Robustness analysis

In this Section, a Theorem showing that the trajectory $\phi^o$ of system (3.12), converges to a neighborhood of the origin, whose size depends on the accuracy of the model $f_c^{SS}$, (3.13) will be introduced. Before stating the Theorem, the following candidate Lyapunov function $V : \mathcal{X} \to \mathbb{R}^+$ for system (3.13) is defined:

$$V(x) \doteq \sum_{j=0}^{\widehat{T}-1} \|\phi^c(j,x)\|_2 \tag{3.18}$$

where $\widehat{T} \geq T$ and $T = \inf_{x\in\mathcal{X}} (T \in \mathbb{N} : \|\phi^c(t+T,x)\|_2 < \|x\|_2,\ \forall t \geq 0)$.

$V(x)$ results to be Lipschitz continuous with constant $L_V = \sum_{j=0}^{\widehat{T}-1} (L_{cl})^j$:

$$\begin{aligned}
|V(x^1) - V(x^2)| \leq & \; | \, \|x^1\|_2 - \|x^2\|_2 + \|F^c(x^1)\|_2 - \|F^c(x^2)\|_2 + \ldots + \\
& + \|F^c(\phi^c(\widehat{T}-2,x^1))\|_2 - \|F^c(\phi^c(\widehat{T}-2,x^2))\|_2| \leq \\
& \leq \|x^1 - x^2\|_2 + \|F^c(x^1) - F^c(x^2)\|_2 + \ldots + \\
& + \|F^c(\phi^c(\widehat{T}-2,x^1)) - F^c(\phi^c(\widehat{T}-2,x^2))\|_2 \leq \\
& \leq \|x^1 - x^2\|_2 + L_{cl}\|x^1 - x^2\|_2 + \ldots + (L_{cl})^{\widehat{T}-1}\|x^1 - x^2\|_2 = \\
& = \sum_{j=0}^{\widehat{T}-1} (L_{cl})^j \|x^1 - x^2\|_2 = \\
& = L_V \|x^1 - x^2\|_2,\ \forall x^1, x^2 \in \mathcal{X}
\end{aligned} \tag{3.19}$$

Moreover, the following inequality holds

$$\begin{aligned} &\forall x \in \mathcal{X},\ \forall e : (F^c(x) + e) \in \mathcal{X} \\ &V(F^c(x) + e) \leq V(F^c(x)) + L_V \mu \end{aligned} \tag{3.20}$$

Furthermore,

$$\|x\|_2 \leq V(x) \leq \sup_{x \in \mathcal{X}} \frac{V(x)}{\|x\|_2} \|x\|_2 = b\,\|x\|_2,\ \forall x \in \mathcal{X} \tag{3.21}$$

$$V(F^c(x)) - V(x) = \Delta V(x) = -\frac{\|x\|_2 - \|\phi^c(\widehat{T}, x)\|_2}{\|x\|_2} \|x\|_2 \leq -K\|x\|_2,\ \forall x \in \mathcal{X} \tag{3.22}$$

where

$$b = \sup_{x \in \mathcal{X}} \frac{V(x)}{\|x\|_2} \tag{3.23}$$

and

$$K = \inf_{x \in \mathcal{X}} \frac{\|x\|_2 - \|\phi^c(\widehat{T}, x)\|_2}{\|x\|_2},\ 0 < K < 1 \tag{3.24}$$

Note that $b$ in (3.23) exists finite by definition of $V(x)$.
Therefore, $V(x)$ is a Lyapunov function for system (3.13) over $\mathcal{X}$.

**Theorem 6** *Suppose that Assumptions 1 and 2 hold, then* $\forall x_0 \in \mathcal{X}$ *such that* $\phi^o(t, x_0) \in \mathcal{X} \quad \forall t \geq 0$ *:*

**i)** *the trajectory distance* $d(t, x_0) = \|\phi^o(t, x_0) - \phi^c(t, x_0)\|_2$ *is bounded by* $\Delta$ *which increases monotonically with the bound* $\mu$ *introduced in (3.16), i.e.*

$$\|\phi^o(t, x_0) - \phi^c(t, x_0)\|_2 \leq \Delta = \Delta(\mu)$$

**ii)** *the trajectory* $\phi^o$ *asymptotically converges to a neighborhood of the origin whose size depends linearly on the value of* $\mu$ *introduced in (3.16) (i.e. the worst-case accuracy of the model* $f_c$*)*

$$\lim_{t \to \infty} \|\phi^o(t, x_0)\|_2 \leq q = q(\mu)$$

**Proof 1 i)** *Choose any* $x_0 \in \mathcal{X}$ *as initial condition for system (3.12) and model (3.13).*

*On the basis of (3.16) and of the Lipschitz property of $f_c^{SS}$it can be noted that:*

$$
\begin{aligned}
d(1,x_0) &= \|\phi^o(1,x_0) - \phi^c(1,x_0)\|_2 \leq \mu \\
d(2,x_0) &= \|\phi^o(2,x_0) - \phi^c(2,x_0)\|_2 = \\
&= \|f_o^{SS}({}_0^{SS}(x_0,\kappa(x_0))) - f_c^{SS}(f_c^{SS}(x_0,\kappa(x_0)))\|_2 \leq \\
&\leq \|f_c^{SS}(f_o^{SS}(x_0,\kappa(x_0))) + e - f_c^{SS}(f_c^{SS}(x_0,\kappa(x_0)))\|_2 \leq \\
&\leq \|f_c^{SS}(f_o^{SS}(x_0,\kappa(x_0))) - f_c^{SS}(f_c^{SS}(x_0,\kappa(x_0)))\|_2 + \|e\|_2 \leq \\
&\leq L_{cl}\|f_o^{SS}(x_0,\kappa(x_0)) - f_c^{SS}(x_0,\kappa(x_0))\|_2 + \mu \leq \\
&\leq L_{cl}\mu + \mu = (1+L_{cl})\mu \\
d(3,x_0) &= \|\phi^o(3,x_0) - \phi^c(3,x_0)\|_2 = \\
&= \|f_o^{SS}(f_o^{SS}(f_o^{SS}(x_0,\kappa(x_0)))) - f_c^{SS}(f_c^{SS}(f_c^{SS}(x_0,\kappa(x_0))))\|_2 \leq \\
&\leq \ldots \leq (1+L_{cl}+L_{cl}^2)\mu \\
d(t,x_0) &= \|\phi^o(t,x_0) - \phi^c(t,x_0)\|_2 \leq \sum_{k=0}^{t-1}(L_{cl})^k\mu
\end{aligned}
$$

*Thus, the following upper bound of the distance between trajectories $\phi^o(t,x_0)$ and $\phi^c(t,x_0)$ is obtained:*

$$
d(t,x_0) \leq \sum_{k=0}^{t-1}(L_{cl})^k\mu = \Delta_1(t,\mu)\,,\ \forall x_0 \quad \forall t \geq 1 \tag{3.25}
$$

*Since $L_{cl} \geq 1$ (see (3.17)), it cannot be proved, on the basis of inequality (3.25) alone, that the trajectory distance $d(t,x_0)$ is bounded. However, by means the properties of Lyapunov function (3.18), a second upper bound $\Delta_2(t,\mu)$ of $d(t,x_0)$ can be computed. In fact, through equations (3.20) and (3.22) the following inequality holds:*

$$
V(F^c(x)+e) \leq V(x) - K\|x\|_2 + L_V\mu \tag{3.26}
$$

*then, on the basis of (3.21) and (3.26), the state trajectory $\phi^o(t, x_0)$ is such that:*

$$\begin{aligned}
\|\phi^o(t,x_0)\|_2 &\leq V(\phi^o(t,x_0)) = V(F^o(\phi^o(t-1,x_0))) = \\
&= V(F^c(\phi^o(t-1,x_0)) + e(\phi^o(t-1,x_0))) \leq \\
&\leq V(\phi^o(t-1,x_0)) - K\|\phi^o(t-1,x_0)\|_2 + L_V\mu \leq \\
&\leq V(\phi^o(t-1,x_0)) - \frac{K}{b}V(\phi^o(t-1,x_0)) + L_V\mu = \\
&= \left(1 - \frac{K}{b}\right) V(\phi^o(t-1,x_0)) + L_V\mu = \\
&= \eta V(\phi^o(t-1,x_0)) + L_V\mu \leq \\
&\leq \eta^t V(x_0) + \sum_{j=0}^{t-1} \eta^j L_V\mu \leq \\
&\leq \eta^t V(x_0) + \frac{L_V\mu}{1-\eta}
\end{aligned} \tag{3.27}$$

*with $\eta = \left(1 - \frac{K}{b}\right) < 1$. Thus, the following result is obtained:*

$$\|\phi^o(t,x_0)\|_2 \leq \eta^t V(x_0) + \frac{b}{K}L_V\,\mu \tag{3.28}$$

$$\|\phi^c(t,x_0)\|_2 \leq \eta^t V(x_0) \tag{3.29}$$

*By means of inequalities (3.28) and (3.29) the upper bound $\Delta_2(t,\mu)$ can be computed:*

$$\begin{aligned}
d(t,x_0) &= \|\phi^o(t,x_0) - \phi^c(t,x_0)\|_2 \leq \\
&\leq \|\phi^o(t,x_0)\|_2 + \|\phi^c(t,x_0)\|_2 \leq \\
&\leq 2\,\eta^t V(x_0) + \frac{b}{K}L_V\,\mu \leq \\
&\leq 2\,\eta^t \sup_{x_0\in\mathcal{X}} V(x_0) + \frac{b}{K}L_V\,\mu = \\
&= \Delta_2(t,\mu)\,,\ \forall x_0 \quad \forall t \geq 0
\end{aligned} \tag{3.30}$$

*Note that, since $\mu < \infty$ and $\mathcal{X}$ is compact*

$$\begin{gathered}
\Delta_2(t,\mu) < \infty,\ \forall t \geq 0 \\
\lim_{t\to\infty} \Delta_2(t,\mu) = \frac{b}{K}L_V\,\mu = q \\
q < \Delta_2(t,\mu) < \infty,\ \forall t \geq 0
\end{gathered}$$

*Thus, as $t$ increases towards $\infty$, the bound $\Delta_2(t,\mu)$ (3.30) decreases monotonically from a finite positive value equal to $2\sup_{x_0\in\mathcal{X}} V(x_0)+\frac{b}{K}L_V\,\mu$ towards a finite positive value $q$, while the bound $\Delta_1(t,\mu)$ (3.25) increases monotonically from 0 to $\infty$. Therefore, for a fixed value of $\mu$ there exists a finite discrete time instant $\widehat{t}>0$ such that $\Delta_1(\widehat{t},\mu)>\Delta_2(\widehat{t},\mu)$. As a consequence, by considering the lowest bound between $\Delta_1(t,\mu)$ and $\Delta_2(t,\mu)$ for any $t\geq 0$, the following bound $\Delta(\mu)$ of $d(t,x)$, which depends only on $\mu$, is obtained:*

$$\begin{aligned}&\Delta(\mu)=\sup_{t\geq 0}\min(\Delta_1(t,\mu),\Delta_2(t,\mu))\\&q\leq\Delta(\mu)<\infty\\&\|\phi^o(t,x_0)-\phi^c(t,x_0)\|_2\leq\Delta(\mu),\ \forall x_0\in\mathcal{X}\quad\forall t\geq 0\end{aligned}$$

*Since both $\Delta_1(t,\mu)$ and $\Delta_2(t,\mu)$ increase monotonically with $\mu$, also their pointwise minimum w.r.t. to $t$ does.*

**ii)** *On the basis of (3.28) it can be noted that*

$$\begin{aligned}\lim_{t\to\infty}\|\phi^o(t,x_0)\|_2&\leq\lim_{t\to\infty}\eta^t b\|x_0\|_2+\frac{b}{K}L_V\mu\\&=\frac{b}{K}L_V\mu=q,\ \forall x_0\in\mathcal{X},\end{aligned}\tag{3.31}$$

*and that $q$ is linear in $\mu$.*

■

In the sequel, the following notation will be used:

$$\mathbb{B}(\mathcal{A},r)=\bigcup_{x\in\mathcal{A}}\mathbb{B}(x,r)\quad\mathcal{A}\subset\mathbb{R}^n$$

where $\mathbb{B}(x,r)\doteq\{\xi\in\mathbb{R}^n:\|x-\xi\|_2\leq r\}$.

**Proposition 1** *Suppose there exists a positively invariant set $\mathcal{G}\subset\mathcal{X}$ such that:*

1. $\phi^c(t,x_0)\in\mathcal{G},\quad\forall x_0\in\mathcal{G},\forall t\geq 0$
2. $\mathbb{B}(\mathcal{G},\Delta)\subset\mathcal{X}$

*then points **i)** and **ii)** of Theorem 6 hold $\forall x_0\in\mathcal{G}$.*

*Remark*
The more accurate is the nominal model (i.e. the lower $\mathcal{R}_I$) the stronger are the robust stability properties of the controlled system. Assuming a local Lipschitz constant,

instead of a global one, can be useful in order to obtain improvements in identification accuracy. A very simple local approach is based on the identification of an improved model exploiting an existing model $\widehat{f}$ (obtained by any desired technique) and input/output process data. In particular, the NSM methodology is applied to the residue function $f_{\Delta}(\varphi) \doteq f_o(\varphi) - \widehat{f}(\varphi)$, using the data $\Delta y^{t+1} = \widetilde{y}^{t+1} - \widehat{f}(\widetilde{\varphi}^t), t \in \mathcal{T}$. See [44] for more details.

The main consequence of Proposition 1 is that for any initial condition $x_0 \in \mathcal{G}$ it is guaranteed that the state trajectory is kept inside the set $\mathcal{X}$ and converges to the set $\mathbb{B}(0, q)$, whose size depends on the accuracy of the model $f_c$. Theorem 6 is to be intended mainly as a qualitative result that establishes local robust attractivity of the origin of the closed-loop system. The difficulty of using this result also for quantitative analysis lies in the practical computation of the involved quantities and in the related conservativeness. On the other hand, to find non-conservative and practically useful results for nonlinear systems is quite a hard task, unless some more restrictive assumptions on the structure of the system and of the problem are made.

### 3.3.1 Vehicle yaw control application

In order to show the effectiveness of the proposed SMPC methodology, an application to a vehicle yaw stability control system is presented here. A brief description of yaw stability control systems is in Section 2.3.

#### Control Requirements

The control objective is the tracking of a reference yaw rate value $\dot{\psi}_{\text{ref}}(t)$, whose course is designed in order to improve the vehicle maneuverability, and to assist the driver in keeping directional stability under different driving conditions. In the considered situation, the vehicle front steering angle $\delta$ represents the control input, while the yaw rate $\dot{\psi}$ is the controlled output.
A feedback control law receives as input the reference yaw rate value, together with the measured yaw rate $\dot{\psi}$, and computes a suitable command current for the steer-by-wire device, that imposes accordingly the pinion angle and, consequently, the steering angle $\delta$ of the front wheels. The desired vehicle behavior is taken into account in the control design by a suitable choice of the reference signal $\dot{\psi}_{\text{ref}}$. Details on the computation of the $\dot{\psi}_{\text{ref}}$ can be found in [37]. The tracking of $\dot{\psi}_{\text{ref}}$ can be taken into account by minimizing the amount of the tracking error $e$, defined as:

$$e = \dot{\psi}_{\text{ref}} - \dot{\psi}$$

The value of the front steering angle $\delta$, generated by the employed active device, is subject to its physical limits. In particular, the range of allowed front steering angles that can be

mechanically generated is $\pm$ 35°, thus, saturation of the control input (i.e. the angle $\delta$) has to be taken into account in the control design.

**Vehicle model identification and SMPC design**

A set of measured values of $\tilde{\dot{\psi}}_t$ and $\tilde{\delta}_t$ are collected in order to identify the NSM vehicle model $f_c$ (A.8).
The number of output and input regressors, $n_y$ and $n_u$, have to be chosen in order to achieve a suitable tradeoff between model complexity and accuracy, while the values of the Lipschitz constant $\gamma$ and of the noise bound $\varepsilon$ are estimated from the data in order to achieve a non-empty $FSS$ (for more details on the regressor choice and on the computation of $\gamma$ and $\varepsilon$, the interested reader is referred to [1]).
According to equation (3.4) the pseudo–state results to be:

$$x_t = \left[ \; \dot{\psi}_t \dots \dot{\psi}_{t-n_y} \delta_{t-1} \dots \delta_{t-n_u} \; \right] \in \mathbb{R}^{n-1} \tag{3.32}$$

The control move is obtained, according to the RH strategy (Section 3.1), by optimizing the following cost function:

$$\min_{U} \quad \sum_{j=1}^{N_p} Q\, e_{t+j+1|t}^2 + R\, \delta_{t+j|t}^2 \tag{3.33}$$

subject to

$$x_{t+j+1|t} = f_c^{SS}(x_{t+j|t}, \delta_{t+j|t}),\ j \in [0, Np-1] \tag{3.34}$$

$$U \in \mathbb{U} = \left\{ \delta_{t+j|t} \,:\, |\delta_{t+j|t}| \leq \bar{\delta},\ j \in [1, N_c] \right\} \tag{3.35}$$

$$e_{t+Np|t} = 0 \tag{3.36}$$

$$u_{t+N_c|t}, \dots, u_{t+N_p-1|t} = u_{t+N_c-1|t} \tag{3.37}$$

where $Q$, $R \in \mathbb{R}^+$ are suitable weights, $e_{t+j|k}$ is the $j^{th}$ step ahead prediction of the tracking error obtained as

$$e_{t+j|t} \doteq \dot{\psi}_{\text{ref},t} - \dot{\psi}_{t+j|t}$$

The terminal state (3.36) equality constraint induces asymptotic closed loop stablity of the nominal model as required by Assumption 1, since, in the presence of this constraint, the optimal cost function turns out to be a Lyapunov function for the tracking error's dynamics. Please refer to [45] for more details.

The saturation value $\bar{\delta}$ is the maximum steering angle that can be mechanically generated i.e. $\bar{\delta} = \pm 35°$. The values of $Q$, $R$, $N_p$, $N_c$ are design parameters suitably chosen in order to achieve a good compromise between closed loop stability and performance (see e.g. [40]).

### Simulation results

In order to evaluate the effectiveness of the proposed approach in a realistic way, a detailed 14 degrees of freedom (d.o.f.) Simulink® vehicle model is employed. Such a model gives an accurate description of the vehicle dynamics as compared to actual measurements and includes nonlinear suspension, steer and tyre characteristics, obtained on the basis of measurements on the real vehicle (see [37] for a detailed description of such a model). The 14 d.o.f. model has been employed at first stance to generate $\tilde{\dot{\psi}}_t$ and $\tilde{\delta}_t$ data with sampling time $T_s = 0.01\,\text{s}$, by simulating a series of standard maneuvers. Then, such data have been divided into two subsets: i.e. the identification and the validation data. The identification data have been employed to derive the NSM vehicle model (A.8) while the validation ones to evaluate its accuracy and to tune the values of $n_u$, $n_y$, $\gamma$ and $\varepsilon$. In particular, after a series of trial-and-error iterations, the values $n_y = 1$, $n_u = 3$, $\gamma = 3$ and $\varepsilon = 0.02\,\text{rad/s}$ have been chosen. The SMPC law has then been designed using the following parameters $N_p = 30$, $N_c = 3$, $Q = 10$ and $R = 5$.

In order to evaluate the proposed SMPC approach, a performance comparison with a NMPC controller designed using the nonlinear single–track vehicle model described by the state equations (3.38) (see [36] and Figure 3.1 for more details) has been carried out:

$$\begin{aligned} mv(t)\dot{\beta}(t) + mv(t)\dot{\psi}(t) &= F_{yf}(t) + F_{yr}(t) \\ J_z\ddot{\psi}(t) &= aF_{yf}(t) - bF_{yr}(t) \end{aligned} \tag{3.38}$$

where $m$ is the vehicle mass, $J_z$ is the moment of inertia around the vertical axis, $\beta$ is the sideslip angle, $\psi$ is the yaw angle, $v$ is the vehicle speed, $a$ and $b$ are the distances between the center of gravity and the front and rear axles respectively.
The nominal parameter values used are: $m = 1715\,\text{kg}$ $J_z = 2700\,\text{kgm}^2$ $a = 1.07\,\text{m}$ $b = 1.47\,\text{m}$. The sampling time $T_s = 0.01\,s$ is used to discretize the model by means the forward difference approximation. $F_{yf}$ and $F_{yr}$ are the front and rear tyre lateral forces, which can be expressed as nonlinear functions of the state, the input and of the vehicle speed (see [37] and [46] for more details):

$$\begin{aligned} F_{yf} &= F_{yf}(\beta, \dot{\psi}, v, \delta) \\ F_{yr} &= F_{yr}(\beta, \dot{\psi}, v, \delta) \end{aligned} \tag{3.39}$$

At first, the NMPC parameters $Q$, $R$, $N_p$ and $N_c$, were set to be the same of the SMPC ones. In such a way, the performance of the NMPC controller was significantly worse than that of the SMPC. After that, in order to make a fair comparison, the NMPC parameters have been tuned via a trial-and-error procedure in order to improve the performance. The final choice was: $Q = 2$, $R = 10$, $N_p = 80$ and $N_c = 2$.
In both cases the control move computation has been performed using the MatLab® optimization function `fmincon`.

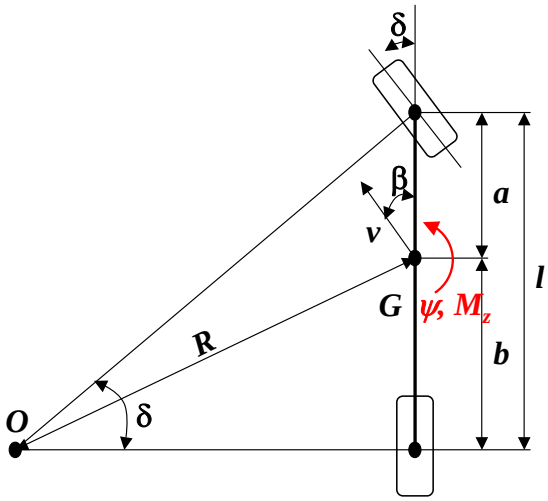


Figure 3.1. Single track model schematic.

Assumptions 1-3 have been checked through numerical inspection using an approach similar to the estimation of the Lipschitz constant proposed in [1] and [47].

An open loop (i.e. without driver's feedback) maneuver has been chosen to test the control effectiveness and to compare the two approaches. In particular, a 50° handwheel step at 100 km/h, with a handwheel speed of 400°/s has been performed in different conditions:

- with nominal vehicle parameters
- with increased vehicle mass, +100 kg, with consequent variations of the other involved inertial and geometrical characteristics
- with a lateral wind gust, which exerts on the vehicle a lateral force and a moment of 800 N and 500 Nm, respectively, for a period of 1 s

Such tests aimed at evaluating both the transient and steady state performance of the controlled vehicle.
The obtained results in nominal conditions (i.e. when the parameters of the 14 d.o.f. model match with those of the physical model (3.38)) are reported in Figure 3.2. It can be noted that the NMPC law based on the physical model achieves a steady–state regulation error of about 3%. This is due to the neglected dynamics and under-modeling of the physical model. On the other hand, the SMPC approach, by employing a model identified directly from data, achieves better regulation precision with 0.9% steady–state tracking error. The advantages of the SMPC technique are also evident in an handwheel step test with increased vehicle mass. The result of this test is shown in Figure 3.3: while the

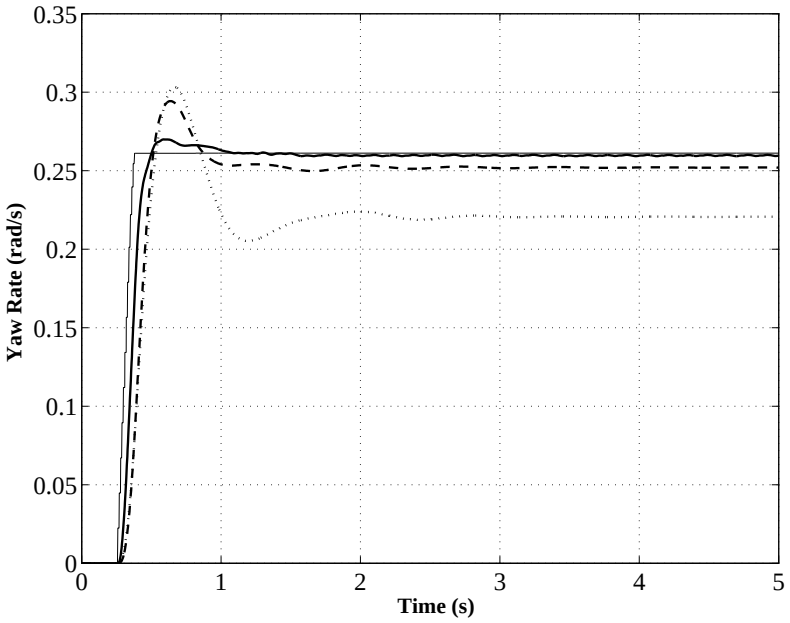


Figure 3.2. Results of the 50° handwheel step test with nominal parameters. Uncontrolled vehicle yaw rate (dotted), reference yaw rate (thin solid line), and yaw rate obtained with the SMPC (solid) and NMPC based on a physical model (dashed) control laws.

SMPC law is able to keep a nearly zero tracking error (0.9%), the NMPC law based on the physical model achieves a slightly higher steady–state tracking error (1.9%) w.r.t the SMPC law. Further, Figure 3.4 shows that the SMPC controller is more robust w.r.t. with the NMCP controller when an external disturbance occurs (0.9% versus 3.8%).
Thus, the presented simulation results highlight that the proposed SMPC methodology improves both robustness and regulation precision of the closed loop system w.r.t. NMPC one, based on physical modelling of the system.

## 3.4 Robust design

Recalling the state space representation (3.6) and (3.9), of $f_0^{SS}$ and $f_c^{SS}$, with a slight abuse of notation, it can be obtained that

$$\begin{aligned} f_c^{SS}(x_t,u_t) &- f_0^{SS}(x_t,u_t) = \\ &= \begin{bmatrix} f_c(x_t,u_t) - f_0(x_t,u_t) \\ 0 \\ \vdots \\ 0 \end{bmatrix} \\ &\doteq w_t(x_t,u_t) \end{aligned} \tag{3.40}$$

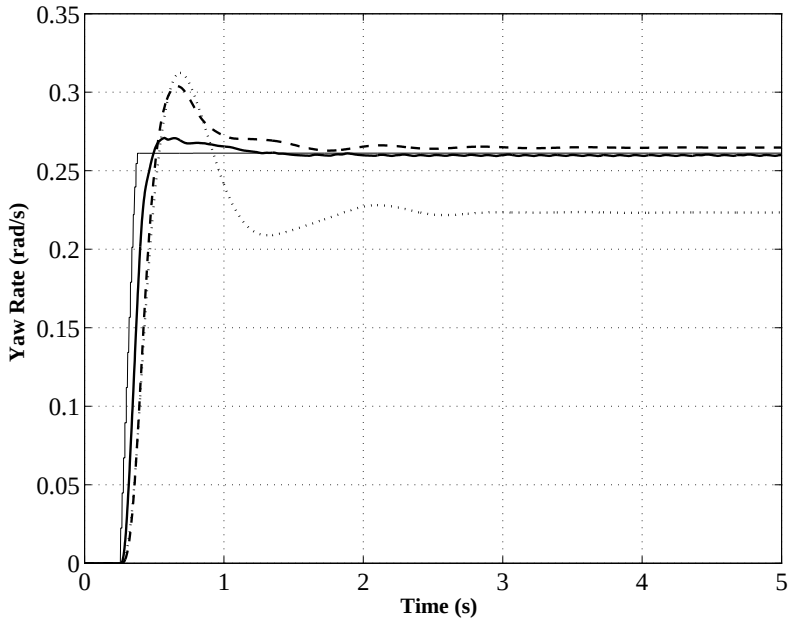


Figure 3.3. Results of the 50° handwheel step test with increased mass. Uncontrolled vehicle yaw rate (dotted), reference yaw rate (thin solid line), and yaw rate obtained with the SMPC (solid) and NMPC based on a physical model (dashed) control laws.

thus the following equation can be derived:

$$x_{t+1} = f_0^{SS}(x_t, u_t) = f_c^{SS}(x_t, u_t) + w_t(x_t, u_t) \tag{3.41}$$

i.e. the model uncertainty is described in terms of an additive, input-and-state-dependent perturbation $w_t(x_t, u_t) \in \mathbb{R}^{n_y+n_u+1}$, whose elements are all equal to zero except for the first one. Then, according to Theorem 8-3), it can be shown that the quantity $w_t(x_t, u_t)$ is pointwise bounded as:

$$\begin{aligned} |w_t(x_t, u_t)| &\leq \frac{1}{2}|\overline{F}(x_t, u_t) - \underline{F}(x_t, u_t)| \\ &\doteq \overline{w}(x_t, u_t), \text{ for any } (x_t, u_t) \in \Phi, \end{aligned} \tag{3.42}$$

where the bound $\overline{w}(x_t, u_t)$ is computed in the NSM approach together with the estimate $f_c^{SS}(x_t, u_t)$. Note that, in (3.42), $w_t \in \mathbb{R}^{n_y+n_u+1}$, while $\overline{F}(x_t, u_t)$, $\underline{F}(x_t, u_t) \in \mathbb{R}$: yet, eq. (3.42) holds due to the particular structure of $w_t$ (3.40).
In principle, one could use the nominal model (3.8) and the uncertainty bound (3.42) to design a robust controller for the system (3.5). However, the related control design may be too complex. Thus, in this work a "global", rather than pointwise, uncertainty bound is employed, derived by using Theorem 8-4) with the $\infty$-norm as a measure of accuracy

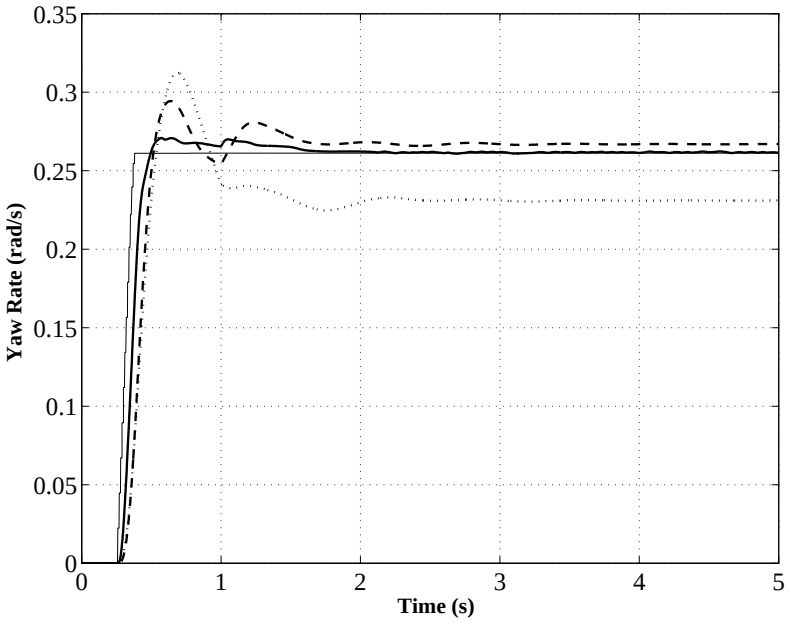


Figure 3.4. Results of the 50° handwheel step test when a blust of wind occurs at 1 s. Uncontrolled vehicle yaw rate (dotted), reference yaw rate (thin solid line), and yaw rate obtained with the SMPC (solid) and NMPC based on a physical model (dashed) control laws.

of the estimate $f_c$ w.r.t. the real system:

$$\begin{aligned} \forall (x,u) \in \Phi,\, \overline{w}(x,u) &= \frac{1}{2}|\overline{F}(x,u) - \underline{F}(x,u)| \\ &\leq \frac{1}{2}\|\overline{F}(x,u) - \underline{F}(x,u)\|_\infty = \mathcal{R}_{I,\infty} \doteq \mu. \end{aligned} \tag{3.43}$$

Summing up, on the basis of eqs. (3.41)-(3.43) the pseudo-state model to be employed in the robust SMPC design is the following:

$$x_{t+1} = f_c^{SS}(x_t, u_t) + w_t,\ |w_t| \leq \mu, \tag{3.44}$$

where $x_t,\ w_t \in \mathbb{R}^{n_u+n_y+1} = \mathbb{R}^r$ and $u_t \in \mathbb{R}$. An estimate of the bound $\mu$ can be computed e.g. by using the approach of [32].

In the sequel the robust design of a SMPC control law is introduced.
In the following, the sequence of $\overline{k}$ control inputs $\{u_t\}_{t_1}^{t_1+\overline{k}-1}$, starting from the generic time instant $t = t_1$ up to time instant $t = t_1 + \overline{k} - 1$, is indicated as $U_{t_1}^{\overline{k}}$. Similarly, $W_{t_1}^{\overline{k}}$ indicates a sequence $\{w_t\}_{t_1}^{t_1+\overline{k}-1}$ of "disturbances" from time instant $t_1$ up to time instant $t_1 + \overline{k} - 1$. The set of all the possible state values at

time $t_1 + \overline{k}$, that originate from the generic state value $x_{t_1}$ at time $t_1$ by applying the input sequence $U_{t_1}^{\overline{k}}$ to system (3.44), is defined as:

$$\begin{aligned} \mathcal{S}(x_{t_1}, U_{t_1}^{\overline{k}}) &\doteq \{\{x_t\}_{t_1}^{t_1+\overline{k}} : \\ x_{t_1+k+1} &= f_c^{SS}(x_{t_1+k}, u_{t_1+k}) + w_{t_1+k}, \\ \forall k \in [0, \overline{k}-1] &, \quad \forall w_{t_1+k} : |w_{t_1+k}| \leq \mu\} \end{aligned} \tag{3.45}$$

while $\phi(x_{t_1}, U_{t_1}^{\overline{k}})$ indicates the nominal state value (i.e. with $w_t = 0\,\forall t$) and $\phi_0^{SS}(x_{t_1}, U_{t_1}^{\overline{k}})$ is the state value of the real plant at time $t_1 + \overline{k}$, obtained starting at $x_{t_1}$ and applying the input sequence $U_{t_1}^{\overline{k}}$. Clearly, it holds that
$\{\phi(x_{t_1}, U_{t_1}^{\overline{k}}), \phi^0(x_{t_1}, U_{t_1}^{\overline{k}})\} \subset \mathcal{S}(x_{t_1}, U_{t_1}^{\overline{k}})$. The Hausdorff distance (see e.g. [48]) between any two sets $\mathcal{S} \in \mathbb{R}^r$ and $\mathcal{X} \in \mathbb{R}^r$ is defined as:

$$\begin{aligned} &d(\mathcal{S}, \mathcal{X}) = \\ &\max\left(\sup_{x^1 \in \mathcal{S}} \inf_{x^2 \in \mathcal{X}} |x^1 - x^2|, \sup_{x^1 \in \mathcal{X}} \inf_{x^2 \in \mathcal{S}} |x^1 - x^2|\right) \end{aligned}$$

It is assumed that the control problem is to robustly asymptotically regulate the state of system (3.44) to a convex and compact neighborhood of the origin, indicated as $\mathcal{X}_f \subseteq \mathbb{R}^r$, under state and input constraints, indicated respectively by a convex set $\mathbb{X} \subseteq \mathbb{R}^r$ and a convex, compact set $\mathbb{U} \subseteq \mathbb{R}$, both containing the origin in their interiors. The notation $U_{t_1}^{\overline{k}} \in \mathbb{U}$ indicates that each one of the elements of the sequence $U_{t_1}^{\overline{k}}$ belongs to $\mathbb{U}$. The following assumption is considered for $\mathcal{X}_f$:

**Assumption 3**
$\forall x_t \in \mathcal{X}_f$, $\forall \overline{k} \in [1, \infty)$, $\exists U_t^{\overline{k}} \in \mathbb{U} : \mathcal{S}(x, U_t^{\overline{k}}) \in \mathcal{X}_f$,

i.e. there exists a feasible control sequence that robustly keeps the state inside the set $\mathcal{X}_f$ for any future time step. The set $\mathcal{X}_f \subset \mathbb{X}$ is a design parameter that has to be chosen according to a tradeoff between better regulation precision and NMPC problem feasibility, as it will be clear in the following. Obviously, $\mathcal{X}_f$ can not be chosen arbitrarily small, due to the presence of the uncertainty $w$. By indicating as $N \in \mathbb{N}$ the prediction horizon, the following cost function $J$ can be defined:

$$J(x_t, U_t^N) = d(x_t, \mathcal{X}_f) + \sum_{k=1}^{N-1} d(\mathcal{S}(x_t, U_t^k), \mathcal{X}_f) \tag{3.46}$$

then, the FHOCP to be solved in the SMPC approach is:

$$J^*(x_t) = \min_{U_t^N} J(x_t, U_t^N) \tag{3.47a}$$

subject to

$$\mathcal{S}(x, U_t^k) \in \mathbb{X},\ \forall k \in [1, N] \tag{3.47b}$$

$$U_t^N \in \mathbb{U} \tag{3.47c}$$

$$\mathcal{S}(x, U_t^N) \in \mathcal{X}_f \tag{3.47d}$$

A (possibly local) optimal control sequence is indicated as $U_t^{N*}(x_t)$. The following assumption is considered about the constrained FHOCP (3.47):

**Assumption 4** *There exists a set $\mathcal{F} \in \mathbb{R}^r$ such that the FHOCP (3.47) is feasible $\forall x \in \mathcal{F}$.*

**Remark 7** *The feasibility of (3.47) depends on many factors, such as the model (3.44), the related uncertainty bound, the constraint sets and the choice of the terminal set $\mathcal{X}_f$. In the quite general settings of this work, it is difficult to derive sufficient conditions on these factors to satisfy Assumption 4 and to evaluate the feasibility set $\mathcal{F} \in \mathbb{R}^r$. These aspects are beyond the scope of this thesis and are subjects of future research.*

The FHOCP (3.47) is typically solved numerically. In particular, it is assumed that the employed algorithm, denoted as $U_t^{N*}(x_t) = \lambda(x_t)$, enjoys the following properties:

**Assumption 5** *For any $x \in \mathcal{F}$, $\lambda(x)$ returns a (eventually local) minimum $J^*(x)$ and the related minimizer $U_t^{N*}(x)$*

**Assumption 6**

**(a)** *For any predicted time instant $t + \underline{k}$ and any control sequence $U_t^{\underline{k}} \in \mathbb{U}$ such that $\mathcal{S}(x_t, U_t^{\underline{k}}) \in \mathcal{X}_f$, the algorithm $\lambda(x_t)$ is able to compute a control sequence $\hat{U}_{t+\underline{k}}^{N-\underline{k}} \in \mathbb{U}$, such that*
*$\mathcal{S}(\mathcal{S}(x_t, U_t^{\underline{k}}), \hat{U}_{t+\underline{k}}^k) \in \mathcal{X}_f,\ \forall k \in [1, N - \underline{k}]$.*

**(b)** *The minimizer $U_t^{N*}(x_t)$ provided by $\lambda(x_t)$ is such that, for any predicted time instant $t + \underline{k} : \mathcal{S}(x_t, U_t^{\underline{k}*}) \in \mathcal{X}_f,\ \underline{k} \in [0, N]$, it happens that*
*$\mathcal{S}(x_t, U_t^{\underline{k}+k*}) \in \mathcal{X}_f,\ \forall k \in [1, N - \underline{k}]$, i.e. the state trajectories are robustly kept inside the terminal set $\mathcal{X}_f$.*

**Remark 8** *Assumptions 5-6 are quite mild, provided that Assumptions 3-4 hold. In particular, with the settings of this work Assumption 5 is satisfied if the problem is feasible and the solver is initialized with a feasible solution (or is able to find a feasible solution). Assumption 6(a) can be satisfied if Assumption 3 holds (so that there exists a sequence*

*that robustly keeps the state inside the terminal set) and if the algorithm $\lambda(x_t)$ is able to find a sequence $\hat{U}_{t+\underline{k}}^{N-\underline{k}}$ and a scalar $\hat{t} = 0$ that solve the following optimization problem:*

$$\left(\hat{t},\, \hat{U}_{t+\underline{k}}^{N-\underline{k}}\right) = \arg \min_{t, U_{t+\underline{k}}^{N-\underline{k}}} t$$

*s.t.*

$$\mathcal{S}(\mathcal{S}(x_t, U_t^{\underline{k}}), \hat{U}_{t+\underline{k}}^{k}) \leq t,\, \forall k \in [1, N - \underline{k}].$$

*Finally, it can be noted that Assumption 6(b) holds as a consequence of Assumption 6(a), by considering that, according to the chosen cost function (3.46), the stage cost related to any predicted set $\mathcal{S}(x_t, U_t^k) : \mathcal{S}(x_t, U_t^k) \in \mathcal{X}_f$ is zero (i.e. minimal).*
*Assumptions 6(a)-(b) can be replaced by assuming that a terminal control policy is known, under which the set $\mathcal{X}_f$ is robustly positively invariant (see e.g. [40]). In some sense, in this work the terminal control policy is not known a priori, while it is assumed that the algorithm $\lambda(x_t)$ is able to derive it.*

According to the RH strategy, the SMPC controller is implemented as follows:

**Algorithm 1**

1. *At time instant $t$, get $x_t$.*
2. *Solve (3.47), by initializing the algorithm $\lambda(x_t)$ with the optimal sequence $\tilde{U}_t^{N*}$, computed at time instant $t-1$ and suitably shifted.*
3. *Apply the first element of the solution sequence $U_t^{N*}$ as the actual control action $u_t$.*
4. *Repeat the whole procedure at time $t+1$.*

The control law resulting from Algorithm 1 is indicated here as $u_t = \kappa^*(x_t)$, and the related sequence, starting from the generic time instant $t_1$ up to time $t_1 + k - 1$, is denoted as $K_{t_1}^k = \{\kappa^*(x_t)\}_{t_1}^{t_1+k-1}$. The following stability result holds.

**Theorem 7** *Under Assumptions 3-6, the distance between the state of system (3.44), controlled by the feedback law $\kappa^*$, and the terminal set $\mathcal{X}_f$ asymptotically robustly converges to zero for any initial condition $x_t \in \mathcal{F}$, i.e.:*

$$\forall x_t \in \mathcal{F},\ \lim_{k\to\infty} d(\mathcal{S}(x_t, K_t^k), \mathcal{X}_f) = 0$$

**Proof 2** *At first, the recursive feasibility of Algorithm 1 is analyzed. Take any $x_t \in \mathcal{F}$. Assumptions 4 and 5 imply that the algorithm $\lambda(x_t)$ is able to find a feasible, locally optimal solution sequence. Such a sequence is indicated here as $U_{t|t}^{N*} \in \mathbb{U}$, to highlight that it is the solution of (3.47) at time $t$. By applying the first element of such a sequence to the system, the state $x_{t+1} = \phi^P(x_t, U_{t|t}^{1*})$ is obtained at the following time step, $t+1$.*

*By initializing the algorithm $\lambda(x_{t+1})$ with the shifted optimal sequence $U^{N-1*}_{t+1|t}$ computed at time step $t$, it can be noted that $S(x_{t+1}, U^{k*}_{t+1|t}) \in \mathbb{X}$, $\forall k \in [0, N-1)$ and that the set $S(x_{t+1}, U^{N-1*}_{t+1|t}) \in \mathcal{X}_f$, i.e. at the second last prediction step the state trajectory is robustly inside the terminal set $\mathcal{X}_f$. Then, according to Assumptions 3 and 6, the algorithm $\lambda(x_{t+1})$ is able to find a control input $\hat{u}_{t+N} \in \mathbb{U}$ so that $S(x_{t+1}, \hat{U}^{N*}_{t+1|t}) \in \mathcal{X}_f$, where the sequence $\hat{U}^{N*}_{t+1|t} \in \mathbb{U}$ is constructed by using as first $N-1$ components the elements $\{u^*_t\}^N_{t+1|t}$ of the optimal sequence $U^{N*}_{t|t}$, and as the last component the value $\hat{u}_{t+N}$. The sequence $\hat{U}^{N*}_{t+1|t}$ provides a feasible input sequence for the problem (3.47) at time $x_{t+1}$. Such a reasoning can be iterated for any time instant $t+k, k \in [2, \infty)$, so that recursive feasibility is proved. The asymptotic convergence of the distance $d(\mathcal{S}(x_t, K^k_t), \mathcal{X}_f)$ to zero, as $k \to \infty$, will be now proved. For any state value $x_t \in \mathcal{F}$, consider the optimal cost $J^*(x_t)$, computed at time $t$ by algorithm $\lambda(x_t)$, corresponding to the optimal solution sequence $U^{N*}_{t|t}(x_t)$. For the sake of simplicity of notation, define $d(x_t) \doteq d(x_t, \mathcal{X}_f)$. From the definition of the cost function $J$ (3.46), it can be noted that*

$$0 \leq d(x_t) \leq J^*(x_t), \tag{3.48}$$

*i.e. the distance between the state $x_t$ and the set $\mathcal{X}_f$ is upper-bounded by $J^*(x_t)$. Moreover, due to Assumptions 3 and 6,*

$$J^*(x_t) = 0 \iff d(x_t) = 0 \tag{3.49}$$

*so that $J^*(x_t) = 0$ if and only if $x_t \in \mathcal{X}_f$. Finally, consider the difference $J^*(x_{t+1}) - J^*(x_t)$. Since the algorithm $\lambda(x_{t+1})$ at time $t+1$ is provided with the feasible input sequence $\hat{U}^{N*}_{t+1|t}$, which is suboptimal, it holds that:*

$$J^*(x_{t+1}) \leq J(x_{t+1}, \hat{U}^{N*}_{t+1|t}). \tag{3.50}$$

*$J(x_{t+1}, \hat{U}^{N*}_{t+1|t})$ is such that:*

$$J(x_{t+1}, \hat{U}^{N*}_{t+1|t}) \leq J^*(x_t) - d(x_t) \tag{3.51}$$

*By combining eqs. (3.50) and (3.51), it can be noted that:*

$$J^*(x_{t+1}) - J^*(x_t) \leq -d(x_t) \tag{3.52}$$

*with:*

$$J^*(x_{t+1}) - J^*(x_t) = 0 \iff d(x_t) = 0, \tag{3.53}$$

*in which case $J^*(x_{t+1}) = J^*(x_t) = 0$, due to Assumption 4. Thus, it holds that:*

$$\begin{aligned} J^*(x_{t+1}) - J^*(x_t) < 0 \, \forall x_t \in \mathcal{F} \setminus X_f \\ J^*(x_{t+1}) - J^*(x_t) = 0 \iff x_t \in \mathcal{X}_f \end{aligned} \tag{3.54}$$

*Equations (3.48) and (3.54) are sufficient to prove robust asymptotic convergence of $d(x_t)$ to 0:*

$$\lim_{t\to\infty} d(x_t) \leq \lim_{t\to\infty} J^*(x_t) = 0,\ \forall x_0 \in \mathcal{F} \tag{3.55}$$

■

**Remark 9** *Theorem 7 also implies that the distance between the state $\phi^P(x_{t_1}, U_{t_1}^{\overline{k}})$ of the controlled system and the set $\mathcal{X}_f$ asymptotically converges to zero.*

**Remark 10** *In order to reduce the conservativeness of the presented approach and to improve the feasibility of (3.47), the FHOCP can be generalized by optimizing over control policies $\kappa$, i.e. $U_{t_1}^N = \{\kappa(x_t)\}_{t_1}^{t+N-1} + V_{t_1}^{t+N-1}$, so that the predictions involved in (3.47) can be carried out in a closed-loop fashion. It is widely recognized (see e.g. [49]) that this approach leads to better performance and reduced feasibility problems. Optimization over control policies has not been adopted in the theoretical framework of this study just for simplicity of notation, yet it can be straightforwardly used and indeed it has been employed in the numerical example of Section 3.4.1*

**Remark 11** *It has to be noted that the set $\mathcal{F}$ has to be a subset (with lower dimension) of the set $\Phi$, over which the NSM identification procedure is applied.*

### 3.4.1 Nonlinear oscillator application

Consider the following two-dimensional, discrete-time nonlinear oscillator obtained from the Duffing equation (see e.g. [50]):

$$\begin{aligned} \xi_{t+1} &= \begin{bmatrix} 1 & T_s \\ -T_s\,\omega^2 & 1-2\,\zeta\,T_s \end{bmatrix} \xi_t + \\ &\quad \begin{bmatrix} 0 & 0 \\ -T_s & 0 \end{bmatrix} \xi_t^3 + \begin{bmatrix} 0 \\ T_s \end{bmatrix} u_t \\ y_t &= \begin{bmatrix} 1\ 0 \end{bmatrix} \xi_t + v_t \end{aligned} \tag{3.56}$$

where $\xi_t = [\xi_t^{(1)}\ \xi_t^{(2)}]^T$ is the system state (the symbol $\cdot^T$ denotes the transpose operator), $v_t \in [-0.01, 0.01]$ is an unknown-but-bounded measurement noise, $\zeta = 0.3$, $\omega = 1$ and $T_s$ = 0.05 s.
The control objective is to regulate the output $y$ to the origin, under the following output and input constraints:

$$|y| \leq 3 \qquad |u| \leq 5 \tag{3.57}$$

The system (3.56) is supposed to be unknown, but a set of noise-corrupted measurements can be collected through preliminary experiments. Note that the origin of system (3.56) is an open-loop asymptotically stable fixed point for any initial condition $\xi_0 \in \mathbb{R}^2$, so that the preliminary experiment can be carried out in open-loop fashion. In particular, 30 experiments have been carried out, starting from 30 different initial conditions $\xi_0 \in \mathbb{R}^2 : \|\xi_0\|_\infty \leq 3$. In each one of these experiments, a uniformly distributed random sequence $\{\tilde{u}_t\}_0^{1 \cdot 10^3} : \forall t, |\tilde{u}_t| \leq 5$ has been used as input, and a second uniformly distributed random sequence $\{\tilde{v}_t\}_0^{1 \cdot 10^3} : \forall t, |\tilde{v}_t| \leq 0.01$ has been employed as measurement noise. The overall collected data form a set of $3 \cdot 10^4$ samples $(\tilde{y}, \tilde{u})$ (A.2), which has been split in an identification set of $2.5 \cdot 10^4$ samples, to be used in the NSM identification procedure, and in a validation set containing the remaining $5 \cdot 10^3$ samples. The number of output and input regressors, $n_y$ and $n_u$ respectively, have been chosen in order to achieve a suitable tradeoff between model complexity and accuracy, while the values of the Lipschitz constant $\gamma$ and of the noise bound $\varepsilon$ have been estimated from the data in order to achieve a non-empty $FSS$ (for more details on the regressor's choice and on the computation of $\gamma$ and $\varepsilon$, the interested reader is referred to [1]). In this case, the values $n_y = 2$, $n_u = 2$, $\gamma = 2.3$ and $\varepsilon = 0.02$ have been chosen. The obtained NSM model has the form (3.44):

$$x_{t+1} = f_c^{SS}(x_t, u_t) + w_t$$

where

$$x_t = \begin{bmatrix} x_t^{(1)} \\ x_t^{(2)} \\ x_t^{(3)} \end{bmatrix} = \begin{bmatrix} y_t \\ y_{t-1} \\ u_{t-1} \end{bmatrix}$$

$$f_c^{SS}(x_t, u_t) = \begin{bmatrix} f_c(x_t, u_t) \\ x_t^{(1)} \\ u_t \end{bmatrix} \tag{3.58}$$

and $f_c(x_t, u_t)$ is the identified NSM model (see (3.9)). The estimated uncertainty bound $\mu$ results to be equal to 0.1. The derived model is then employed to design the SMPC law, according to Algorithm 1, by optimizing over linear feedback control policies of the form $u_t = K\, x_t + u_t'$ (see Remark 10). In particular, the horizon $N = 30$ and the terminal set $\mathcal{X}_f = \{x \in \mathbb{R}^3 : |x^{(1)}|, |x^{(2)}| \leq 0.1; |x^{(3)}| \leq 2\}$ have been employed. Finally, on the basis of the constraints (3.57) on the actual system and of the pseudo-state choice (3.4.1), the sets $\mathbb{X}$ and $\mathbb{U}$ are selected as follows:

$$\begin{aligned} \mathbb{X} &= \left\{x \in \mathbb{R}^3 : |x^{(1)}|, |x^{(2)}| \leq 3;\ |x^{(3)}| \leq 5\right\} \\ \mathbb{U} &= \left\{u \in \mathbb{R} : |u| \leq 5\right\} \end{aligned}$$

The obtained results, starting as an example from the initial state $\xi_0 = [1.85, -3.41]^T$ (and initial pseudo-state $x_0 = [1.85, 2, 0]^T$), are shown in Figure 3.5-3.7, where they are compared to the results achieved in an "ideal" case, i.e. with a NMPC law designed

and implemented assuming exact knowledge of the system equations (3.56) and measurement of the whole state with zero noise. In particular, Figures 3.5 and 3.6(a)-(b) show the trajectories of the system output $y$ and state $\xi$ respectively. It can be noted that quite good regulation precision is achieved by the SMPC law (see Figure 3.6(b)), while its performance in the transient phase are worse w.r.t. the standard NMPC law, due to the conservativeness of the robust design employed in SMPC and the presence of measurement noise. The courses of the input $u$ are shown in Figure 3.7, where it can be noted that the input constraints are always satisfied by both controllers.

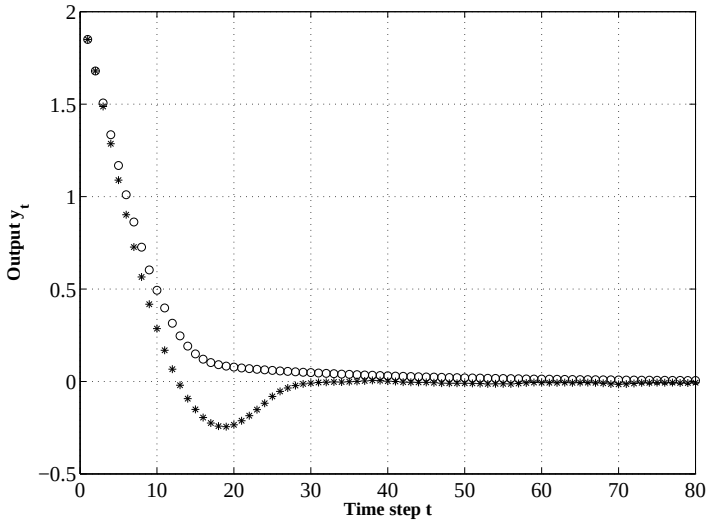


Figure 3.5. Numerical example: courses of the system output $y$ with the SMPC control law ($*$) and with a state-feedback NMPC law ($\circ$). Initial state: $\xi_0 = [1.85,\ -3.41]^T$, initial pseudo-state: $x_0 = [1.85,\ 2,\ 0]^T$.

(a)

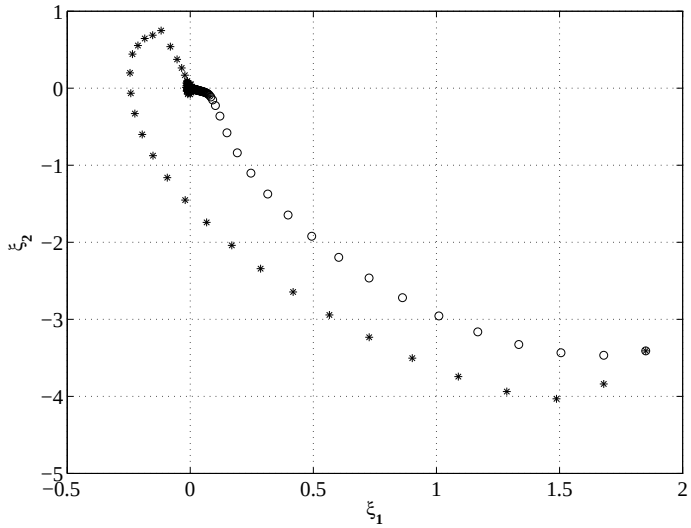


(b)

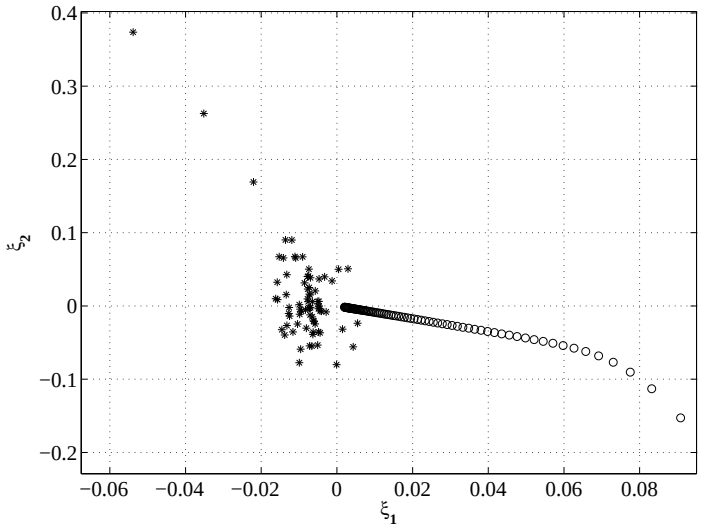


Figure 3.6. Numerical example: (a) Trajectories of the system state $\xi$ with the SMPC control law ($*$) and with a state-feedback NMPC law ($\circ$). (b) Zoom of the trajectories close to the origin. Initial state: $\xi_0 = [1.85,\ -3.41]^T$, initial pseudo-state: $x_0 = [1.85,\ 2,\ 0]^T$.

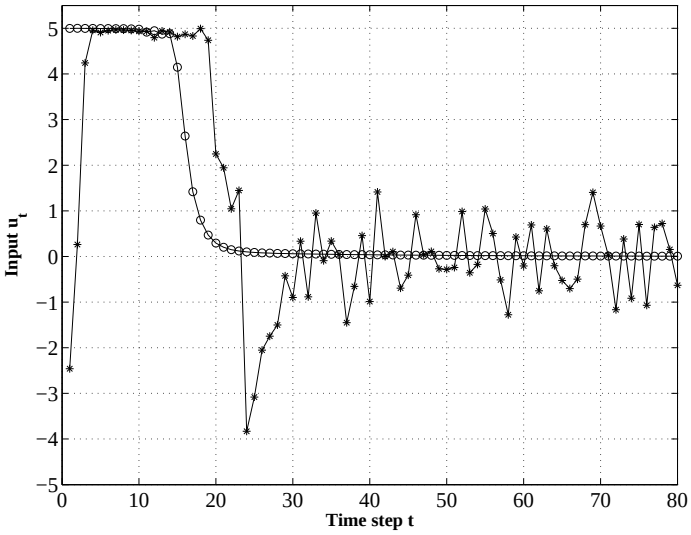


Figure 3.7. Numerical example: courses of the system input $u$ with the SMPC control law ($*$) and with a state-feedback NMPC law ($\circ$). Initial state: $\xi_0 = [1.85,\ -3.41]^T$, initial pseudo-state: $x_0 = [1.85,\ 2,\ 0]^T$.

# Chapter 4

# Stability control systems using Direct Virtual Sensors

Lateral stability control systems significantly enhance safety and handling properties by modifying the dynamics of the passive vehicle (see [51]). These systems usually employ a closed loop control strategy with a yaw rate feedback (see [36]). Clearly, the yaw rate sensor plays a crucial role for the correct operation of the control system and sensor faults may lead to performance deterioration or even safety risks, unless a proper recovery strategy is adopted. In this context, virtual sensors can be employed to carry out a recovery strategy. Once the sensor fault has been detected, the measure of the yaw rate can be replaced by its estimate, provided by the virtual sensor.
In this thesis, the design of a linear yaw rate Direct Virtual Sensor (DVS) and its use in feedback control is studied.
A quite extensive literature can be found regarding yaw rate estimation using the measures of wheel speeds, steering angle and/or lateral acceleration (see [12] and the reference therein for more details). However, few works investigate the use of combined yaw rate estimation and feedback for yaw control and none of them addresses the issue of guaranteeing closed loop system stability in the presence of virtual sensor.
Here, such issues are investigated. At first, the problem of how to make a suitable choice of the measured variables needed by the DVS is studied in order to enhance the estimation accuracy. It is shown that, using data collected in a closed loop fashion, better overall estimation performance can be obtained, with a reduced number of measured variables. The stability of the controlled system using the DVS is studied via an a posteriori robustness analysis. Finally, through simulations, the performance of the controlled vehicle is evaluated in critical conditions and when a recovery strategy is used in order to face a yaw rate sensor fault.

## 4.1 Vehicle modeling

Vehicle stability control systems usually employ a feedback control structure where the controlled variable is the yaw rate $\dot{\psi}(t)$ and the controller is designed on the basis of a linear vehicle model. The control input is able to modify the vehicle dynamics by influencing the longitudinal and/or lateral tyre forces, using several physical mechanisms. Among the existing solutions (see e.g. [52–57]), in this paper an approach similar to AFS systems (see e.g. [52]) is adopted: the steering angle $\delta(t)$ of the front wheels is the sum of the contribution $\delta_d(t)$, issued by the driver via the conventional steering system, with the contribution $\delta_f(t)$, provided by the active system via an electromechanical device:

$$\delta(t) = \delta_d(t) + \delta_f(t) \tag{4.1}$$

Angle $\delta_d$ is related to the handwheel angle $\delta_v$, provided by the driver, through the steering ratio $\tau$, i.e. $\delta_d = \delta_v/\tau$. The value of $\delta_f(t)$ is restricted in the range $\pm 5^\circ$ due to the actuator limitations in the considered AFS system. The adopted actuation solution is motivated by safety reasons, since the driver intervention on the front steering angle is always kept.
For the control design, a linear single track vehicle model is considered, assuming that angle $\delta$(t) is the control input (see e.g. [36] for details). Under the typical assumptions for single track models, for a fixed vehicle speed $\overline{v}$ the following dynamic equilibria hold:

$$\begin{aligned} a_y(t) &= \overline{v}(\dot{\beta}(t) + \dot{\psi}(t)) = (F_{yf}(t) + F_{yr}(t))/m \\ J\ddot{\psi}(t) &= aF_{yf}(t) - bF_{yr}(t) \end{aligned} \tag{4.2}$$

where $m$ is the vehicle mass, $J$ is the moment of inertia around the vertical axis, $\beta$ is the side–slip angle, $a$ and $b$ are the distances between the center of gravity and the front and rear axles respectively and $F_{yf}$ and $F_{yr}$ are the front and rear axle lateral forces, respectively. The dynamic generation of tyre forces is also taken into account through the following first order equations:

$$\begin{aligned} F_{yf}(t) + \tfrac{l_f}{\overline{v}}\dot{F}_{yf}(t) &= -c_f\left(\beta(t) + a\tfrac{\dot{\psi}(t)}{\overline{v}} - \delta(t)\right) \\ F_{yr}(t) + \tfrac{l_r}{\overline{v}}\dot{F}_{yr}(t) &= -c_r\left(\beta(t) - b\tfrac{\dot{\psi}(t)}{\overline{v}}\right) \end{aligned} \tag{4.3}$$

where $l_f$ and $l_r$ are the front and rear tyre relaxation lengths and the variables $c_f$ and $c_r$ stand for the front and rear axle cornering stiffnesses (see [58]).
In the presence of a physical yaw rate sensor, the measure of $\dot{\psi}(t)$ is employed for feedback control and the controller design is carried out on the basis of the transfer function $G_{\dot{\psi}}(s)$, between the steering angle $\delta(t)$ and the yaw rate $\dot{\psi}(t)$:

$$G_{\dot{\psi}}(s) = \frac{b_2 s^2 + b_1 s + b_0}{a_4 s^4 + a_3 s^3 + a_2 s^2 + a_1 s + a_0} \tag{4.4}$$

where

$$\begin{aligned}
&a_4 = mJl_f l_r,\ a_3 = m\overline{v}J(l_f + l_r)\\
&a_2 = J(m\overline{v}^2 + c_f l_r + c_r l_f) + m(c_f a^2 l_r + c_r b^2 l_f)\\
&a_1 = \overline{v}(J(c_f + c_r) + m(c_f a(a - l_r) + c_r b(b + l_f)))\\
&a_0 = c_f c_r l^2 - m\overline{v}^2(c_f a - c_r b)\\
&b_2 = m\overline{v}ac_f l_r,\ b_1 = m\overline{v}^2 ac_f,\ b_0 = \overline{v}c_f c_r l
\end{aligned} \tag{4.5}$$

Transfer function $G_{\dot{\psi}}(s)$ can be derived, for a fixed value of the speed $\overline{v}$, by applying the Laplace transform to equations (4.1)–(4.3). It is also useful to describe the relationships between the vehicle input $\delta$ and the lateral acceleration $a_y$, the difference between the angular speeds of the front wheels, $\Delta\omega_f$, and of the rear wheels, $\Delta\omega_r$. Such variables have been considered since their measures are either usually available on vehicles, due to the presence of electric power steering (EPS) and anti–lock braking (ABS) systems and thus they can be used as inputs for the yaw rate virtual sensor. Moreover, as a first approximation, under the same assumptions of the single track vehicle model, the values of $\Delta\omega_f(t)$ and $\Delta\omega_r(t)$ are related to $\dot{\psi}(t)$ through the following equations (see e.g. [36]):

$$\begin{aligned}
\Delta\omega_f(t) &= \dot{\psi}(t)d_f/R_w\\
\Delta\omega_r(t) &= \dot{\psi}(t)d_r/R_w
\end{aligned} \tag{4.6}$$

where $R_w$ is the nominal wheel radius (supposed to be the same for all of the four wheels) and $d_f$, $d_r$ are the front and rear wheelbases respectively. Note that variables $\Delta\omega_f$ and $\Delta\omega_r$ are defined as:

$$\begin{aligned}
\Delta\omega_f &= \omega_{f,h} - \omega_{f,v}\\
\Delta\omega_r &= \omega_{r,h} - \omega_{r,v}
\end{aligned}$$

where $\omega$ denotes the wheel angular speed and the subscripts $f,\ r,\ h,\ v$ stand for front, rear, right and left wheel position, respectively. On the basis of equations (4.1)–(4.6), transfer functions $G_{a_y}(s)$, $G_{\Delta\omega_f}(s)$ and $G_{\Delta\omega_r}(s)$ are derived, respectively between the input $\delta$ and the output variables $a_y$, $\Delta\omega_f$ and $\Delta\omega_r$:

$$\begin{aligned}
G_{a_y}(s) &= \frac{c_3 s^3 + c_2 s^2 + c_1 s + c_0}{a_4 s^4 + a_3 s^3 + a_2 s^2 + a_1 s + a_0}\\
G_{\Delta\omega_f}(s) &= \frac{g_2 s^2 + g_1 s + g_0}{a_4 s^4 + a_3 s^3 + a_2 s^2 + a_1 s + a_0}\\
G_{\Delta\omega_r}(s) &= \frac{h_2 s^2 + h_1 s + h_0}{a_4 s^4 + a_3 s^3 + a_2 s^2 + a_1 s + a_0}
\end{aligned} \tag{4.7}$$

where

$$\begin{aligned}
&c_3 = Jl_r c_f\overline{v},\ c_2 = J\overline{v}^2 c_f,\ c_1 = \overline{v}blc_f c_r,\ c_0 = \overline{v}^2 c_f c_r l\\
&g_2 = m\overline{v}ac_f l_r d_f/R_w,\ g_1 = m\overline{v}^2 ac_f d_f/R_w\\
&g_0 = \overline{v}c_f c_r l d_f/R_w,\ h_2 = m\overline{v}ac_f l_r d_r/R_w\\
&h_1 = m\overline{v}^2 ac_f d_r/R_w,\ h_0 = \overline{v}c_f c_r l d_r/R_w
\end{aligned} \tag{4.8}$$

## 4.2 Vehicle yaw control using physical sensor

In this Section, the adopted control structure is presented, together with its design procedure(Figure 4.2). The control objective is to track a reference yaw rate value $\dot{\psi}_{ref}(t)$, whose course is designed in order to improve the vehicle maneuverability, and to assist the driver in keeping directional stability under the different driving conditions. In particular, $\dot{\psi}_{ref}(t)$ is computed by means of a static map whose inputs are the handwheel angle $\delta_v(t)$, issued by the driver, and the vehicle speed $v(t)$. For given values of $\delta_v$ and $v(t)$, the map is designed so that the desired yaw rate is higher than the one obtained by the uncontrolled vehicle, thus obtaining a higher lateral acceleration value and narrower paths, i.e. better maneuverability. At the same time, the reference yaw rate map is designed in such a way that the related side-slip angle $\beta$ is limited, so to improve directional stability. Finally, the map also takes into account the nonlinear behaviour of the vehicle as it approaches its lateral acceleration limit. The reference yaw rate map employed in this paper is shown in Figure 4.1. For a detailed description of the criteria followed in the map construction, the

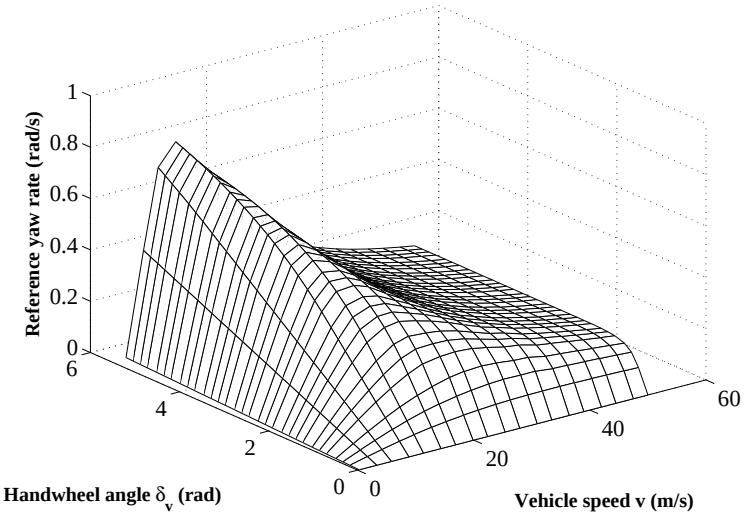


Figure 4.1. Yaw-rate reference map employed in the control system.

interested reader is referred to [37] and [59].
In the considered control structure, denoted as $(Q + \dot{\psi})$ in the following, the value of the control input $\delta_f(t)$ is the sum of a feedback contribution $\delta_{fb}(t)$ with a feedforward one $\delta_{ff}(t)$. The feedback controller is designed using IMC methodologies, since they have been proved to be effective in the context of robust vehicle stability control (see e.g. [37, 53, 59] for their application in different contexts).
The IMC controller $Q(s)$ is designed to optimize the vehicle performance, while guaran-

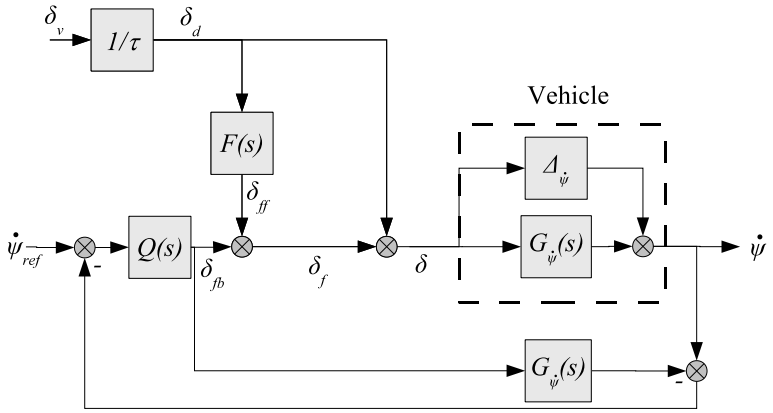


Figure 4.2. Control structure with measured yaw rate feedback and IMC controller $Q(s)$ ($Q + \dot{\psi}$).

teeing robust stability in the presence of the model uncertainty induced by the wide range of operating conditions. In order to take into account such uncertainty in the control design, an additive model set of the following form is employed:

$$\mathcal{G}_{\dot{\psi}}(G_{\dot{\psi}}, \Gamma_{\dot{\psi}}) = \{(G_{\dot{\psi}}(s) + \Delta_{\dot{\psi}}(s)) : |\Delta_{\dot{\psi}}(j\omega)| \leq \Gamma_{\dot{\psi}}(\omega)\} \tag{4.9}$$

$\Delta_{\dot{\psi}}(s)$ is the unstructured additive uncertainty (see e.g. [60]), while $\Gamma_{\dot{\psi}}(\omega)$ is an upper bound on the magnitude of $\Delta_{\dot{\psi}}(j\omega)$. Such model set can be obtained considering variations of the vehicle and tyre parameters with respect to their nominal values (see [60]), as described in Section 4.5. The design of $Q(s)$ is performed by means of the following optimization problem (see e.g. [39]):

$$Q(s) = \underset{\left\|Q(s)\bar{\Gamma}_{\dot{\psi}}(s)\right\|_\infty < 1}{\arg\min} \left\|W_S^{-1}(s)\, S(s)\right\|_\infty \tag{4.10}$$

where $\bar{\Gamma}_{\dot{\psi}}(s)$ is a suitable real rational stable function, whose magnitude strictly overbounds $\Gamma_{\dot{\psi}}(\omega)$ (4.9) and $W_S(s)$ is a weighting function which accounts for the desired performance on the nominal sensitivity $S(s) = 1 - G_{\dot{\psi}}(s)Q(s)$. $W_S(s)$ is chosen to achieve good closed loop damping properties and to slightly improve the system bandwidth with respect to the uncontrolled vehicle.
The feedforward contribution $\delta_{ff}$, computed through the filter $F(s)$ from the measure of angle $\delta_d$, issued by the driver, has been added to improve the dynamic response characteristic. In particular, the filter $F(s)$ is designed to match the desired open loop yaw rate behavior, between the driver input $\delta_d$ and vehicle yaw rate $\dot{\psi}$, with the one described by an objective transfer function $T^{\text{des}}(s)$:

$$\dot{\psi}(s) = T^{\text{des}}(s)\delta_d(s) \tag{4.11}$$

According to the scheme in Figure 4.2, it results that

$$\begin{aligned} T^{\text{des}}(s)\delta_d(s) &= G_{\dot{\psi}}(s)\delta_d(s) + G_{\dot{\psi}}(s)\delta_{ff}(s) = \\ &= G_{\dot{\psi}}(s)\delta_d(s) + G_{\dot{\psi}}(s)F(s)\delta_d(s) \end{aligned}$$

thus the filter $F(s)$ can be computed as

$$F(s) = \frac{T^{\text{des}}(s)}{G_{\dot{\psi}}(s)} - 1 \tag{4.12}$$

Moreover, since $F(s)$ aims at enhancing the transient response only, its contribution should be deactivated in steady state conditions. This is achieved when the dc–gains of $T^{\text{des}}(s)$ and $G_{\dot{\psi}}(s)$ are equal.

## 4.3 Virtual Sensors vs Direct Virtual Sensors

### 4.3.1 Virtual Sensors

Let us consider a process $\mathcal{S}$ with a set of known inputs $u \in \mathbb{R}^m$, some unknown inputs (named disturbances) $w \in \mathbb{R}^r$, a set of measured outputs $y \in \mathbb{R}^q$ and an internal variable of interest $z \in \mathbb{R}$, to be estimated. A virtual sensor (see e.g. [61]) is a causal and stable dynamic system that takes as inputs the known inputs $u$ and a subset of the measured outputs $y$ of $\mathcal{S}$, and whose output is an estimate $\hat{z}$ of the internal variable $z \in \mathbb{R}$. In the linear case, the virtual sensor dynamic behavior can be described as:

$$\hat{Z}(s) = H_{\hat{z},y}(s)Y(s) + H_{\hat{z},u}(s)U(s) \tag{4.13}$$

where $H_{\hat{z},u}(s)$ and $H_{\hat{z},y}(s)$ are real rational stable transfer matrices of suitable dimension. Figure 4.3 shows the general process–virtual sensor scheme together with the approximation error $\epsilon$. Different methodologies can be employed to build a virtual sensor, according to the considered prior information and assumptions. The most common techniques rely on the use of a (usually linear) process model and particular hypotheses about disturbances. Some of these approaches are the minimum variance (Kalman) and $\mathcal{H}_\infty$ filtering techniques. With these techniques, the obtained estimation accuracy may be poor due to neglected dynamics in the employed model and due to the presence of (often uncertain) nonlinear characteristics in the real process (see [62]).

### 4.3.2 Direct Virtual Sensors

When the process is not completely known, a data–driven approach to the virtual sensor design problem can be considered. In this paper, a direct procedure is followed, in which

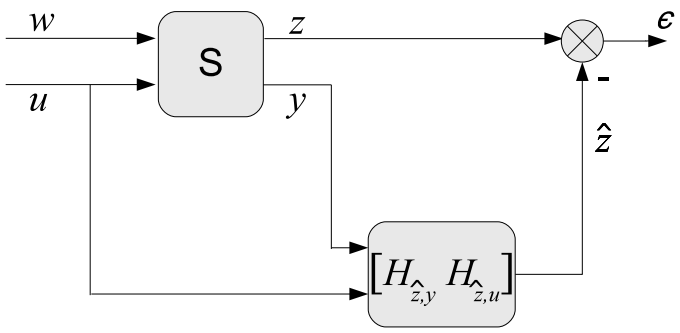


Figure 4.3. Process–virtual sensor scheme.

suitable process input–output experimental data are used to design a DVS in one step, avoiding the identification of a model of the process. A preliminary experiment can be performed also when the variable $z$ is measured. This assumption is not restrictive, since some measurements of $z$ are needed to evaluate the performance of any virtual sensor, independently on the employed design methodology. Moreover, in the considered automotive context, extensive experimental testing campaigns are usually carried out, in order to tune the control algorithms and to assess the active system performance. During such experimental tests, in order to collect large quantities of data, the employed prototype car is equipped with a full set of sensors that, usually, are not all installed on the final commercialized vehicle due to their excessive costs.
Denote with $u_k$, $y_k$ and $z_k$ the sampled values of $u$, $y$ and $z$ respectively, corresponding to any sampling instant $k \in \mathbb{N}$, with fixed sampling period $T_s$. $N$ measurements of $u_k$, $y_k$ and $z_k$, corresponding to sampling instants $k\,T_s,\ \forall k \in [1, N]$, are collected in the preliminary experiment. In the following, the values of $u_k,\ y_k,\ z_k$, $k = 1, ..., N$, are referred to as the "data set". Since a virtual sensor must be a stable system, its impulse response has an exponential decay and it can be approximated with desired precision by a Finite Impulse Response (FIR) filter that uses present and past values of $u_k$ and $y_k$ to give an estimate $\hat{z}_k$ of $z_k$, that is:

$$\hat{z}_k = \sum_{j=0}^{n_u} \alpha_j^T u_{k-j} + \sum_{j=0}^{n_y} \beta_j^T y_{k-j} \tag{4.14}$$

where $n_u$, $n_y$ are design parameters which define the structure of the DVS and $\alpha_j \in \mathbb{R}^m,\ j = 0, \ldots, n_u$ and $\beta_j \in \mathbb{R}^q,\ j = 0, \ldots, n_y$ are the filter coefficients, whose values are constrained by the following exponential decay:

$$\|\alpha_j\|_\infty \leq L_u \rho^j,\ j \in [0,1, \ldots, n_u]$$
$$\|\beta_j\|_\infty \leq L_y \rho^j,\ j \in [0,1, \ldots, n_y]$$

where $L_u > 0$, $L_y > 0$ and $0 < \rho < 1$. $L_u$, $L_y$ and $\rho$ are the parameters that define the model class where the DVS is looked for. In particular, $L_u$ and $L_y$ define the maximum

absolute value of any one of the elements of the first coefficients in the impulse response (i.e. $\alpha_0$ and $\beta_0$), while $\rho$ is the decay rate.
Assuming that $z$ is observable from $y$, it can be shown that the estimation error $\epsilon_k = z_k - \hat{z}_k$ is bounded for any bounded input sequence (see [63]). Using FIR filters with the structure (4.14), the DVS can be designed by minimizing a weighted $p$–norm of the estimation error on the collected data set, i.e. on the collected values of $u_k$, $y_k$ and $z_k$ for any $k \in [\underline{k}, N]$, where $\underline{k} = \max(n_u, n_y)$:

$$[\hat{\alpha}_0, \ldots, \hat{\alpha}_{n_u}, \hat{\beta}_0, \ldots, \hat{\beta}_{n_y}] = \arg\min \left( \sum_{k=\underline{k}}^{N} \left| \mathrm{w}_k^{-1} \epsilon_k \right|^p \right)^{1/p}$$

such that

$$\begin{cases} \epsilon_k = z_k - \sum_{j=0}^{n_u} \alpha_j u_{k-j} - \sum_{j=0}^{n_y} \beta_j y_{k-j} \quad k \in [\underline{k}, N] \\ \|\alpha_j\|_\infty \leq L_u \rho^j, \ j \in [0,1,\ldots,n_u] \\ \|\beta_j\|_\infty \leq L_y \rho^j, \ j \in [0,1,\ldots,n_y] \end{cases} \tag{4.15}$$

This convex optimization problem with linear constraints can be efficiently solved. By suitably selecting the weights $\mathrm{w}_k$ in (4.15), it is possible to consider noise measures dependent on $k$, for example relative measurement errors. Details on how to select the exponential decay parameters $L_u$, $L_y$ and $\rho$ and weights $\mathrm{w_k}$ are given in [64].
Depending on the data set employed in the design, the obtained linear DVS is able to give good estimation performance also in nonlinear process operating conditions, when the linear models used in classic approaches suffer from under–modeling (for a complete comparison, see [63]).
Regardless of the used norm, solution to problem (4.15) is usually a high order FIR filter. Then, model order reduction techniques are used to fit the identified impulse responses with a stable and causal IIR filter of a prefixed order $n$. An $n$-th order state-space realization is obtained by singular value decomposition of the Hankel matrix of the filter impulse response, such that the $H_\infty$ distance between the original and the low order filter is bounded, see [65]. Finally, a bilinear transformation is applied to the resulting estimator in order to obtain the form (4.13).

### 4.3.3 Direct Virtual Sensors for yaw rate

The design and the use of a yaw rate DVS for feedback control is now studied. Thus, referring to Section 4.3.2, the variable $z$ to be estimated is the yaw rate $\dot{\psi}$, while the variable $u$ is the front steering angle, i.e. $u = \delta$. As to variable $y$, it is assumed that the measures of the lateral acceleration $a_y$ and of the differences between the wheel angular speeds of the front and rear axles, $\Delta\omega_f$ and $\Delta\omega_r$ respectively, are available. Therefore, the considered output $y$ is composed of a suitable subset of the variables $a_y$, $\Delta\omega_f$ and $\Delta\omega_r$. Table 4.1 lists all the possible virtual sensors.

| DVS | Measurements |
|---|---|
| 1 | $[\delta, a_y]$ |
| 2 | $[\delta, \Delta\omega_f]$ |
| 3 | $[\delta, \Delta\omega_r]$ |
| 4 | $[\delta, a_y, \Delta\omega_f]$ |
| 5 | $[\delta, a_y, \Delta\omega_r]$ |
| 6 | $[\delta, \Delta\omega_f, \Delta\omega_r]$ |
| 7 | $[\delta, a_y, \Delta\omega_f, \Delta\omega_r]$ |

Table 4.1. Subsets of measurements used for the DVS design

By intuition, it could be expected that the best estimation accuracy can be obtained when all of the possible available measurements are used. However, an interesting outcome of this paper is that this is not true in general, since the use of all of the three measures of $a_y$, $\Delta\omega_f$ and $\Delta\omega_r$ does not always lead to the best accuracy results. In particular, it will be shown that, if the initial experiment is performed in closed loop fashion, the DVS which achieves the best accuracy employs the measures of $a_y$ and $\Delta\omega_r$ only. Moreover, such DVS has better accuracy than those designed using data collected with the uncontrolled vehicle, independently on the number of employed measurements. However, figuring out a priori which measured variables should be used to obtain good accuracy appears to be a hard task: physical insight and trial–and–error procedures can be used to practically establish the best combination of measurements to be employed.

## 4.4 Vehicle yaw control using Direct Virtual Sensor

Closed loop stability when the DVS is used for feedback control is now investigated. Figure 4.4 shows the considered control scheme where the yaw rate DVS replaces the physical one, e.g. to recover the yaw rate sensor fault. This scheme is denoted $(Q+DVS)$ for brevity. Since the estimated variable $\hat{z}$ is the yaw rate $\widehat{\dot{\psi}}$ and the input $u$ is the steering angle $\delta$, the transfer matrices of the DVS (see (4.13))are denoted with $H_{\widehat{\dot{\psi}},y}$ and $H_{\widehat{\dot{\psi}},\delta}$. A sufficient robust stability condition, based on the small gain theorem (see e.g. [60]), is employed to assess if the controller $Q(s)$ is still able to robustly stabilize the system in the presence of the DVS. To this end, the nominal transfer matrix $G_y(s)$, from input $\delta$ to the considered output $y$, is computed. $G_y(s)$ is a single–column transfer matrix whose components are one or more of the transfer functions (4.7), depending on the particular considered variable $y$. For example, the transfer matrix $G_y(s)$ related to DVS 4 (see Table 4.1 and (4.7)) is defined as:

$$G_y(s) = \begin{bmatrix} G_{a_y}(s) \\ G_{\Delta\omega_f}(s) \end{bmatrix}$$

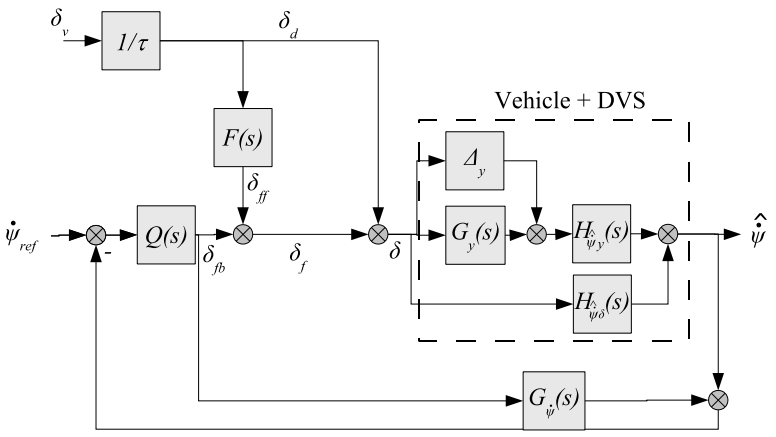


Figure 4.4. Control structure with estimated yaw rate feedback and IMC controller $Q(s)$ $(Q + DVS)$.

Model uncertainty is taken into account by the following additive model set:

$$\mathcal{G}_y(G_y, \Gamma_y) = \{G_y(s) + \Delta_y(s) : \bar{\sigma}\left(\Delta_y(j\omega)\right) \leq \Gamma_y(\omega)\} \tag{4.16}$$

where $\bar{\sigma}(\cdot)$ is the maximum singular value and $\Delta_y(s)$ is the transfer matrix of the additive uncertainty associated to $G_y(s)$, while $\Gamma_y(\omega)$ is an upper bound of $\bar{\sigma}\left(\Delta_y(j\omega)\right)$, which can be computed by considering variations of the vehicle and tyre parameters with respect to their nominal values (as described e.g. in [60]).
Referring to Figure 4.4 and defining the functions:

$$\begin{aligned} G_{DVS}(s) &= H_{\hat{\dot{\psi}},y}(s)G_y(s) + H_{\hat{\dot{\psi}},\delta}(s) \\ \Delta_{DVS}(s) &= H_{\hat{\dot{\psi}},y}(s)\Delta_y(s) \\ C(s) &= Q(s)(1 - G_{\dot{\psi}}(s)Q(s))^{-1} \end{aligned}$$

the following sufficient condition can be used to check robust stability of control scheme $(Q + DVS)$.

**Robust stability of control scheme ($Q + DVS$)**
The control scheme $(Q + DVS)$ is robustly stable with respect to the model uncertainty $\Delta_y$ in the model set (4.16) if

$$\left\|\Gamma_{DVS}(s)C(s)(1 + C(s)G_{DVS}(s))^{-1}\right\|_\infty < 1 \tag{4.17}$$

where $\Gamma_{DVS}(s)$ is a stable real rational transfer function, such that

$$\bar{\sigma}\left(\Delta_{DVS}(j\omega)\right) \leq |\Gamma_{DVS}(j\omega)|$$

**Proof**. $C(s)$ is the equivalent feedback controller of the IMC loop formed by $Q(s)$ and $G_{\dot{\psi}}(s)$, $G_{DVS}(s)$ is the nominal transfer function from $\delta$ to $\hat{\dot{\psi}}$ and $\Delta_{DVS}(s)$ is the resulting additive uncertainty of $G_{DVS}(s)$. Equation (4.17) follows from the application of the

small gain theorem to the equivalent feedback loop with additive uncertainty. ■

## 4.5 Vehicle yaw control design using Direct Virtual Sensor

### 4.5.1 Yaw control design

The IMC design has been performed using transfer function $G_{\dot{\psi}}(s)$ (see (4.4)) and vehicle parameter values as shown in Table 4.2. Model sets (4.9) and (4.16) have been obtained

| Model parameters | Values |
|---|---|
| $m$ | 1715 kg |
| $\overline{v}$ | 100 km/h |
| $J$ | 2697 kgm$^2$ |
| $a$ | 1.07 m |
| $b$ | 1.47 m |
| $l_f$ | 1 m |
| $l_r$ | 1 m |
| $c_f$ | 89733 Nm/rad |
| $c_r$ | 114100 Nm/rad |
| $R_w$ | 0.303 m |
| $d_f$ | 1.48 m |
| $d_r$ | 1.35 m |
| $\tau$ | 15.4 |

Table 4.2. Vehicle model parameters

by considering variations of the vehicle nominal speed between 70 and 130 km/h, independent variations of rear and front tyre cornering stiffness between [-30%, +10%], increments of vehicle mass up to +20% distributed as 30% on the front axle and 70% on the rear axle, with the consequent changes of distances between the center of gravity and the front and rear axles and of moment of inertia. Moreover, a variation of $\pm 10\%$ of the tyre radius has been considered too. The control input $\delta_f$ is supposed to be mechanically limited such that $|\delta_f| \leq 5^\circ$.
The IMC controller $Q(s)$ has been obtained as the solution of (4.10), using the following weighting function:

$$W_S(s) = 1.06\frac{s}{s+5} \tag{4.18}$$

The feedforward filter $F(s)$ in (4.12) has been computed using the following transfer function $T^{\text{des}}(s)$:

$$T^{\text{des}}(s) = \frac{4.488}{(1 + s/20)^2}.$$

Functions $W_S(s)$ and $T^{\text{des}}(s)$ have been chosen and tuned in order to achieve a good compromise between steady state behavior and closed loop specifications. In particular, for $W_S(s)$, a zero at the origin has been employed to ensure servo performance, so that in steady-state conditions the reference yaw rate, which has been chosen in order to improve vehicle maneuverability, is attained with zero tracking error. The gain and the pole of $W_S(s)$ have been chosen to impose a limited resonance peak and larger bandwidth with respect to the uncontrolled vehicle, so to improve the damping of the vehicle transient response and reduce the response time, thus enhancing the vehicle handling performance.

### 4.5.2 Direct Virtual Sensor design and performance

A 14 d.o.f. nonlinear vehicle model has been used to generate the data sets required for the design and the validation of the virtual sensors. Nonlinear characteristics obtained on the basis of measurements on a real vehicle have been employed to model the tyre, steer and suspension behavior. A first-order dynamical model of each wheel has been used to compute the wheel speed. The employed tyre model, described e.g. in [58], takes into account the interaction between longitudinal and lateral slip, as well as vertical tyre load and suspension motion, to compute the tyre longitudinal and lateral forces and self–aligning moments. An example of the employed tyre friction ellipses is shown in Figure 4.5, where the lateral friction coefficient is reported as a function of the exploited longitudinal friction (during traction) and of the tyre slip angle $\alpha$.

Figure 4.6 shows a comparison between the yaw rate measured on the real vehicle during a track test, and the one obtained in simulation with the considered model.
Using such detailed 14 d.o.f. vehicle model, two data sets have been obtained through two different experiments, lasting 90 s each. In both experiments, the vehicle speed is kept constant at 70 km/h during the first 25 s, then it is gradually increased up to 100 km/h at 35 s, from 35 s to 55 s it is kept at 100 km/h, in the next 10 s the speed is gradually increased up to 130 km/h and maintained at this value for the last 25 s.
In the first experiment, the vehicle has been driven in open loop, by imposing a suitably designed course $\delta_d^{\text{id}}(t)$ of $\delta_d$, composed of quick ramps and constant intervals plus a pseudo–random binary signal. The second experiment has been performed in closed loop fashion using the control scheme $(Q + \dot{\psi})$. In this case, the vehicle is driven by means of the same driver input $\delta_d^{\text{id}}(t)$ and employing the controller $Q(s)$ and the filter $F(s)$ designed as described in Section 4.2 and 4.5.1.
Seven DVS have been designed for each data set, considering all possible combination of the available measurements (see Table 4.1). Each DVS has been identified by solving the

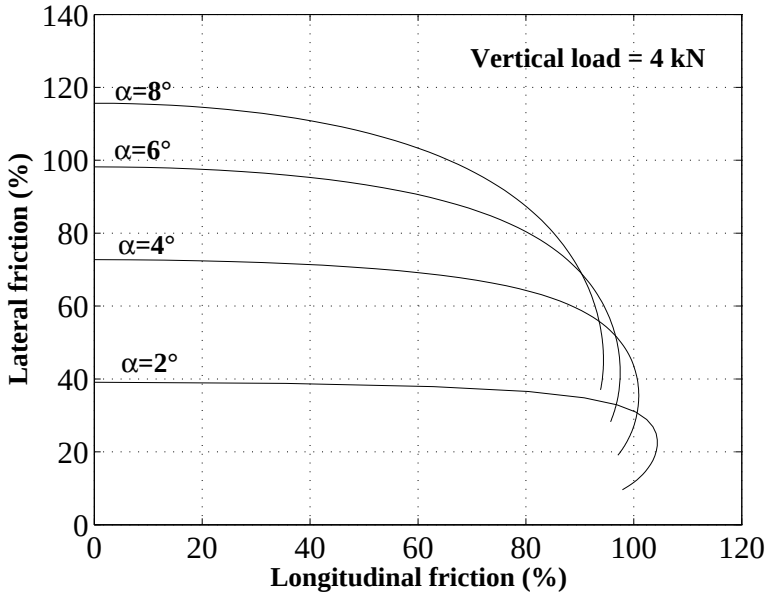


Figure 4.5. Front tyre friction ellipses considered in the 14 degrees of freedom model, with different values of lateral slip angle $\alpha$, for a constant vertical load of 4 kN.

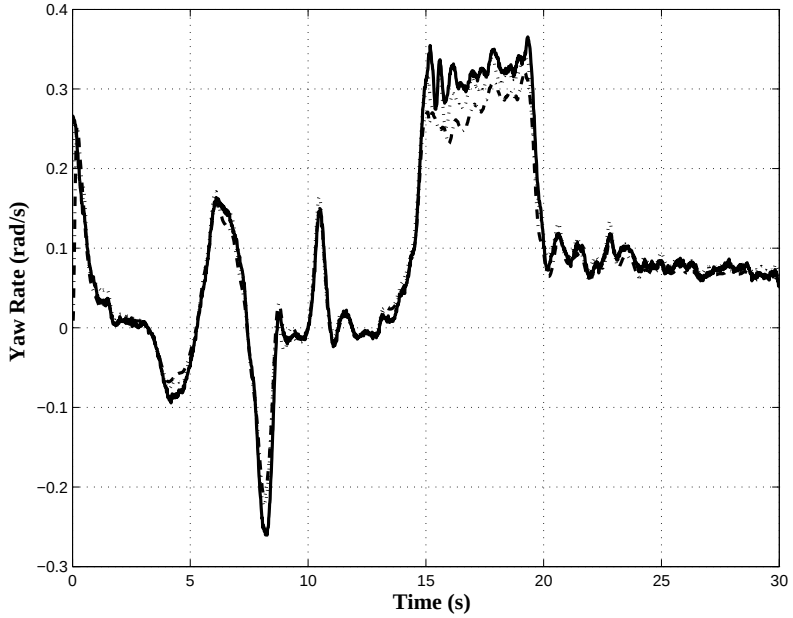


Figure 4.6. Comparison between the measured yaw rate (solid) during a track test on the real vehicle, the simulated yaw rate obtained with the 14 d.o.f. model (dotted) and the estimate provided by the DVS (dash-dotted).

optimization problem (4.15) using either the open or the closed loop data set, for $p = 2$ and unitary weights, i.e. the resulting filter is the FIR model that minimizes the sum of squared errors, while having an impulse response bounded by the decay rate defined by $L$ and $\rho$.
Different bounds on the decay rate have been considered for each DVS, adjusting the filter lengths accordingly, and the ones giving the lowest estimation error, while satisfying the robust stability condition (4.17), have been selected. Table 4.3 shows the length $n_{FIR} = n_u = n_y$ and decay rate constraints $L = L_u = L_y$ and $\rho$ of the designed DVSs, and the order $n$ of the corresponding virtual sensors obtained after the order reduction step.
In order to evaluate the control system performance when the yaw rate estimate $\widehat{\dot{\psi}}$ given

| DVS | $L$ | $\rho$ | $n_{FIR}$ | $n$ |
|---|---|---|---|---|
| 1 | 0.4 | 0.96 | 150 | 10 |
| 2 | 0.3 | 0.92 | 100 | 8 |
| 3 | 0.3 | 0.92 | 100 | 8 |
| 4 | 0.6 | 0.92 | 100 | 8 |
| 5 | 0.6 | 0.90 | 100 | 10 |
| 6 | 0.3 | 0.95 | 150 | 8 |
| 7 | 0.3 | 0.95 | 150 | 10 |

Table 4.3. Parameters for DVS design

by the DVS is used, simulations have been performed employing the 14 d.o.f. nonlinear vehicle model and the control structure ($Q + DVS$). In particular, the following maneuvers have been considered:

- constant speed steering pad at 100 km/h: the handwheel angle is increased slowly ($1°$/s) to evaluate the steady state tracking behavior
- steer reversal test with handwheel angle of $5°$ and $50°$, at 90 km/h, to evaluate steady state and transient vehicle performance in linear and nonlinear operating conditions.

Table 4.4 shows the obtained accuracy results for the steering pad tests, in terms of maximum relative estimation error $\hat{E}_{\text{max}}$ and mean relative estimation error $\hat{E}_{\text{mean}}$:

$$\hat{E}_{\text{max}} = \max_{t\in[t_0,t_{end}]} \hat{e}(t) \tag{4.19}$$

$$\hat{E}_{\text{mean}} = \frac{1}{t_{end} - t_0} \int_{t_0}^{t_{end}} \hat{e}(t)dt \tag{4.20}$$

where

$$\hat{e}(t) = \left| \frac{\hat{\dot{\psi}}(t) - \dot{\psi}(t)}{\dot{\psi}(t)} \right|, \ \dot{\psi}(t) \neq 0$$

and $t_0$, $t_{end}$ are the starting and final test time instants respectively. Since the steering pad is a steady state maneuver, the values of $\hat{E}_{\text{max}}$ and $\hat{E}_{\text{mean}}$ can be considered as measures of the static DVS performance.

The results presented in Table 4.4 show that a bounded estimation error is obtained with

| | Open loop | | Closed loop | |
|---|---|---|---|---|
| DVS | $\hat{E}_{\text{max}}$ | $\hat{E}_{\text{mean}}$ | $\hat{E}_{\text{max}}$ | $\hat{E}_{\text{mean}}$ |
| 1 | 34.9% | 24.8% | 43.8% | 30.8% |
| 2 | 22.4% | 14.3% | 16.2% | 9.3% |
| 3 | 24.5% | 16.2% | 17.3% | 9.7% |
| 4 | 19.8% | 13.4% | 12.8% | 8.5% |
| 5 | 20.6% | 13.6% | **12.2%** | **6.9%** |
| 6 | 20.0% | 9.5% | 19.6% | 13.2% |
| 7 | **14.7%** | **7.1%** | 13.3% | 8.2% |

Table 4.4. Steering pad test using DVS

all the considered virtual sensors. DVS 1, which employs the measure of $a_y(t)$ only, gives the worst performance, while all of the other filters show similar estimation errors. In most cases, the use of closed loop data gives better results than using open loop data.

| | Open loop | | Closed loop | |
|---|---|---|---|---|
| DVS | $\hat{E}_{\text{mean}}$ | $E_{\text{mean}}$ | $\hat{E}_{\text{mean}}$ | $E_{\text{mean}}$ |
| 1 | 37.1% | 37.2% | 33.7% | 29.8% |
| 2 | 31.3% | 24.6% | 20.4% | 16.0% |
| 3 | 33.0% | 25.2% | 20.9% | 16.2% |
| 4 | 21.9% | 21.6% | 16.4% | **13.5%** |
| 5 | 24.8% | 23.2% | **16.0%** | 13.9% |
| 6 | 23.2% | 17.3% | 24.2% | 18.7% |
| 7 | **21.2%** | **17.8%** | **16.0%** | 14.0% |

Table 4.5. $5^\circ$ steer reversal test using DVS

Tables 4.5 and 4.6 show the obtained performance in the steer reversal tests in terms of the index $\hat{E}_{\text{mean}}$ (4.20) and of the mean relative tracking error $E_{\text{mean}}$:

$$E_{\text{mean}} = \frac{1}{t_{end} - t_0} \int_{t_0}^{t_{end}} e_{ref}(t) dt \tag{4.21}$$

where

$$e_{ref}(t) = \left| \frac{\dot{\psi}_{ref}(t) - \dot{\psi}(t)}{\dot{\psi}_{ref}(t)} \right|, \; \dot{\psi}_{ref}(t) \neq 0$$

| | Open loop | | Closed loop | |
|---|---|---|---|---|
| DVS | $\hat{E}_{\text{mean}}$ | $E_{\text{mean}}$ | $\hat{E}_{\text{mean}}$ | $E_{\text{mean}}$ |
| 1 | 20.0% | 22.4% | 16.4% | 12.6% |
| 2 | 12.5% | 8.4% | 9.0% | 4.7% |
| 3 | 13.2% | 10.6% | 8.6% | 5.0% |
| 4 | 12.3% | 10.8% | 8.6% | 5.1% |
| 5 | 9.5% | 15.4% | **6.8%** | **2.8%** |
| 6 | **8.4%** | **4.4%** | 8.4% | 4.8% |
| 7 | 10.3% | 6.2% | 7.2% | 3.2% |

Table 4.6.
$50^\circ$ steer reversal test using DVS

Note that virtual sensors identified from closed loop data perform better than those identified from open loop data, especially in the $50^\circ$ steer reversal maneuver. This is due to the fact that, in the presence of the control action, the closed loop vehicle transient response is different from the open loop one. Thus, by using closed loop experimental data a more appropriate information about the process is taken into account in the DVS design.
Moreover, it can be noted (see Tables 4.4–4.6, bold–faced text) that the best overall estimation accuracy is given by DVS 5, obtained using the closed loop data set and the measures of $a_y(t)$ and $\Delta\omega_r(t)$ only, which performs better than DVS 7 that exploits all of the possible available measurements, designed either using the closed loop or the open loop data sets. It is not trivial to explain, from the practical point of view, why such a result has been obtained. From a theoretical point of view, the signals with higher correlation with the estimated variables are those that give more information and that should be employed. This is surely the case, in this particular application, of the lateral acceleration, as it is intuitive and also evident by the poor results achieved by DVSs n. 2, 3 and 6, and of at least one of the two wheel speed differentials, since DVS 1 (that does not employ the measure of wheel speed difference) also has bad performance. The remaining DVSs n. 4, 5 and 7 have very similar estimation accuracy. The employed vehicle is an all-wheel drive one, so that wheel slip during traction is present on all wheels, which may explain why the results of DVSs 4,5 and 7 (closed-loop) are so close one to the other. With a 2-wheel drive vehicle, one would expect the non-driven wheel speeds to give a more accurate yaw-rate estimate.
Finally, the accuracy of the DVS 5 has been evaluated on experimental data measured on the real vehicle during a track test with vehicle speed varying between 50 km/h and 120 km/h and lateral acceleration up to $7.5$ m/s$^2$. In Figure 4.6, the estimate provided by DVS 5 is compared to the yaw rate measured during a track test and to the yaw rate course obtained with the 14 d.o.f. vehicle model. The mean relative error between the measured yaw rate and the simulated one is 8.6%, while the mean relative error between

the measured yaw rate and the one given by DVS 5 is 13%.

### 4.5.3 Simulation results

According to the results reported in Tables 4.4–4.6, DVS 5, identified from closed loop data, has been chosen to compare performance of the control structures $(Q + \dot{\psi})$ and $(Q + DVS)$ which use, respectively, the measured and estimated yaw rate. In Figure 4.7, sensitivity functions of the considered control schemes are compared with the desired sensitivity described by the weighting function $W_S(s)$ (4.18). It can be noted that the magnitude course of sensitivity functions related to the scheme $(Q + \dot{\psi})$ satisfies the nominal performance. Although the magnitude of the nominal sensitivity of the closed loop system $(Q+DVS)$ shows a higher peak value, it has a greater noise attenuation level at low frequencies.

In order to assess the behaviour of the control systems when a DVS is employed for

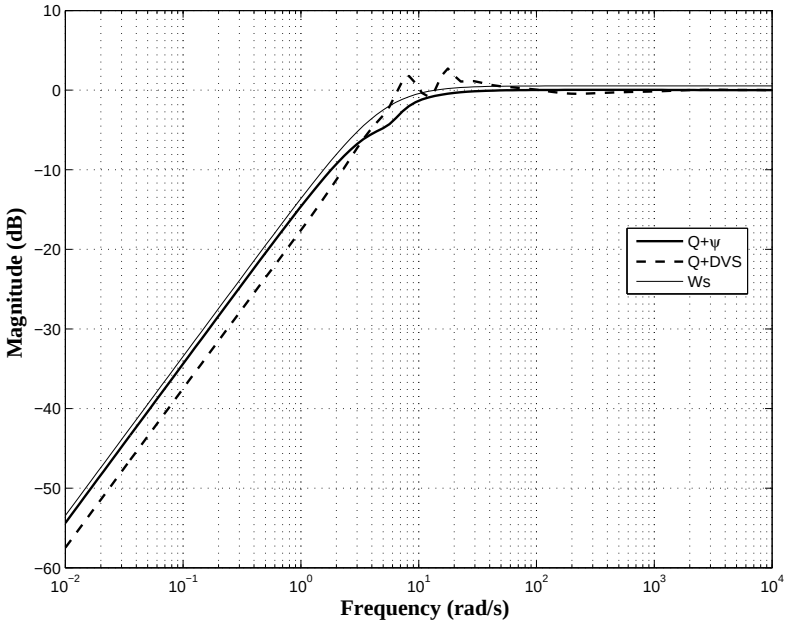


Figure 4.7. Thin solid line: weighting function $W_S$. Sensitivity functions of the control scheme $(Q + \dot{\psi})$ (solid), $(Q + DVS)$ (dashed).

feedback and to analyze the results of the recovery strategy when a fault of the yaw rate sensor occurs, the following simulation tests have been performed:

- 50° steer reversal maneuver performed on dry road with vehicle speed varying between 50 km/h and 120 km/h. This test aims to assess the robustness of the control system both in the absence and in the presence of DVS, in different operating conditions.

- brake–in–a–turn test performed at 110 km/h with handwheel angle of $15^\circ$ and a braking action of $0.5g$ ($g$ is the gravitational acceleration). The braking occurs when the transient phase of the step steer has been finished and lasts 3 s, from the 5$^{\text{th}}$ until the 8$^{\text{th}}$ second of the maneuver. Note that during this maneuver the vehicle is subject to significant lateral acceleration and non constant longitudinal speed (from 110 to 50 km/h) due to the sudden braking, thus making this a quite demanding robustness test. The maneuver has been also performed when a fault of the yaw rate sensor occurs after 7 s from the beginning.

- ISO double lane change maneuver as reported in [58]. This maneuver has been performed once on wet road with constant speed $v_{\text{ref}} = 100$ km/h and with vehicle mass increased by +200 kg and then on iced road, with constant speed $v_{\text{ref}} = 50$ km/h in a fault recovery situation. After 6 s from the start of the maneuver, a fault of the yaw rate sensor occurs and the measure of the yaw rate is replaced by its estimate provided by the DVS. The following driver's model has been used:

$$\tau_d \dot{\delta}_v(t) + \delta_v(t) = K_d \left(\psi_{\text{ref}}(t) - \psi(t)\right) \tag{4.22}$$

  where $\psi_{\text{ref}}(t)$ is the course of the reference yaw angle, corresponding to the ISO double lane change path at the considered speed (see [58]), and $K_d$, $\tau_d$ are the driver gain and the driver time constant respectively. Although more complex driver models could be employed (see e.g. [58]), the simple model (4.22) has been considered in this work because the purpose here is to make a comparison between the behavior of the uncontrolled vehicle and of the controlled ones, given the same driver model, rather than to use a detailed driver model. As regards the driver's model parameters, the values $K_d = 10.8$ and $\tau_d = 0.2$ s have been considered. Note that the values of $\tau_d$ roughly range from 0.08 s (experienced driver) to 0.25 s (unexperienced driver), while the higher is the driver gain, the more aggressive is the driving action which could more likely cause vehicle instability.

Figure 4.8 shows the variation of time responses of the controlled vehicle with physical sensor and DVS in terms of normalized yaw rate $\dot{\psi}(t)/\dot{\psi}_{ref}(t)$. As expected, the vehicle using the measured yaw rate shows better performance both in transient and steady state however robust stability is achieved in both cases. It can be noted that the DVS tends to underestimate the vehicle yaw rate, so that the actual yaw rate results to be higher than the reference one (see Figure 4.8, bottom), thus bringing the vehicle closer to its lateral acceleration limit. This issue can be circumvented both by designing a reference yaw rate map that takes into account the potential estimation errors of the DVS (i.e. leaving some "margin" between the reference yaw rate and the limits of handling) and by alerting the driver, in case of sensor fault, through suitable warning lights and/or sounds that notify that the yaw control systems is running in recovery regime, so to induce a more cautious driving behavior.

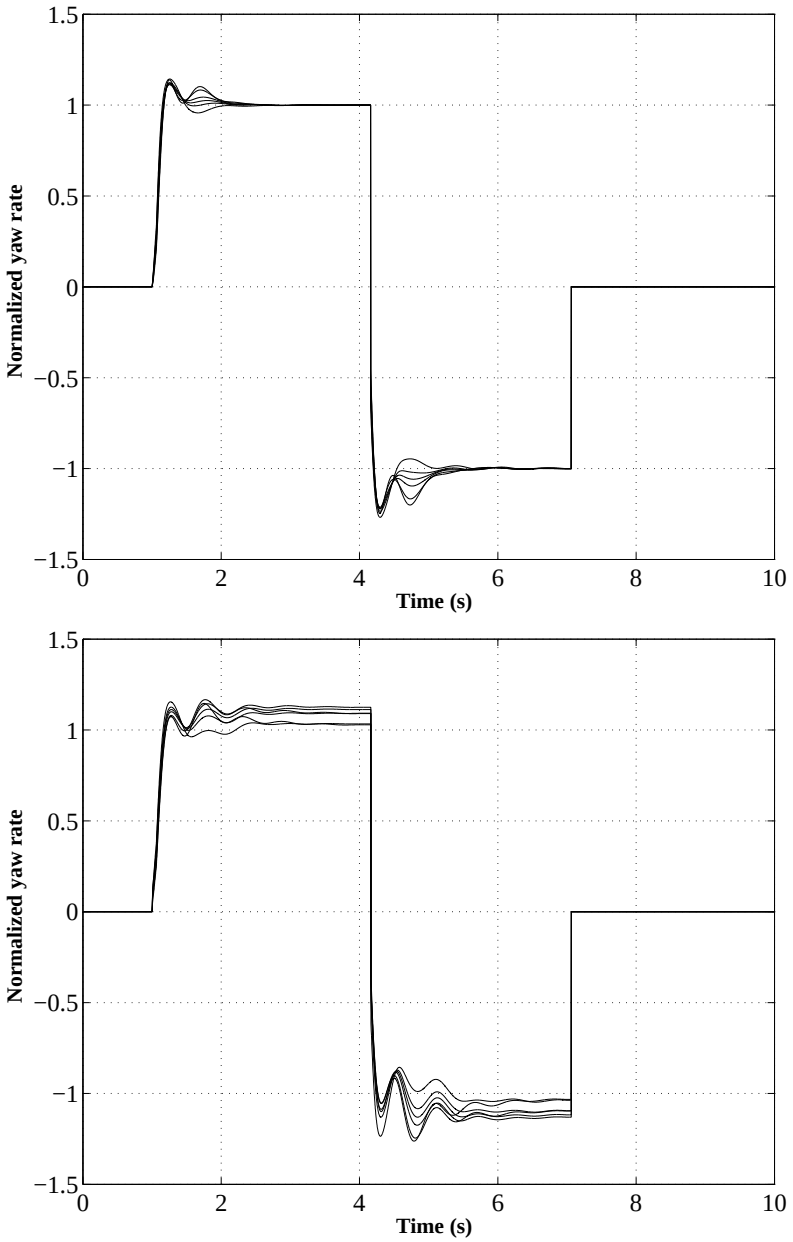


Figure 4.8. Steer reversal test with handwheel angle value of 50°, performed with varying vehicle speed between 50 km/h and 120km/h. Courses of the normalized yaw rate $\dot{\psi}(t)/\dot{\psi}_{ref}(t)$ of the vehicle controlled with $(Q + \dot{\psi})$ (top) and with $(Q + DVS)$(bottom).

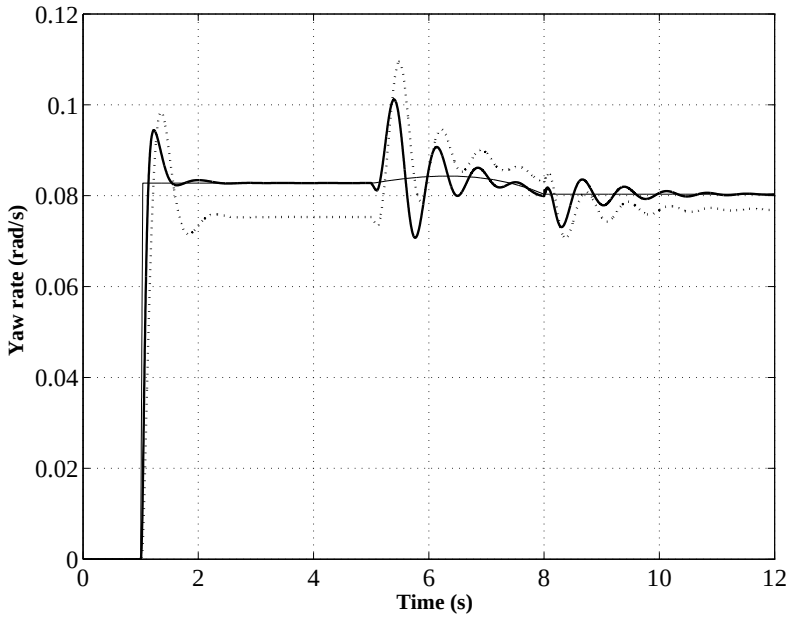


(a)

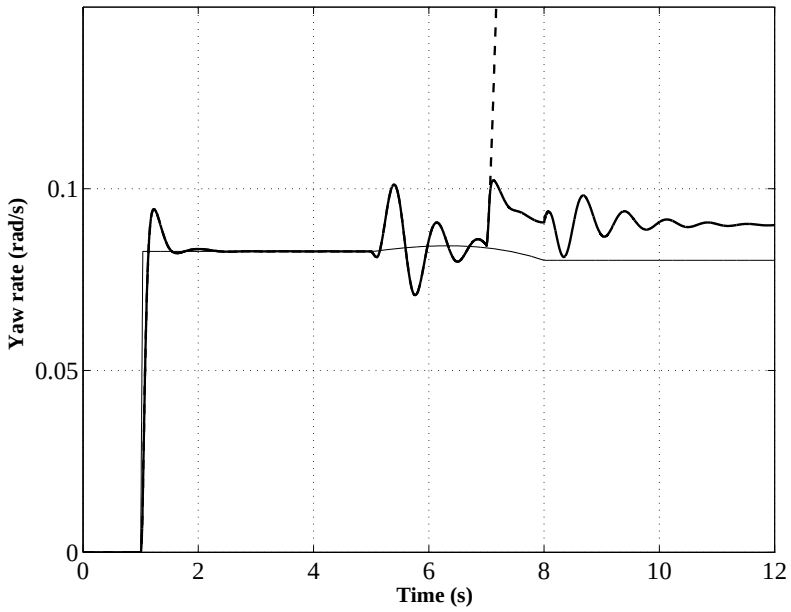


(b)

Figure 4.9. Brake in a turn test at 110 km/h with 15° handwheel angle and deceleration of 0.5g. Thin line: reference yaw rate. (a) Dotted line: uncontrolled vehicle, solid: vehicle controlled with (Q + $\dot{\psi}$). (b) Solid: vehicle controlled with (Q + $\dot{\psi}$) until 7 s when the sensor fault occurs and then with (Q + DVS). Dashed: vehicle controlled with (Q + $\dot{\psi}$) until 7 s and then it remains in open loop.

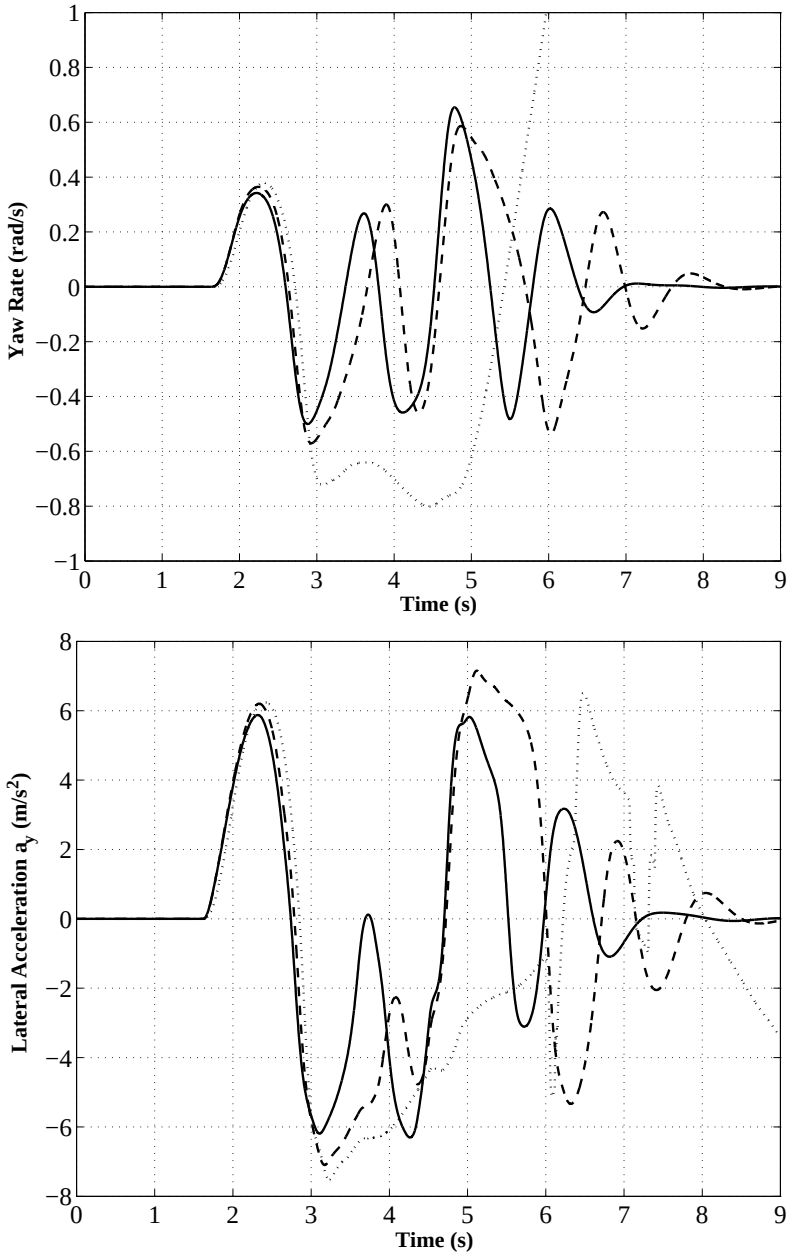


Figure 4.10. ISO double line change test at 100 km/h on wet road with vehicle mass increased by +200 kg w.r.t. nominal conditions. From top to bottom: vehicle yaw rate, vehicle lateral acceleration. Dotted line: uncontrolled vehicle, solid line: vehicle controlled with $(Q + \dot{\psi})$, dashed line: vehicle controlled with $(Q + DVS)$.

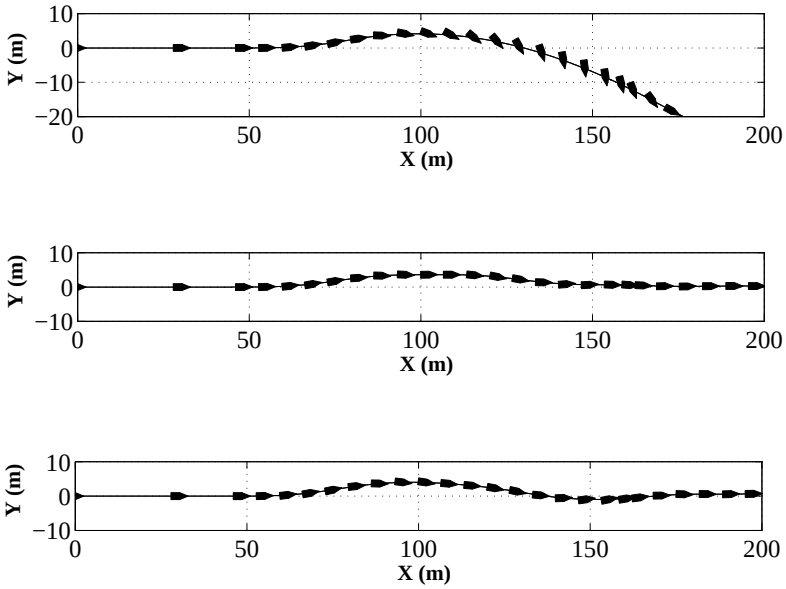


Figure 4.11. Vehicle trajectories obtained in the ISO double line change test at 100 km/h on wet road with vehicle mass increased by +200 kg w.r.t. nominal conditions. From top to bottom: uncontrolled vehicle, vehicle controlled with $(Q + \dot{\psi})$, vehicle controlled with $(Q + DVS)$.

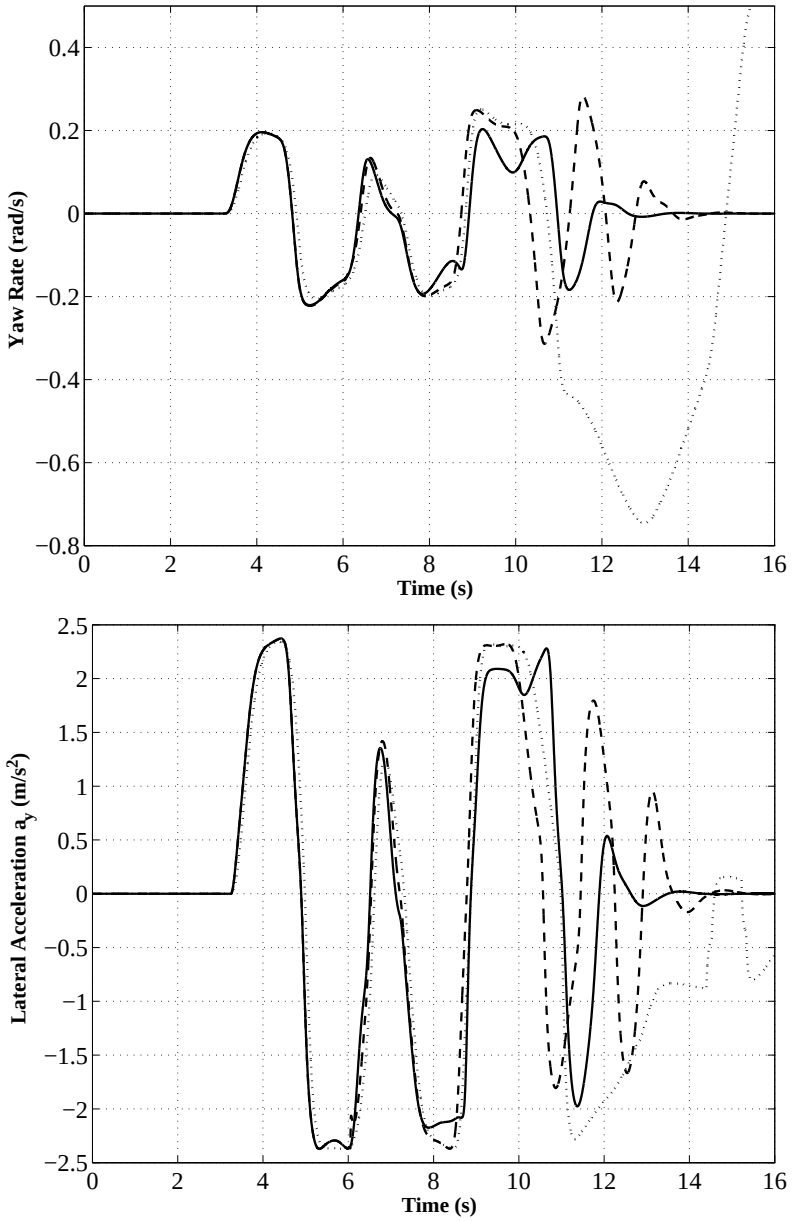


Figure 4.12. ISO double line change test at 50 km/h on iced road. From top to bottom: vehicle yaw rate, vehicle lateral acceleration. Dotted line: uncontrolled vehicle, solid line: vehicle controlled with $(Q + \dot{\psi})$, dashed line: vehicle controlled with $(Q + \dot{\psi})$ until 6 s when the fault occurs and then with $(Q + DVS)$.

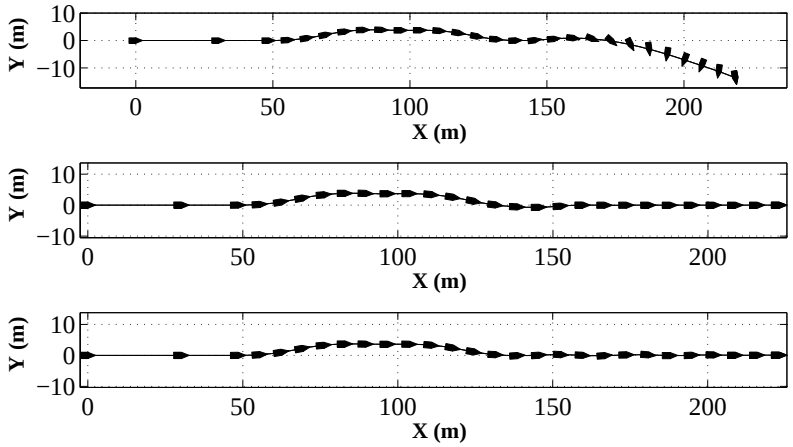


Figure 4.13. Vehicle trajectories obtained in the ISO double line change test at 50 km/h on iced road. From top to bottom: uncontrolled vehicle, vehicle controlled with $(Q + \dot{\psi})$, vehicle controlled with $(Q + \dot{\psi})$ until 6 s when the fault occurs and then with $(Q + DVS)$.

Figure 4.9 shows the results of the brake–in–a–turn maneuver. The results of this test indicate that the designed yaw control system is able to effectively intervene when the vehicle is driven in a turn at high speed and significant braking forces occur. Note that such a test is quite demanding for the considered control system, since braking forces have not been considered neither in the control design (based on a LTI single track model), nor in the DVS design (since no such maneuvers have been included in the data set collected in the preliminary experiments). Moreover, from Figure 4.9.a it can be noted that while the passive vehicle is stable, the controlled one becomes unstable when a fault of the yaw rate sensor occurs and it is not recovered, see Figure 4.9.b. In fact, since no yaw rate measure is provided in feedback, the control loop is open. On the other hand, recovery of the fault is allowed when the DVS gets on duty ensuring stability and acceptable performance on the controlled system.
Figures 4.10–4.11 show the results obtained in the ISO double lane change maneuver on wet road, in absence of fault, when the vehicle mass is increased of 200 kg. It can be noted that the uncontrolled vehicle shows excessive oversteering and instability in the last part of the maneuver. On the other hand the controlled vehicles (i.e. using the $(Q + \dot{\psi})$ and $(Q + DVS)$ schemes) are able to successfully complete the test giving a further evidence of the robustness properties of $Q + DVS$ structure. Note that, as shown in Figure 4.10, a lateral acceleration value of about 7.3 m/s$^2$, corresponding to about 95% of the maximal vehicle lateral acceleration, is reached by the vehicles controlled using the schemes $(Q + DVS)$. Thus, the results of this test indicate that the designed yaw control system is able to effectively aid the driver, also when the DVS is used instead of a physical sensor, despite the presence of driver's feedback, wet road and increased mass, that were not considered in the preliminary experiments performed to collect the data for the DVS identification.
Figures 4.12–4.13 show the results obtained with the ISO double lane change maneuver on iced road when the yaw rate sensor fault occurs. It can be noted that the uncontrolled vehicle is unstable in the last part of the maneuver, while the controlled ones are able to successfully complete the test. In particular, the controlled vehicle remains stable when, at 6 s, the physical sensor is no more able to provide the measure of the yaw rate and it is replaced by the DVS which estimates the yaw rate.

# Chapter 5

# Conclusion

This thesis investigated the robust control of nonlinear dynamic systems from data. Such approach is particularly interesting when the plant is not completely known or its laws are too complex thus it is not possible or convenient to derive a mathematical model. At this aim two methodologies were developed to control unknown and nonlinear systems employing a model derived from data. In order to derive data based model, the NSM identification was used. Such a technique provides both a system model and a model uncertainty bound; moreover, the model accuracy can be improved by using a greater number of data from different experiments for the identification.
The research focused on model-based techniques such as NIMC and NMPC, which employ the system model, respectively, as a part of the controller and of the prediction algorithm. Indeed, considering the developed NIMC methodology [2], the novelty consists in deriving the controller by cascading a filter describing the desired input/output system behavior and the inverse of the system model. Such a novel procedure exploits the recent results on the right-inversion and, above all, does not require the knowledge and the invertibility of the system. The last one is a not negligible advantage because the inversion of nonlinear systems is not trivial and sometimes impossible.
The knowledge of the uncertainty bound of the NSM model is of great importance to assess the robustness of the closed loop systems designed applying the proposed methodologies. A robust stability study showed that the obtained NIMC control structure is input/output stable by imposing a small gain condition in the control design phase [4]. Concerning the proposed NMPC control structure, instead, the robust stability was verified first through an a posteriori analysis [7] and then guaranteed by means a robust design procedure [8]. The carried out robust stability studies represent some of the main contributions of this thesis, because, at the best of author's knowledge, no similar results can be found in literature. As a matter of fact, for nonlinear systems, the robust stability issue is not tackled systematically since it is not available a suitable description of the uncertainty associated with the system models usually employed.

As minor research theme, it was investigated the design of vehicle stability control systems using the technology of Direct Virtual Sensors (DVSs) [11]. DVSs are software algorithms able to estimate a variable of interest of a system exploiting some available measures. It was shown that the direct identification from data implies a greater accuracy of the estimate w.r.t. the classical two steps approach (e.g. Kalman filter) [10]. Further, it was shown that using data collected in closed loop fashion allows to obtain a much accurate estimate than using open loop data. Then, the DVSs were used to develop a fault tolerant vehicle yaw control system: the DVS gets on duty and replaces the physical yaw rate sensor when a fault of the last one occurs [12]. Thus the novelty is that the feedback variable is replaced by the estimate yaw rate provided by the DVS guaranteeing the right working of the stability control system and hence the vehicle safety. Finally, through an a posteriori analysis, it was shown that the closed loop system employing the DVS is robustly stable.

# Appendix A

# Nonlinear Set Membership Identification

In this Appendix the main arguments of the Nonlinear Set Membership Identification (NSM) methodology are introduced, for more details see [1].
Consider a nonlinear discrete-time dynamic system in regression form:

$$\begin{aligned} y_{t+1} &= f_o\left(\mathbf{y}_t, \mathbf{u}_t\right) \quad t \in \mathbb{Z} \\ \mathbf{y}_t &= [y_t; \ldots; y_{t-n_y}] \\ \mathbf{u}_t &= [u_t; \ldots; u_{t-n_u}] \end{aligned} \tag{A.1}$$

where $u_t \in U \subset \mathbb{R}$, $y_{t+1} \in Y \subset \mathbb{R}$, $f_o : \Phi \subset \mathbb{R}^n \to \mathbb{R}$, $n = n_y + n_u$. $U$, $Y$ and $\Phi$ are convex compact sets. The regression function $f_o$ is assumed differentiable. The notation $[\ldots;\ldots;\ldots]$ indicates vertical concatenation.
Suppose that the system to be controlled $\mathbf{f}_o$ is not known, but a set of noise-corrupted measurements is available

$$(\widetilde{y}_t, \widetilde{u}_t) \quad t \in \mathcal{T} \doteq \{-T+1, -T+2, ...,0\} \tag{A.2}$$

Measurements (A.2) can be collected in a initial experiment on the plant to be controlled. Note that such measurements are needed also in the case of physical models, in order to tune the model parameters. Let $\widetilde{\varphi}_t \doteq [\widetilde{\mathbf{y}}_t; \widetilde{\mathbf{u}}_t]$ where $\widetilde{\mathbf{y}}_t = [\widetilde{y}_t; \ldots; \widetilde{y}_{t-n_y}]$ and $\widetilde{\mathbf{u}}_t = [\widetilde{u}_t; \ldots; \widetilde{u}_{t-n_u}]$.
Then, (A.1) can be re-written as

$$\widetilde{y}_{t+1} = f_o(\widetilde{\varphi}_t) + d_t, \ t \in \mathcal{T} \tag{A.3}$$

where the term $d_t$ accounts for the fact that $y_t$ and $\varphi_t \doteq [\mathbf{y}_t; \mathbf{u}_t]$ are not exactly known.
The aim is to derive a model $f$ of $f_o$ from the available measurements $(\widetilde{y}_t, \widetilde{u}_t)$. The estimate $f$ should be chosen to give small (possibly minimal) $L_p$ error $||f_o - f||_p$ , where the

$p-$norm of a given function $F(\varphi)$ is defined as $\|F\|_p \doteq \left[\int_\phi |F(\varphi)|^p \, d\varphi\right]^{\frac{1}{p}}, p \in (1,\infty)$, where $\|F\|_\infty \doteq \operatorname{ess\,sup}_{\varphi\in\Phi} |F(\varphi)|$, $|\cdot|$ denotes the Euclidean norm and $\Phi$ is a bounded set in $\mathbb{R}^n$.
Whatever estimate is chosen, no information on the identification error can be derived, unless some assumptions are made on the function $f_o$ and on the noise $d$.

**Assumption 7**

- $f_o \in \mathcal{F}(\gamma)$

$$\mathcal{F}(\gamma) \doteq \{F \in C^1 : |F(\varphi) - F(\bar{\varphi})| \leq \gamma|\varphi - \bar{\varphi}| \quad \forall \varphi, \bar{\varphi} \in \Phi \subset \mathbb{R}^n\}$$

- $|d_t| \leq \varepsilon < \infty,\ t \in \mathcal{T}$.

Thus, $\mathcal{F}(\gamma)$ is the set of Lipschitz continuous functions on $\Phi$ with Lipschitz constant $\gamma$. It is assumed that $\Phi$ is a compact set. Assumption 7 represents the only restriction imposed on the model "structure" in this study.

A key role in the SM framework is played by the Feasible Systems Set, often called "unfalsified systems set", i.e. the set of all systems consistent with prior assumptions and measured data.

**Definition 7** *Feasible Systems Set:*

$$FSS \doteq \{F \in \mathcal{F}(\gamma) \colon |\widetilde{y}_t - F(\widetilde{\varphi}_t)| \leq \varepsilon, t \in \mathcal{T}\}. \tag{A.4}$$

■

If Assumption 7 is "true", then $f_o \in FSS$.
For a given estimate $f \simeq f_o$, the related $L_p$ error $\|f_o - f\|_p$ cannot be exactly computed, but its tightest bound is given by

$$\|f_o - f\|_p \leq \sup_{F\in FSS} \|f_o - f\|_p$$

This motivates the following definition of worst-case identification error.

**Definition 8** *The worst-case identification error of the estimate $f$ is*

$$E(M) \doteq \sup_{F\in FSS} \|F - M\|_p .$$

■

Looking for estimates that minimize the worst-case identification error leads to the following optimality concept.

**Definition 9** *An estimate $F^*$ is optimal if*

$$E\left(F^*\right) = \inf_{M} E\left(M\right) = \mathcal{R}_{I,p}.$$

■

The quantity $\mathcal{R}_{I,p}$, called *radius of information*, gives the minimal worst-case identification error that can be guaranteed by any estimate based on the available information. Define the following functions:

$$\begin{aligned} \overline{F}\left(\varphi\right) &\doteq \min_{t\in\mathcal{T}} \left(\overline{h}_t + \gamma|\varphi - \widetilde{\varphi}_t|\right) \\ \underline{F}\left(\varphi\right) &\doteq \max_{t\in\mathcal{T}} \left(\underline{h}_t - \gamma|\varphi - \widetilde{\varphi}_t|\right) \\ \overline{h}_t &\doteq \widetilde{y}_t + \varepsilon \\ \underline{h}_t &\doteq \widetilde{y}_t - \varepsilon \end{aligned} \tag{A.5}$$

The next Theorem shows that the estimate

$$f_c \doteq \frac{1}{2}(\underline{F} + \overline{F}) \tag{A.6}$$

is optimal for any $L_p$ norm.

**Theorem 8** *For any $L_p$ norm, with $p \in [1, \infty]$:*

1. $f_c \in FSS$
2. *The estimate $f_c = \frac{1}{2}(\underline{F} + \overline{F})$ is optimal*
3. *The worst case identification error $E\left(f_c\right)$ is given by:*

$$E\left(f_c\right) = \frac{1}{2}\left\|\overline{F} - \underline{F}\right\|_p = R_{I,p} \tag{A.7}$$

4. *For any $\varphi \in \Phi$, $|f_c(\varphi) - f_o(\varphi)| \leq \frac{1}{2}|\overline{F}(\varphi) - \underline{F}(\varphi)|$*

■

The model $f_c$ (A.6) can be written as a nonlinear regression:

$$y_{t+1} = f_c(y_t; \ldots; y_{t-n_y}, u_t; \ldots; u_{t-n_u}) \qquad t \in \mathbb{Z} \tag{A.8}$$

where $f_c$ is a Lipschitz continuous function with Lipschitz constant $\gamma$ (see [1] for more details).

**Remark 12** *A global Lipschitz constant over all $\Phi$ has been assumed. However, a local Lipschitz constant can be useful in order to obtain improvements in identification accuracy. A very simple local approach is based on the identification of an improved model exploiting an existing model $\widehat{f}$ (obtained by any desired technique) and input/output process data. In particular, the NSM methodology is applied to the residue function $f_{\Delta}(\varphi) \doteq f_o(\varphi) - \widehat{f}(\varphi)$, using the data $\Delta y^{t+1} = \widetilde{y}^{t+1} - \widehat{f}(\widetilde{\varphi}^t)$, $t \in \mathcal{T}$. See [44] for more details.*

# Bibliography


[1] M. Milanese and C. Novara. Set membership identification of nonlinear systems. *Automatica*, 40:957–975, 2004.

[2] M. Canale, C. Novara, and M. C. Signorile. A nonlinear IMC approach to vehicle yaw control. In *European Control Conference*, Budapest, Hungary, 2009.

[3] C. Novara, M. Canale, and M. Milanese. Left-inversion of nonlinear fading memory systems from data. In *47th IEEE Conference on Decision and Control and European Control Conference*, Cancun, Mexico, 2008.

[4] M. Canale, C. Novara, and M. C. Signorile. A nonlinear IMC approach using model inversion from data. In *48th IEEE Conference on Decision and Control and European Control Conference*, Shangai, China, 2009.

[5] C. Novara, M. Canale, M. Milanese, and M. C. Signorile. Set membership inversion and robust control from data of nonlinear systems. *submitted to International Journal of Robust Nonlinear Control*.

[6] M. Canale, L. Fagiano, and M. C. Signorile. Vehicle lateral stability using a front steer by wire device and set membership predictive control techniques. In *American Control Conference*, Baltimore, Maryland, 2010.

[7] M. Canale, L. Fagiano, and M. C. Signorile. On the robustness of receding horizon control using nonlinear approximated models. In *$8^{th}$ IFAC Symposium on Nonlinear Control Systems NOLCOS 2010*, Bologna, Italy, September 2010.

[8] M. Canale, L. Fagiano, and M. C. Signorile. Robust design of predictive controllers using set membership identifed models. In *18th World Congress of the International Federation of Automatic Control (IFAC)*, Milan, Italy, 2011.

[9] M. Canale, L. Fagiano, and M.C. Signorile. A model predictive control approach to vehicle yaw control using identified models. *Proceedings of the institution of mechanical engineers. Part D, Journal of automobile engineering*. 10.1177/0954407011424098 - in press.

[10] M. Canale, L. Fagiano, F. Ruiz, and M. C. Signorile. On the design of linear virtual sensors for low cost vehicle stability control. In *2nd IEEE Multi-conference on Systems and Control*, San Antonio, Texas, 2008.

[11] M. Canale, L. Fagiano, F. Ruiz, and M. C. Signorile. A study on the use of virtual sensors in vehicle control. In *47th IEEE Conference on Decision and Control*,

Cancun, Mexico, 2008.

[12] M. Canale, L. Fagiano, F.Ruiz, and M. C. Signorile. Vehicle stability control using direct virtual sensors. *Vehicle System Dynamics, Taylor and Francis*. 10.1080/00423114.2011.607253 - in press.

[13] C.E. Garcia and M. Morari. Internal model control. 1. A unifying review and some new results. *Ind. Eng. Chem Process Des. Dev.*, 21:308–323, 1982.

[14] C.G. Economou, M. Morari, and B.O. Paisson. Internal model control. 5. Extension to nonlinear systems. *Ind. Eng. Chem Process Des. Dev.*, 25:403–411, 1986.

[15] L. Silverman. Inversion of multivariable linear systems. *IEEE Transactions on Automatic Control*, 14(3):270–276, 1969.

[16] W. Rugh. An extended linearization approach to nonlinear system inversion. *IEEE Transactions on Automatic Control*, 31(8):725–733, 1986.

[17] S. Devasia, C. Degang, and B. Paden. Nonlinear inversion-based output tracking. *IEEE Transactions on Automatic Control*, 41(7):930–942, 1996.

[18] M.D. Di Benedetto and P. Lucibello. Inversion of nonlinear timevarying systems. *IEEE Transactions on Automatic Control*, 38(8):1259–1264, 1993.

[19] K.J. Hunt and D. Sbarbaro. Neural networks for nonlinear internal model control. *IEE Proceedings-D*, 138(5):431–438, 1991.

[20] M.D. Di Benedetto and P. Lucibello. Stable inversion of continuous-time nonlinear systems by finite-difference methods. *IEEE Transactions on Automatic Control*, 47(3):537–542, 2002.

[21] Q. Hu, P. Saha, and G.P. Rangaiah. Experimental evaluation of an augmented imc for nonlinear systems. *Control Engineering Practice*, 8(10):1167–1176, 2000.

[22] Li Haijun, H. Xianlin, and B. Xiaojun. Nonlinear autopilot design based on inversion system and fuzzy logic. In *Chinese Control Conference*, pages 2399–2404, Munich, Germany, 2007.

[23] D. Schwarzmann, R. Nitsche, J. Lunze, and A. Schanz. Pressure control of a two-stage turbocharged diesel engine using a novel nonlinear imc approach. In *2006 IEEE International Conference on Control Applications*, pages 357–360, Zhangjiajie, China, 2006.

[24] B.Y. Zhang and B. Morton. Robustness analysis of dynamic inversion control laws applied to nonlinear aircraft pitch-axis models. *Nonlinear Analysis*, 32(4):501–532, 1998.

[25] I. Rivals and L. Personnaz. Nonlinear internal model control using neural networks: application to processes with delay and design issues. *IEEE Trans. on Neural Networks*, 11(1):80–90, 2000.

[26] C. Novara, M. Canale, and M. Milanese. Left–inversion of nonlinear fading memory systems from data. In *47$^{th}$ IEEE Conference on Decision and Control*, Cancun, Mexico, 2008.

[27] M.A. Dahleh, E. Sontag, D.N. Tse, and J. Tsitsiklis. Worst-case identification for a class of fading memory systems. *Automatica*, 31(3):503–508, 1995.

[28] L. Ljung. Convergence analysis of parametric identification methods. *IEEE Transactions on Automatic Control*, 23(5):770–783, 1978.

[29] E. Hansen. Global optimization using interval analysis: the one-dimensional case. *Journal of optimization theory and applications*, 29(3):331–344, 1979.

[30] A. Törn and A. Žilinskas. *Global optimization*. Springer, 1989.

[31] Y. Sergeyev. *Global one-dimensional optimization using smooth auxiliary functions*. New York: Springer-Verlag, 1998.

[32] M. Milanese and C. Novara. Computation of local radius of information in SM–IBC identification of nonlinear systems. *Journal of Complexity*, 4(6):937–951, August 2007.

[33] C. Economou, M. Morari, and B. Paisson. Internal model control. 5. extension to nonlinear systems. *Ind. Eng. Chem Process Des. Dev.*, 25:403–411, 1986.

[34] H.K. Khalil. *Nonlinear Systems*. Prentice Hall, 1996.

[35] G.C. Goodwin, S.F. Graebe, and M.E. Salgado. *Control System Design*. Prentice Hall, 2001.

[36] Rajesh Rajamani. *Vehicle Dynamics and Control*. Springer Verlag, 2005.

[37] M. Canale, L. Fagiano, M. Milanese, and P. Borodani. Robust vehicle yaw control using an active differential and imc techniques. *Control Engineering Practice*, 15:923–941, 2007.

[38] P. Yih and C. Gerdes. Modification of vehicle handling characteristics via steer-by-wire. *IEEE Transactions on Control Systems Technology*, 13(6):965–976, November 2005.

[39] M. Morari and E. Zafiriou. *Robust Process Control*. Prentice Hall, Englewood Cliffs, NJ, 1989.

[40] D. Q. Mayne, J. B. Rawlings, C. V. Rao, and P.O.M. Scokaert. Constrained model predictive control: Stability and optimality. *Automatica*, 36:789–814, 2000.

[41] M. Morari and J.H. Lee. Model predictive control: past, present and future. *Computers and Chemical Engineering*, 23:667–682, 1999.

[42] M. Baes, M. Diehl, and I. Necoara. Every continuous nonlinear control system can be obtained by parametric convex programming. *IEEE Transactions on Automatic Control*, 53(8):1963–1967, 2008.

[43] M. Baes and S. Dempe. Directional derivatives of the solution of a parametric nonlinear program. *Mathematical programming*, 70(1), 1995.

[44] M. Canale, L. Fagiano, M. Milanese, and M.C. Signorile. Nonlinear model predictive control using set membership approximated models. In *UKACC International Conference on Control (CONTROL 2010)*, Coventry, UK, September 2010.

[45] L. Grüne and J. Pannek. *Nonlinear Model Predictive Control: Theory and Algorithms*. Springer, 2011.

[46] E. Bakker, L. Lidner, and H.B. Pacejka. A new tyre model with an application in vehicle dynamics studies. In *SAE Paper 890087*, 1989.

[47] M. Canale, L. Fagiano, and M. Milanese. Set membership approximation theory for fast implementation of model predictive control laws. *Automatica*, 45(1):45–54, 2009.

[48] Ch. S. Blagovest. *Hausdorff Approximations*. Springer, 1990.

[49] P. J. Goulart, E. C. Kerrigan, and J. M. Maciejowski. Optimization over state feedback policies for robust control with constraints. *Automatica*, 42:523–533, 2006.

[50] D.W. Jordan and P. Smith. *Nonlinear ordinary differential equations*. Oxford University Press, 1987.

[51] G. J. Forkenbrock, D. Elsasser, and B. O'Hara. NHTSA's light vehicle handling and ESC effectiveness research program. *ESV Paper Number 05-0221*, 2005.

[52] P. Kohen and M. Ecrick. Active steering - the BMW approach towards modern steering technology. In *SAE Technical Paper No. 2004-01-1105*, 2004.

[53] M. Canale and L. Fagiano. Vehicle yaw control using a fast NMPC approach. In *47$^{th}$ IEEE Conference on Decision and Control*, pages 5360–5365, Cancun, Mexico, 2008.

[54] A. T. Van Zanten, R. Erhart, and G. Pfaff. VDC, the vehicle dynamics control system of bosch. In *SAE Technical Paper No. 95759*. 1995.

[55] A. T. Van Zanten. Bosch ESP systems: 5 years of experience. In *SAE Technical Paper No. 2000-01-1633*, 2000.

[56] J. Ackermann and W. Sienel. Robust yaw damping of cars with front and rear wheel steering. *IEEE Trans. on Control Systems Technology*, 1(1):15–20, 1993.

[57] B. A. Güvenç, T. Bünte, and L. Güvenç. Robust two degree-of-freedom vehicle steering controller design. *IEEE Trans. on Control System Technology*, 12(4):627–636, 2004.

[58] G. Genta. *Motor Vehicle Dynamics, II ed.* World Scientific, 2003.

[59] M. Canale and L. Fagiano. Comparing rear wheel steering and rear active differential approaches to vehicle yaw control. *Vehicle System Dynamics*, 48(5):529–549, 2009.

[60] S. Skogestad and I. Postlethwaite. *Multivariable Feedback Control. 2$^{nd}$ edition*. Wiley, 2005.

[61] P. Albertos and G. C. Goodwin. Virtual sensors for control applications. *Annual Reviews in Control*, 26:101–112, 2002.

[62] M. Milanese, C. Novara, K. Hsu, and K. Poolla. Filter design from data: direct vs. two-step approaches. In *American Control Conference*, pages 4466–4470, Minneapolis, MN, 2006.

[63] M. Milanese, F. Ruiz, and M. Taragna. Virtual sensors for linear dynamic systems: structure and identification. In *3$^{rd}$ International IEEE Scientific Conference on Physics and Control (PhysCon 2007)*, Postdam, Germany, 2007.

[64] Mario Milanese, Fredy Ruiz, and Michele Taragna. Direct data-driven filter design for uncertain lti systems with bounded noise. *Automatica*, 46(11):1773 – 1784, 2010.

[65] U. Al-Saggaf and G. Franklin. An error bound for a discrete reduced order model of a linear multivariable system. *Automatic Control, IEEE Transactions on*, 32(9):815 – 819, September 1987.